Volume-02
Issue-04
April-May-2014

ISSN: 2348-4098

International Journal of Science, Engineering and Technology

Editor-in-Chief
Dr. Kavita Sharma

Published by :
Innovative Journal Publication and Research Consultancy
E-mail : editor@ijset.in • Website: www.ijset.in/www.ijprc.com

APRIL- MAY 2014
ONLINE & PRINT VERSION

INTERNATIONAL JOURNAL OF SCIENCE, ENGINEERING AND TECHNOLOGY

(IJSET)

Print Version, Volume 02, Issue 04
April- May 2014 Edition
ISSN: 2348-4098

IJSET
www.ijset.in

International Journal of Science, Engineering and Technology

GENERAL INFORMATION:
IJSET, International Journal of Science, Engineering and Technology publish Bi- Monthly Journal under ISSN: 2250-3153

ONLINE VERSION
http://www.ijset.in/e-journal
PRINT VERSION
http://www.ijset.in/print-journal

CONTACT INFORMATION

Dr. Kavita Sharma
Editor-in-Chief
E-mail: editor@ijset.in
Website: http://www.ijset.in

TABLE OF CONTENTS

ISSN:2348-4098

EFFECTS OF TEMPERATURE ON ATTENUATION OF SEISMIC WAVES THROUGH CONSOLIDATED ROCKS IN NIGERIA

Olorode, Deborah Oluwaseun

Senior Lecturer, Physics Department, University of Lagos, Lagos, Nigeria

ABSTRACT

The factors affecting attenuation of seismic waves are numerous and one major factor considered in this study is anelasticity - the departure from ideal elastic behavior in the interior of the Earth. Studies of the anelasticity of the Earth had begun in Nigeria by seismologists using various techniques, but at room temperature, to investigate what could be responsible for this mechanism. This study employs the use of the continuous-wave transmission and spectral amplitude wave-ratio techniques to investigate the effects of temperature on the attenuation of seismic waves propagating through three different rock types (sandstone, limestone and shale) from the upper crust. Three different sedimentary rock types were collected from Ewekoro Cement factory in Ogun State of Nigeria for this study. The research study was carried out experimentally in the Solid Earth and Space Physics Research Laboratory; University of Ibadan using a special kiln.The study covers the frequency range 10Hz to 1000Hz while the temperature varies from 344K to 774K. Results obtained show that attenuation is affected by many mechanisms including presence of organic matter and seashells, presence of impurities or hydrocarbons in the rock matrix and presence of isolated pin-points. There is a general increase in the attenuation of the rock samples when heated; this is attributable to the thermal agitation of the internal constituents in the rock matrix, causing annealing in it. The rock samples reacted differently when heated. These reactions were shown by the different plots obtained from the data recorded.

Index Terms: *Anelasticity, Annealing, Attenuation, Impurities, Isolated pin-points, rock matrix, and thermal agitation.*

1. INTRODUCTION

ISSN:2348-4098

Elasticity is the property of a body or substance by which it tends to resume its original size and shape after being subjected to deforming forces. Hooke's law that strain is linearly related to stress applied until a certain point of stress, known as the field strength for the material. Anelasticity on the other hand is a process which describes the dissipation of energy in materials under stress. It is responsible for the damping of force oscillations as well as the attenuation of seismic waves. Anelasticity is also the departure of a material from being perfectly elastic. Anelastic properties are controlled by thermal and defect properties of the rock samples. These properties are influenced by thermal conductivity, grain-size, defect concentration, defect mobility, diffusion rate and other grain boundary effects. Many of these mechanisms are strongly dependent on the temperature within the material and to a small extent on the pressure. Scientists [1] have worked on thermally activated mechanisms assuming internal friction (or attenuation coefficient) $Q^{-1}$of the form

$$Q^{-1} = C\, e^{[-(E+PV)/RT]} \quad \ldots\ldots 1$$

Where C = constant depending on temperature, pressure or frequency;
E and V are activation energy and activation volume respectively;
P and T are pressure and temperature.

These processes will explain the apparent high-attenuation zone in the upper mantle in terms of temperature and pressure variations alone. In the upper mantle, the effect of temperature predominates and internal friction is high, but in the lower mantle the effect of pressure suppresses this mechanism and Q^{-1}decreases.

Attenuation of seismic waves has been investigated for many rock types under various physical conditions. In the laboratory, attenuation is generally measured using one of several techniques. Each technique determines a different measure of attenuation. These include continuous-wave transmission technique [2], pulse-echo transmission technique [3] and [4]; slow stress-strain cycles technique [5], [6] and[7] ; resonant bars technique [8], [9],[10],[11] , [12] and [13]) or pulse transmission technique [14], [15],[16] and [17] . Much work has been done in the laboratory on linear viscoelastic behavior, creep and

ISSN:2348-4098

anelasticity of the Earth using various rock types ([18], [19], [20] and [21]) and observations show that anelastic behavior at high temperatures and pressures is non-linear, whereas, at low temperatures and pressures, anelastic behavior is linear. The assumption of linear elastic behavior is much less secured for high sub-solidus temperatures than for low temperatures.

Observations of anelasticity in rocks at high temperature and pressure by [22], [23] show that non-linear behavior holds for anelasticity. Linear anelastic behavior in transient creep experiments on mantle peridotite was reported [24] at a temperature of 1250 ^{0}C for strain levels up to 5 x 10^{-5}. However, considerations of partial melting casts doubt on the validity of his result as an indicator of anelastic behavior in the mantle.

It is worth mentioning that the geometrical effects affecting attenuation of elastic waves, which include refraction, reflection and scattering can be thought of as resulting from boundary conditions imposed on the wave-propagation problem and do not reflect the anelastic properties of the medium of propagation.

There are many other mechanisms, which affect attenuation of seismic waves such as damped resonance, static hysteresis, relaxation and viscosity. Some researchers [25] suggested that sliding friction might account very well for most of the attenuation measured in rocks in the laboratory but very unlikely to cause significant attenuation of seismic waves in the mantle. The anelastic behavior of rocks subjected to high temperatures has not been of interest to Nigerian geophysicists. The present study, therefore, focuses on the effects of temperature on the anelastic properties of Nigerian rocks with the aim of obtaining the empirical relations between attenuation and wave frequency; as well as the anelastic behavior of the heated crustal rocks for comparison with attenuation measurements elsewhere.

2. EXPERIMENTAL ARRANGEMENTS AND TECHNIQUES

The experimental set-up mainly comprises a sine-audio signal generator, a heating chamber (or kiln), a double-beam standard oscilloscope, modular cable

ISSN:2348-4098

probes and a pair of quartz transducers. The signal generator generates the continuous sinusoidal waveforms, which propagates through the rock samples in turn while these are heated in the kiln. There is a pair of receiving and transmitting transducers fixed to either side of the rock sample. The experiments were carried out on three rock samples in rectangular shape having thickness approximately 2cm. The samples are: shale, sandstone and limestone from Ewekoro cement factory, Ogun state of Nigeria, located on Eastern Dahomey Basin. The kiln, with dimensions 15cm x I8cm x 25 cm, was designed and constructed by the author for this study. Proper insulation was made between its walls and the rock sample housed by it. A 0 – 200 mV thermoelectric transducer (thermocouple) which measures the temperature of the heater in millivolts was also constructed and calibrated to measure in degree Kelvin. Details of the experimental set-up and arrangements are well explained in [26].

Continuous-wave transmission and spectral amplitude wave-ratio techniques were adapted and extended for measurements of attenuation in the crustal rocks. A continuous sinusoidal wave with frequency in the range 10 Hz to 1000Hz was passed in steps of 10Hz from the sine-audio signal generator into the rock sample housed by the kiln. Records of the incident (A_i) and transmitted (A_t) waves were obtained from the double-beam oscilloscope. The relation between the incident and transmitted wave has been given by [27] as

$$A_t(f) = A_i(f)e^{-\pi ft/Q} \quad \ldots\ldots 2$$

Or

$$\ln[A_i/A_t] = -\pi ft/Q \quad \ldots\ldots 3$$

$$= -2kr \quad \ldots\ldots 4$$

From where

$$\pi ft/Q = 2kr$$

and $$\pi f/Q\, v = 2kr \quad \ldots\ldots 5$$

Where v is the velocity of the wave propagated through the rock.
f is the frequency of the wave
r is thickness of rock samples in meters.
And k is the attenuation coefficient in m^{-1}

Measurements were first taken for each rock type at room temperature. The samples were then placed in turn inside

ISSN:2348-4098

tile kiln and the temperature was varied slowly in the range 2.6 mV to 14.6 mV [i.e. 70 ^{o}C to 500^{o}C]. Equation (5) above was used to compute the attenuation coefficient k for all the rock samples. The heated rock samples were allowed to cool down to room temperature and attenuation coefficient was measured again to see the effect of heat on those samples. The right hand side of equation (3) was plotted against f to get a straight-line graph from whose slope the value of $Q$was calculated. The results obtained are presented in tables 1 to 4 and Figs 1 to 6.

Table 1. Attenuation data for Shale

Temp (K)	**k10**	**100**	**600**	**1000Hz**
344.6	15.75	14.29	11.61	9.22
380.3	13.08	9.22	7.05	5.07
416.1	6.54	5.07	4.14	3.25
451.7	5.61	4.14	3.25	1.57
487.4	3.86	1.57	0.77	0.77
523.2	-3.91	-6.54	-6.54	-7.65
558.9	-6.18	-12.06	-12.5	-12.5
594.6	-15.75	-17.57	-17.92	-18.6
630.3	-24	-26.44	-27.36	-27.36
666.1	-34.18	-36.27	-36.27	-36.88
701.7	-40.72	-42.42	-42.66	-43.12
737.4	-47.61	-49.94	-49.94	-50.76
773.2	-53.71	-55.57	-55.84	-55.84

Table 2 Attenuation with temp for limestone

Temp	k @ 10	100	600	1000Hz
344.6	15.7	12.91	9.22	7.05
380.3	14.38	11.61	10.38	7.05
416.1	10.68	9.22	7.05	7.05
451.7	8.52	7.05	7.05	7.05
487.4	10.68	9.22	9.22	9.22
523.2	0.68	9.22	8.11	8.11
558.9	9.57	7.04	7.05	6.04
594.6	7.51	6.04	5.07	5.07
630.3	5.61	3.61	3.25	3.25
666.1	4.72	3.25	2.39	2.39
701.7	4.37	2.39	2.39	1.57

ISSN:2348-4098

737.4	0	-1.61	-1.61	-1.68
773.2	-0.7	-2.17	-2.84	-2.84

Table 3. Attenuation data for Sandstone

Temp	k@100	600	1000Hz
344.6	-17.5	-17.5	-18
380.3	-18	-18	-18.4
416.1	-18	-18.4	-18.8
451.7	-18.6	-18.6	-18.8
487.4	-17.1	-16.6	-16.6
523.2	0	0	-1.15
558.9	-1.15	-1.15	-1.15
594.6	10.14	10.14	10.14
630.3	6.37	5.54	4.75
666.1	2.56	1.88	1.23
701.7	-1.15	-1.7	-2.24
737.4	-4.22	-4.22	-5.14
773.2	-6.43	-6.84	-7.24

Table 4 Attenuation of limestone with frequency

Freq.Hz	**Lim344k**	**473 K**	**558 K**	**737K**
10	15.75	10.68	9.573	0
20	15.75	10.68	9.573	0
30	15.75	10.68	9.573	0
40	14.38	10.68	9.573	0
50	14.38	10.68	9.573	0
60	14.38	10.68	9.573	0
70	14.38	10.68	9.573	0
80	14.38	10.68	9.573	0
90	14.38	10.68	9.573	0
100	12.91	9.215	7.049	1.608

3. DISCUSSIONS

The continuous-wave transmission and spectral amplitude wave -ratio techniques have been used to measure seismic wave attenuation in the crustal

ISSN:2348-4098

rocks at many frequencies over tile frequency range of 10 to 1000Hz. The temperature of the heating chamber was recorded using the thermoelectric thermocouple in millivolts and converted to Kelvin after being calibrated to Celsius scale. The data obtained from the experiments on sandstone, shale and limestone were analyzed using GRAF4WIN on a computer. The calculated attenuation coefficients for the rock samples were plotted on graphs attached. Results show that at room temperature, sandstone attenuates most, while shale attenuates least. These agree well with experimental results of [28].

As soon as temperature of sandstone increases, attenuation goes from positive to negative from temperature of 334 K to 558 K for sandstone. At temperature 630 K however, there is an inversion in attenuation of sandstone as it suddenly increases from negative to positive values. Any further increase in temperature decreases attenuation of the sandstone sample (fig 6).

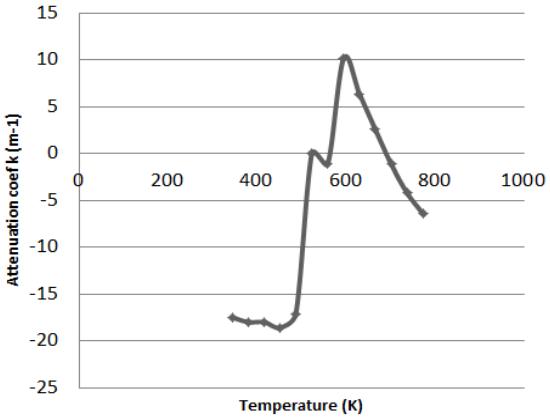

Figure 6 Attenuation of sandstone with temp.

The overall effect of temperature on sandstone shows some picture about its internal structure. The presence of impurities and hydrocarbons may be causing the decrease in attenuation at the onset of heat. Observations by [29] and [30] showed that the presence of impurities can cause great influence on rocks. The latter increase in attenuation of sandstone at higher temperature may be due to thermal vibrations which may unpin the dislocation points in the rock matrix, or it may be due to the effect of sliding friction in the rock matrix and thermal agitations as observed by seismologists for similar rocks ([21], [30] and [1]). The value of attenuation coefficient for limestone at room temperature is also positive and

ISSN:2348-4098

decreases logarithmically with frequency but not as high as that of sandstone. As the temperature of limestone increases, the attenuation coefficient reduces to negative values, giving polynomials at both high and low frequency regions (figs 4&5).

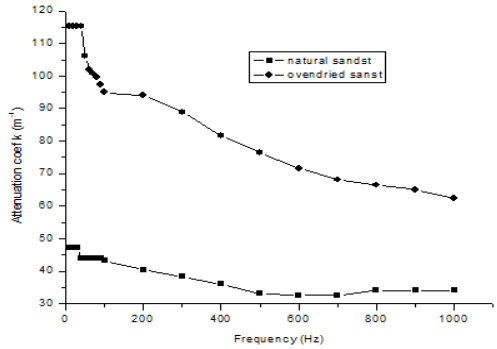

Figure 1 Effect of heat on attenuation of sandstone

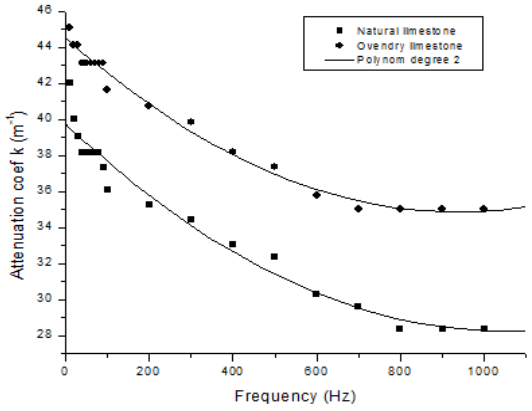

Figure 2 Effect of heat on attenuation of limestone

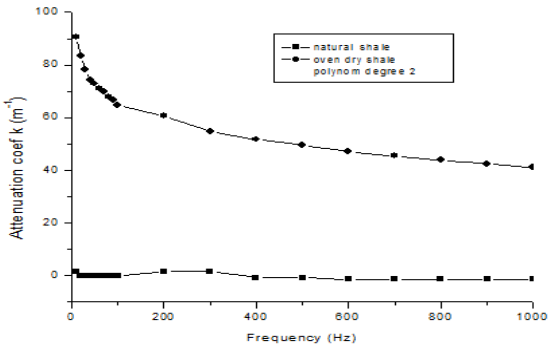

Figure 3 Effect of heat on attenuation of shale

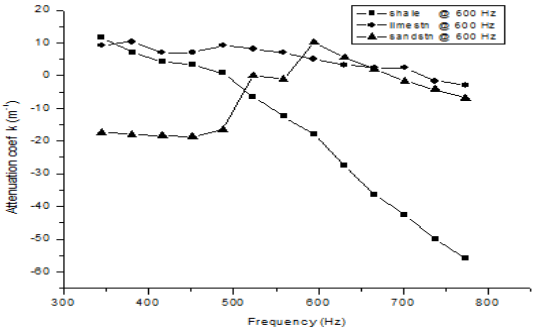

Figure 4 Effect of heat on attenuation of all samples

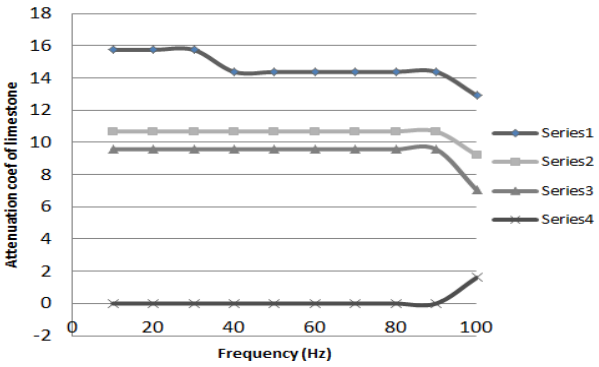

Figure 5 Attenuation of limestone at low frequencies

ISSN:2348-4098

This behavior may be traced to the presence of organic matter, sea-shells, hydrocarbons or other impurities in the sample of limestone. These are thermally agitated when heated and fusion of the materials in the rock matrix then take place thereby reducing attenuation at higher temperatures as recorded by [2] and [29].

Shale has negative values of attenuation coefficient (figs 3&4), which may be attributable to the thermal vibrations within the rock matrix which might have unpinned the dislocation points. This is revealed from the way the shale sample actually separates into thin slates after cooling. Some researchers [24] and [30] made similar observations to this result. Finally, the general increase in the attenuation could be attributable to the thermal agitation in the rock matrix causing its internal constituents to fuse together in a process known as annealing.

4. CONCLUSIONS

The principal aim of the work is to determine the effects of temperature on the attenuation of the consolidated crustal rocks and hence obtain the anelastic behavior of the rocks for this locality when heated. In this study, continuous -wave transmission and spectral amplitude wave- ratio techniques have been used to investigate the effects of temperature on seismic wave attenuation in consolidated sandstone, limestone and shale in the frequency range 10Hz to 1000Hz. Results have shown that they react differently to heat, even when the same waves at the same frequencies were allowed to propagate though them. The fact that the rock samples attenuates more after heatingreveals that if any sudden heat flow takes place underneath the Earth crust, we should expect the properties of the rock materials to change also.

The results so obtained will help to predict how each rock type will react to sudden changes in the internal heat flow of the Lithosphere (crust). Also for in-situ measurements, results presented can be used to extrapolate the value of temperature from attenuation values. This will be easier if the rock types in various layers of the crust are known, Anelastic properties of Earth's crust or the Lithosphere can be predicted from knowledge of the rock types at the site of investigation, hence an estimation of the temperature value at the depth can be made.

ISSN:2348-4098

REFERENCES

[1] Anderson D. L. and C. B. Archambeau,: " The ane1asticity of the Earth " J. Geophys. Res. 69, pp. 2071 No. 10 (1964)

[2] Manghnani, M. R., C. S. Rai, K. W. Katahara and G. R. Olhoeft: "Ultrasonic velocity and attenuation in basalt melt." Geophysics J. Roy. Astr. Soc., 73, pp. 118-122, (1983).

[3] Levykin, A. I.: "Longitudinal and transverse wave absorption and velocity in rock Specimens at multilateral pressure up to 4000 Kb/cm^2 "USSR Geophys. Ser.(Eng. transl.). Physics of the Solid
Earth,.1, pp. 94- 98. (1965).

[4] Gregory, A. R.:"Aspects of rock physics laboratory and log data that are important to seismic interpretation. Seismic stratigraphy- Application to hydrocarbon exploration " AAPG Memoir, 26, pp 15-46.(1977).

[5] Gordon, R. B. and L. A. Davis"Velocity and attenuation of seismic waves in imperfectly elastic rock". J. Geophys. Res.73, pp. 3917- 3935.(1968).

[6] Jackson, D. D.: "Grain boundary relaxation and the attenuation of seismic waves" Ph. D. Thesis Mass. Inst. of Tech., Cambridge. {Culled from Uma (l998)} (1969)

[7] Brennan B. J. "Linear viscoelastic behavior in rocks." Geophys.J. Roy. Astr.Soc., 73.pp 13- 22, (1983).

[8] Born W. T.: "Attenuation constant of Earth materials" Geophysics6, pp 132-148,(1941).

[9] Shumway, C. "A resonant chamber method for sound velocity and attenuation measurements in sediments" Geophys.21, pp 305-319, (1956)

[10] Wyllies, M. R J. , G. H. F. Gardner and A. R. Gregory: " Studies of elastic wave propagation in porous media." Geophys.27,pp. 569-589. (1962)

[11] Gardner, G. H. F., M. R. J. Wyllie and D. M. Droschak:"Effects of pressure and fluid saturation on the attenuation of elastic waves in sands. "J. Petroleum Tech., 16, pp. 189- 198. (1964).

[12] Spetzler, H. and D. L. Anderson "The effect of temperature and partial melting on velocity and attenuation in a simple binary system." J. Geophys. Res. 73, pp.6051- 6060, (1968).

[13] Birch F.: "Velocity and attenuation from resonant vibrations of spheres of rocks, glass and steel " J. Geophys. Res. 80.pp. 756- 764. (1975).

[14] Krishnamurthi, M. and S. Balakrishna: "Attenuation of sound in

ISSN:2348-4098

rocks" Geophysics, 22 pp. 268- 274. (1957).

[15) Datta S.: "Absorption of dilatational waves in rocks" Geoexploration 2 pp.127-139.(1968).

[16] Toksoz, M. N., D. H. Johnston and A. Timur: "Attenuation of seismic waves in dry and saturated rocks. 1 Laboratory measurements". Geophys.44, pp. 453-462, (1979).

[17] Brennan B. J.: "Pulse propagation in media with frequency-dependent Q" Geophys. Res. Lett., *Z,* pp. 211- 214,(1980).

[18] Wahr, J. and M. Wyss ,:" Interpretation of post-seismic deformation with a viscoelastic relaxation model." ." J. Geophys. Res. 85.pp. 6471-6477, (1980)

[19] O'Connell, R J. and B. Budiansky: "Viscoelastic properties of fluid-saturated cracked solids." 1. Geophys. Res. 82, pp. 5719- 5736.(1977)

[20] Rundle, J. B.: "Viscoelastic crustal deformation by finite quasi- static sources" J. Geophys. Res 83, pp. 5937-5945, (1978).

[21] Yuen, D. A. and W. R Peltier:" Mantle plumes and the thermal stability of the D' Layer" Geophys. Res. Lett.Z, NO.9 pp. 625- 628. (1980)

[22] Goetze, C.:" High temperature rheology of westerly granite" J. Geophys. Res.76. pp. 1223- 1230, (1971).

[23] Murell, S. A. F. and S. Chakravarty: "Some new rheological experiments on igneous rocks at temperatures up to 1120 C." Geophysics 1. R. Astro. Soc. 34pp. 211-250, (1973).

[24] BerckhemerH., Auer F. and J. Drisler: "High temperature anelasticity of mantle peridotite" Phys. Earth Planet Int. 20, pp. 48- 59, (1979).

[25] Jackson, D. D. and D. L. Anderson: "Physicalmechanisms of seismic wave attenuation". Rev. Geophys, and Space Phys. Vol. 8 NO.1 pp. 1- 64.(1970).

[26] Olorode, D.O.: "Analysis of the temperature effects on the attenuation coefficients and anelastic properties of three sedimentary rocks from South Western Nigeria" Ph. D. Thesis , University of Ibadan. (2001).

[27] White, R. E.; "The accuracy of estimating Q from seismic data." Geophys. 57 No. 11 pp. 1508-1511, (1992)

[28] Umo, J. A.: " Analysis of the wave amplitudes of broad band seismic waveforms propagated through different geological samples from Abeokuta and Ewekoro formations ,Eastern Dahomey

ISSN:2348-4098

Basin" Ph.D. Thesis, University of Ibadan.(1998)

[29] Granato, A. andK Lucke: "Theory of mechanical damping due to dislocations" J . App1. Phys.27,(2) pp. 583,(1956).

[30] Niblett, D. H. and J. Wilks,:" Dislocation damping in metals" Advances in Physics, Vol 9 (33) pp.1,(1960).

BIOGRAPHIES

Deborah Olorode did her BSc, M.Phil and PhD in Physics at the University of Ibadan, Nigeria. She is a senior lecturer in Physics Department, University of Lagos, Nigeria. Her area of specialization is Solid Earth and Environmental Geophysics.

ISSN:2348-4098

SPECTROPHOTOMETRIC DETERMINATION OF COPPER IN VARIOUS ENVIRONMENTAL SAMPLES USING GREEN REAGENT

K. KIRAN

Young Scientist, Department of Environmental Sciences, S. V. University, Tirupati-517502. Andhra Pradesh, INDIA

ABSTRACT

p-dimethyl amino benzyl ethylene diamine reagent has been successfully synthesized by the author under ordinary laboratory conditions and this reagent was used for the determination of copper metal ions in various environmental samples. Various parameters like effect of pH, reagent concentration; choice of solvent, foreign ions interferences was studied. The molar absorptivity of the complex was calculated and reported as $2.3x10^{4}$ lit mol^{-1} cm^{-1} and the Sandell's sensitivity of the complex was found to be $2.4283x\ 10^{-3}$ µg cm^{-2}.

Key words: copper ion, leaf samples, p-dimethyl amino benzyl ethylene diamine, spectrophotometry, water samples, etc.

1. INTRODUCTION

Copper is a very common substance that occurs naturally in the environment. Humans widely use copper. Copper can be released into the environment by both natural sources and human activities. Copper is often found near mines, industrial settings, landfills and waste disposals. Long-term exposure to copper can cause irritation of the nose, mouth and eyes and it causes headaches, stomachaches, dizziness, vomiting and diarrhea. Intentionally high uptakes of copper may cause liver and kidney damage and even death. Whether copper is carcinogenic or not is yet to be established. Industrial exposure to copper fumes, dusts, or mists may result in metal fume fever with atrophic changes in nasal mucous membranes. Chronic copper poisoning results in Wilson's disease, characterized by a hepatic cirrhosis,

ISSN:2348-4098

brain damage, demyelization, renal disease, and copper deposition in the cornea. Turkoglu et al [1] reported a simple spectrophotometric determination of copper in natural waters and pharmaceutical samples with chloro(phenyl) glyoxime. Copper is quantitatively retained with 1,5-diphenylcarbazone (DPC) on microcrystalline naphthalene in the pH range 6.5 - 8.0 from a large volume of aqueous solutions of various samples as reported by Shishehborea et al [2]. The liquid-liquid extraction of Cu^{2+} ions with organic solutions containing different chelating agents was reported by Marczenko [3] and Eaton [4]. Spectrophotometric determination of copper in environmental water samples by solvent extraction of an ion association complex of the dichlorocuprate(I) ion with ethylviolet has been developed by Yamamoto and Kumamaru [5]. Yamamoto [6] reported Spectrophotometric determination of copper in steel, stainless steel and aluminium alloys by the solvent extraction of an ion associate of dichlorocopper(I) ion with ethyl violet. A new solvent extraction spectrophotometric determination of copper with 2-nitroso-5-dimethyl aminophenol and zephiramine was developed by Cheng [7]. Akaiwa [8] developed a novel method of preconcentration of copper with 4,7-diphenyl-1,10-phenanthroline disulfonic acid-loaded resin. Jun-Ichi [9] reported a method for the interference of organic material with chelating resin preconcentration of trace copper in environmental water and its elimination by photochemical decomposition. Shishehborea et al [10] developed a spectrophotometric method for the determination of trace copper after preconcentration with 1,5-Diphenylcarbazone on microcrystalline naphthalene. The liquid-liquid extraction of Cu^{2+} ions is reported with organic solutions containing different chelating agents [11, 12]. A very simple, highly sensitive and selective spectrophotometric procedure was developed by Ghazy et al [13] for the determination of copper (II) in natural waters, vitamins and certified steel scrap samples. It is based on the reaction at pH 4-9 between the synthesized acetophenone-*p*-chlorophenylthiosemicarbazone (A-*p*-ClPT) and Cu (II) forming a green complex, Cu (II): A-*p*-ClPT (1:2) that floats quantitatively with oleic acid (HOL) surfactant. A facile, sensitive and selective extractive spectrophotometric

ISSN:2348-4098

method was developed by Rekha et al [14] for the determination of copper (II) in various water and alloy samples using a newly synthesized reagent, 3-methoxy-4-hydroxy benzaldehyde 4-bromophenyl hydrazone (3,4-MHBBPH). Jankiewicz et al [15] developed a spectrophotometric determination of copper (II) in soil samples from selected allotment gardens in Lodz. A simple, rapid and sensitive ultraviolet-visible spectrophotometric technique was developed by Liao et al [16] for the determination of ultra-trace copper based on injection-ultrasound-assisted dispersive liquid-liquid microextraction. Spectrophotometric measurement of $Cu(DDTC)_2$ for the simultaneous determination of zinc and copper by Uddin etal [17]. In the present study, the author synthesized *p*-dimethyl amino benzyl ethylene diamine reagent in the laboratory and this reagent was used for the determination of copper metal ions in various environmental samples.

2. EXPERIMENTAL

All the chemicals and solvents used were of analytical reagent grade procured from Sigma – Aldrich Company and double-distilled water was used to prepare all solutions in the experiments. A pH meter (Elico, Model LI-129, India) with combined glass electrode was used for pH measurements. A single pan analytical balance (Dhona, Model 100 DS, India) was employed for weighing the samples. A Systronics UV- Vis Spectrophotometer 118 model with 1 cm matched quartz cells was used for all absorbance measurements.

2.1 Synthesis of *p*-dimethyl amino benzyl ethylene diamine

Equi-molar ratio *of* p-dimethyl amino benzaldehyde and ethylene diamine (1:1) mixture was refluxed at room temperature for 3 h and allowed to stand at room temperature for two hours. Light yellow color crystals were obtained and these crystals were washed with double distilled water and recrystalized from methanol. The melting point of the reagent is 145^0 C .

2.2 General Procedure for the extraction of *p*-dimethyl amino benzyl ethylene diamine-copper complex

Transfer a sample aliquot, 1-10 mL of solution containing up to 50 µg copper,

ISSN:2348-4098

to a 125 mL separatory funnel. Add 1.0 mL of 2.0 M sulfuric acid and make the solution with double distilled water to reach a final volume of about 20 mL. To this add 20 mL of ethyl acetate. Cool the funnel and its contents in an ice water bath at 10^0C for 30 min. All reagents added beyond this point are also cooled to 10^0C. Add 3.0 mL of 3.0 % hydrogen peroxide. Shake the funnel vigorously for 30 s, allow for layer separation, and discard the aqueous phase. Add 10 mL 0.01% *p*-dimethyl amino benzyl ethylene diamine. Again extract for 30 s, allow for layer separation, and discard the aqueous phase. Transfer the organic phase to a 25 mL volumetric flask, warm to room temperature, and add sufficient additional ethyl acetate to achieve a volume of exactly 25 mL. Measure the absorbance of this solution at 480 nm against a reagent blank prepared in the same manner but containing no metal ion.

3 RESULTS AND DISCUSSION

p-dimethyl amino benzyl ethylene diamine yields a yellow colored complex with copper metal solution in acetate buffer of pH 5.0. This complex has maximum absorption at 480 nm and is stable for eight hours. Effects of pH, reagent concentration, choice of the solvent, interference of foreign ions were investigated in order to develop a sensitive spectrophotometric method for the determination of copper ion in various environmental samples.

3.1 Absorption spectrum of the *p*-dimethyl amino benzyl ethylene diamine- copper complex

An aliquot of 1.0 mL of copper solution was transfered into a 25 mL separating funnel. To it, 1.0 mL of *p*-dimethyl amino benzyl ethylene diamine in ethyl acetate solution and 3.0 mL of acetate buffer of pH 5.0 were added. The yellow colored complex was transferred into a 25 mL standard flask and made up to the mark. The reagent blank was prepared by using the same solutions without copper and extracted similarly. The absorption spectrum of the complex is recorded against the reagent blank. The absorption spectrum of the reagent and the complex is shown in Figure 1. The spectrum reveals that the *p*-dimethyl amino benzyl ethylene diamine-copper complex has maximum absorbance at 480 nm. Hence, further absorbance measurements of the complex were made at 480 nm.

ISSN:2348-4098

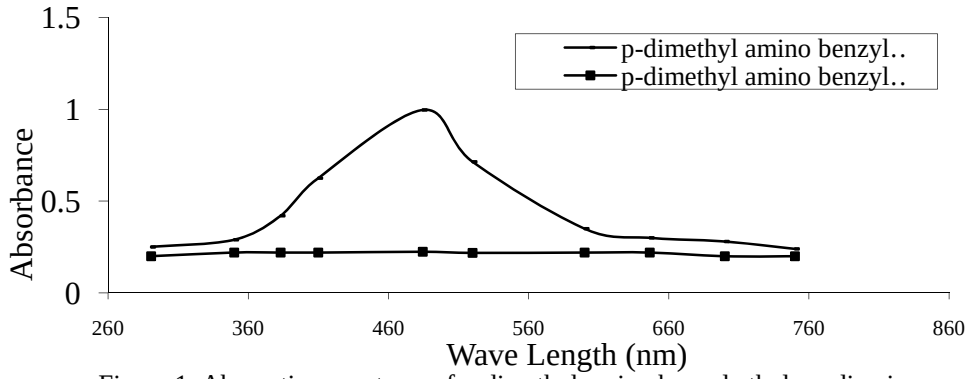

Figure 1. Absorption spectrum of p-dimethyl amino benzyl ethylene diamine-copper complex

3.2 Choice of solvent

Various organic solvents such as chloroform, n-butanol, carbontetrachloride, ethyl acetate, MIBK, benzene, etc, were used for the extraction of *p*-dimethyl amino benzyl ethylene diamine-copper complex. The results show that maximum absorbance was obtained in ethyl acetate medium. Hence, ethyl acetate solvent was chosen for further investigations.

A mixture containing 5.0 µg of copper, 3.0 mL of the suitable buffer and 1.0 mL of reagent solution was taken and the volume was adjusted to 10.0 mL with double distilled water. The experiment was repeated with acetate buffer at different pH values from 3.0 to 9.0. The values obtained were shown in Figure 2. It is observed that the extraction of the metal ion gives maximum abosorbance at pH 5.0. Hence pH 5.0 is selected for further investigations.

3.3 Effect of pH

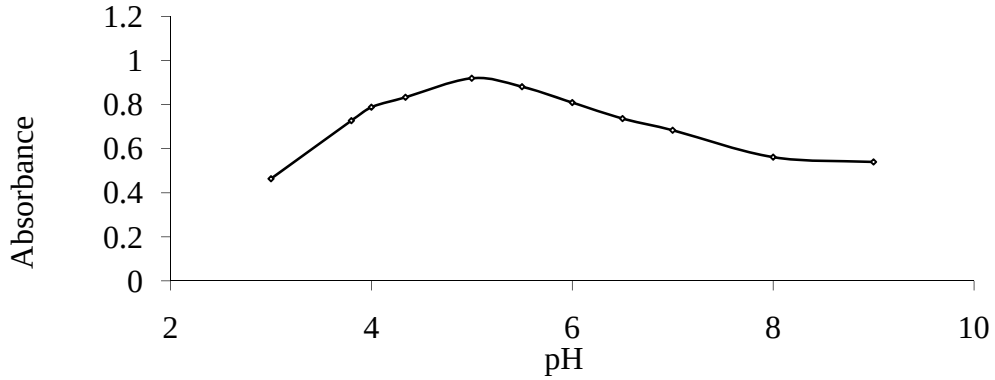

Figure 2. Variation of absorbance with pH for p-dimethyl amino benzyl ethylene diamine- copper complex

ISSN:2348-4098

3.4 Effect of reagent concentration

The effect of reagent concentration has been studied by taking constant 2 mL of copper solution and 3.0 mL of pH 5.0 buffer solution. The reagent concentration varied between 1 µg mL^{-1} and 9 µg mL^{-1} to obtain maximum color formation. The total volume of aqueous phases was brought to 10.0 mL with double distilled water. The absorbance of these phases was measured at 480 nm, against their corresponding reagent blanks. Maximum color development of the complex is absorbed at 3 µg mL^{-1}. Hence, 3 µg mL^{-1} of the reagent is maintained for all further studies.

3.5 Stability of the color reaction

The absorbance values of *p*-dimethyl amino benzyl ethylene diamine- copper complex were noted at different intervals of time at 480 nm. It was observed that the absorbance remained constant upto 8 hours, thereby indicating that the complex is stable for at least 8 hours.

3.6 Sensitivity and molar absorptivity

The molar absorptivity of the complex was calculated and reported as $2.3x10^4$ lit mol^{-1} cm^{-1} and the Sandell's sensitivity of the complex was found to be $2.4283x\ 10^{-3}$ µg cm^{-2}.

3.7 Effect of foreign ions

The effect of diverse ions on the extraction of copper ion was studied by taking known amount of copper in the solution. The results are presented in Table 1.

Table No. 1 Effect of foreign species

Species	**Tolerance limit [µg mL^{-1}]**
Na^+, Mg^{2+},Cl^-, NO_3^-, F^-, $CHCOO^-$, CO_3^{2-}, K^+	<2130
Ba^{2+}, SO_4^{2-}, CN^-, SCN^-, Tartarate	<1000
PO_4^{3-}, Al^{3+}, Cd^{2+}, NO_2^- (a)	800

 ISSN:2348-4098

Fe^{3+} [b], Ni^{2+}, Co^{2+}, Ca^{2+}	84
Zn^{2+}, Pb^{2+}, SO_3^{2-}, NO_3^-, Cr^{3+}, As^{5+}	50
Fe^{2+}, S^{2-}	36

[a]Can be masked up to 750 μg mL^{-1} by the addition of 2 mL of 1 % sulfamic acid.

[b]Can be masked up to 43 μg mL^{-1} by the addition of 1 mL of 5% EDTA.

In this study, it is noticed that there is no interference due to presence of ions such as Ca(II), Mg(II), V(V), Mn(II), Ti(IV), Mo(VI), Sr(II), Bi(III), Sb(III), W(VI), iodide, chloride, bromide, thiourea, nitrate, acetate, citrate, tartrate, phosphate and oxalate up to 2500 μg or more. Cations like Ag(I), Hg(II) and Be(II) can be tolerable up to 1250 μg. The metal ions like Ni(II), Co(II), Fe(III), Zn(II), Cd(II) and Pd(II) and anions interferences was suppressed by adding 1.0 mL of 0.3% oxalate, Ni(II), Zn(II) were suppressed by using 1.0 mL of 0.4% thiourea as masking agents and Cd(II) interference was suppressed by using 1.0 mL 0.3% citrate solution.

4 APPLICATIONS OF THE DEVELOPED METHOD

The procedure developed for the determination of copper was successfully employed to determine the content of copper in various water and industrial effluent samples.

4.1 Application of method to natural water samples

The proposed procedure was applied for the preconcentration and determination of copper metal ion in natural water samples. The natural water samples were collected in and around Tirupati, India. Analysis of copper in natural water samples was carried out as described in general procedure section. The results are presented in Table.2.

 ISSN:2348-4098

Table.2. Determination of copper in various water samples with proposed method

Sample	Cu added (µg mL^{-1})	Found[a]	Recovery (%)[a]
Polluted water[b]	-	0.29 ± 0.05	-
	-	0.37 ± 0.03	-
	-	0.42 ± 0.06	-
	-	0.51 ± 0.03	-
Natural water[c]	0.3	0.28 ± 0.04	93.33
	1.0	0.98 ± 0.03	98.00
	1.3	1.58 ± 0.06	99.30
Bore well water[d]	-	1.0 ± 0.04	-
	-	1.20 ± 0.03	-
Drinking water[e]	0.3	0.38 ± 0.05	97.50
	0.6	0.98 ± 0.02	99.00
	1.0	1.38 ± 0.04	99.20
	1.3	1.58 ± 0.02	98.80

a) Mean ± standard deviation (n=6),

b) Collected from near Gajulamanyam Industrial area, A.P., India

c) Collected from Swarnamukhi river, Srikalahasti, A.P, India.

d) Collected from in and around Tirupati,

e) Collected from municipal water supply, Tirupati.

4.2 Determination of copper in leaf samples

The proposed procedure was applied for the pre concentration and determination of copper in leaf samples following spectrometric method. First 0.1 g of

 ISSN:2348-4098

powdered leaf sample was taken in a 100 mL beaker; to this 5 mL of 1:1 molar ratio of conc. HNO_3 and $HClO_4$ is added and then heated gently until the entire leaf sample becomes digested. After digestion the volume was made upto 25 mL with double distilled water and the copper contents were analyzed following general procedure. The values are recorded and shown in Table 3.

Table.3. Determination of copper in various leaf samples

Leaf sample	**Amount of Cu(II) found (µg mL^{-1})**		**CV (%)**
	Standard Reagent [b]	**Synthesized Reagent**	
Amaranthus gangeticus (Totakura)	0.82	0.80±0.03	3.8
Hibiscus rosasinensis (Mandara)	0.78	0.78±0.02	2.6
Azadirachta indica (Neem)	1.20	1.16±0.02	1.7
Murraya koenigii(L) Spr. (Karivepaku)	0.64	0.62±0.02	3.2
Oscimum sanctum (Tulsi)	0.86	0.84±0.03	3.6

a- average mean for five determination, b- 4-Amino-3-hydroxy naphthalene-1-sulphonic acid regent procured from local market.

5 CONCLUSIONS

The proposed method is sensitive, accurate, and tolerant to many foreign substances, and the reagent used is stable under laboratory conditions. The presented procedure has some advantages over the other spectrophotometric procedures for copper, with high molar absorptivity value, low detection limit, and easy application to the real samples. The method is easily applied for the determination of copper contents of different environmental samples.

ACKNOWLEDGEMENT

I especially thanks to Department of Science and Technology to sanctioned project (Reference No:

ISSN:2348-4098

SR/FTP/ES/125/2009) under fast track young scientist scheme to me. I also thanks to Umesh Kumar Sharma, Scientist-D, for his help throughout my project.

REFERENCES

[1] Turkoglu, O.; Soylak, M., "Spectrophotometric determination of copper in natural waters and pharmaceutical samples with chloro (phenyl) glyoxime" Journal of Chinese chemical society, 52, 2005,575-579.

[2] Shishehborea, M.R,; Nasirizadeha, N. H,; Shabanib, A.M,; Tabatabaeea, M., "spectrophotometric determination of Copper with 1,5-diphenylcarbazone (DPC) on microcrystalline naphthalene of various samples" Canadian Journal of Anal.Sci and Spectroscopy, 50(3), 2005,130-136.

[3] Marczenko, Z., *"separation and spectrophotometric determination of elements*" Horwood, London, 1986.

[4] A.D. Eaton, A.D., "*Standard methods for examination of water and waste water"* 19th Ed., American Public Health Association, Washington, D.C. 1995, 3.

[5] Yamamoto,K,; Motomizu,S., "Solvent extraction of dihalogenocuprate(I) with triphenylmethane dyes and spectrophotometric determination of copper" Analytical Sciences, 5, 1989, 745-749.

[6] Yamamoto,K,; Motomizu,S., "Spectrophotometric determination of copper in steel, stainless steel and aluminium alloys by the solvent extraction of an ion associate of dichlorocopper(I) ion with ethyl violet" Bunseki Kagaku, 36(6), 1987, 343-347.

[7] Cheng, R,S., "solvent extraction spectrophotometric determination of copper with 2-nitroso-5-dimethyl aminophenol and zephiramine" Bunseki Kagaku, 34(10), 1985, 643-648.

[8] Akaiwa,H,; Kawamoto,H,; Kinoshita,H., "Preconcentration of copper (II) with 4,7-diphenyl-1,10-phenanthroline disulfonic acid-loaded resin" Bunseki Kagaku, 36(11), 1987, 662-665.

[9] Itoh,J.I,; Komata,M., " Interference of organic material with chelating resin preconcentration of trace copper in environmental water and its elimination by photochemical decomposition" Bunseki Kagaku, 36(11), 1987, 799-801.

Interference of organic material with chelating resin preconcentration of trace copper in environmental water and its elimination by photochemical decomposition

ISSN:2348-4098

[10]Shishehbore, M,R,; asirizadeh,N,; Haji,A.M,; Shabani,; Tabatabaee,M., Spectrophotometric determination of trace copper after preconcentration with 1,5-diphenylcarbazone on Microcrystalline naphthalene" Canadian Journal of Anal.Sci and Spectroscopy, 50(3), 2005, 130-134.

[11] Eaton,A.D., "*Standard Methods for Examination of Water and Waste Water*". 19th Ed., American Public Heath Association, Washington, D. C. 1995, 3.

[12] Marczenko,Z., *"Separation and Spectrophotometric Determination of Element".* Horwood, London, 1986.

[13] Ghazy,S.E,; EI-Shazly, R.M,; EI-Shahawi, M.S,; AI-Hazmi, G.A.A,; EI-Asmy, A.A., "Spectrophotometric determination of copper(II) in natural waters, vitamins and certified steel scrap samples using acetophenone-p-chlorophenylthiosemicarbazone" Journal of the Iranian Chemical Society, 3(2), 2006, 140-150.

[14] Rekha,D,; Suvardhan,K,; Suresh Kumar,K,; Reddy Prasad,P,; Jayaraj,B,; Chiranjeevi,P., "Extractive spectrophotometric determination of copper (II) in water and alloy samples with 3-methoxy-4-hydroxy benzaldehyde-4-bromophenyl hydrazone" J. Serb. Chem. Soc. 72 (3), 2007, 299-310.

[15] Jankiewicz,B,; Ptaszyński,B,; Turek,A., "Spectrophotometric determination of copper (II) in the soil of selected allotment gardens in Lodz" Polish Journal of Environmental Studies, 8(1), 1999, 35-38.

[16] Liao X,; Liang,B,; Li,Z,; Li,Y., "A simple, rapid and sensitive ultraviolet-visible spectrophotometric technique for the determination of ultra-trace copper based on injection-ultrasound-assisted dispersive liquid-liquid microextraction" Analyst, 136(21), 2011, 4580-6.

[17] Uddin,M.N,; Salam,M.A,; Hossain,M.A., "Spectrophotometric measurement of Cu $(DDTC)_2$ for simultaneous determination of Zinc and Copper" Chemosphere, 90(2), 2013, 366-73.

BIOGRAPHIES

Dr. K. Kiran is currently working as an Young Scientist (DST) at Department of Environmental Sciences, Sri Venkateswara University, Tirupati, INDIA. His research interests are in Nanotechnology and their applications towards Environmental Samples.

ISSN:2348-4098

COMPETITIVE PRIORITIES FOR MANUFACTURING STRATEGY PLANNING IN INDIAN INDUSTRY

M.S. NARWAL

Associate Professor, Dept. of Mechanical Engineering, Deenbandhu Chhotu Ram University of Science and Technology, Sonipat, Haryana, India

ABSTRACT

Researches in the area of manufacturing strategy until recently remain very much at a nascent stage in India. Many of these researches in manufacturing strategy have lack of proper industrial relevance. So, it is a real need to find an improved analytical process for developing the manufacturing strategies that will enable the Organization to remain alive well in the current competitive business environment. The paper is aimed to gain sufficient insights of manufacturing strategy issues such as competitive priorities in Automobile (two-wheeler), Tractor and General manufacturing sector companies. It has been attempted to fill some of the gaps in the contemporary research in manufacturing strategy in selected Indian corporate sectors. It is observed that Indian manufacturing companies are highly emphasizing on quality and the least on flexibility. This paper helps to provide a better understanding of manufacturing competence in a dynamic and fast changing business environment. It also highlights that what manufacturing strategy means for Indian manufacturers.

Key Words: Manufacturing Strategy, Competitive Priorities, Manufacturing Competence, Dynamic Environment, Corporate Sectors.

1. INTRODUCTION

The concept of strategy has been borrowed from the military and adopted for use in business. Strategy bridges the gap between the policy and tactics. According to Hart (1967), strategy and tactics bridge the gap between ends (goals) and means (policies), whereas according to Steiner (1979) strategy refers to basic directional decisions i.e. purposes and missions. Strategy is

ISSN:2348-4098

perspective, i.e. vision and direction. Porter (1986) defined competitive strategy as a combination of goals for which the firm is striving and the policies by which it is seeking to get there. Manufacturing strategy falls within the widely accepted hierarchy of strategy (Fine and Hax, 1985; Hill, 1989). This hierarchy spans four levels i.e. industry level strategy, corporate level strategy, business level strategy, and functional level strategy. Industry level strategy concerns to an industrial sector such as automobile, tractor etc. Corporate level strategy formulation is mainly characterized by the consideration of scope and resource deployments. At the business level, it decides the scope and boundaries of each business unit and the operational links with the corporate strategy. At operational/functional level e.g. manufacturing strategy, marketing strategy, and research and development (R & D) strategy, the objectives is to support the desired business level strategy in a manner that will provide a competitive advantage (Gupta and Lonial, 1998).

2. MANUFACTURING COMPETITIVE PRIORITIES

Manufacturing competitive priorities may be defined as a consistent set of goals for manufacturing. The review of various works enables us to identify the existence of four key manufacturing competitive priorities i.e. quality, cost, delivery, and flexibility. These competitive priorities are compiled, among others, in the works of Hayes and Wheelwright, 1979 and 1984; Buffa, 1984; Wheelwright, 1984; Fine and Hax, 1985; Swamidass and Newell, 1987; Ward et al., 1998; Kathuria et al., 1999. The manufacturing competitive priorities have been referred to as the dimensions of manufacturing strategy or the content of manufacturing strategy. Manufacturing competitive priorities capture how capabilities-based competition will evolve (Roth, 1996). Manufacturing competitive priorities represent a holistic set of tasks, which should be performed by the manufacturing function in order to support the business strategy (Kim and Arnold, 1996).

Skinner (1969) believed that a company in reality may not be able to perform well in all dimensions simultaneously and proposed a trade-off model. Later, Ferdows and De Meyer (1990) challenged

ISSN:2348-4098

trade-off model and presented a new cumulative model named as Sand Cone Model. They argued that many companies in Japan and USA are simultaneously achieving more than one competitive priority. Sand cone model was supported by many researchers (e.g. Skinner, 1985; Noble, 1995; Hill, 1989). They proposed the concept of order winners and order qualifiers. Skinner (1985) and Hill (1989) named two dimensions of delivery i.e. dependable delivery, and delivery speed. The following dimensions of delivery seem to be relevant:

i) Delivery speed: respond quickly to customer orders

ii) Dependable delivery: make on time delivery or meet delivery schedules

Garvin (1987) has identified eight strategic dimensions of quality: performance, features, reliability, conformance, durability, serviceability, aesthetics, and perceived quality. On the other hand, Hill (1989) called these strategic dimensions as an order qualifier. Corbett and Wassenhove (1993) argued that competitive priorities (cost, quality, delivery, flexibility and innovation) might be used as measures of competitiveness (external) and competence (internal). They described these two as different sides of the same coin. Quality refers to all physical aspects of the process and product or service delivered. Khir Harun & Kai Cheng (2010) suggest new quality elements of an aerospace to integrate in existing criteria for manufacturing competitiveness. Low cost is considered as a well-established competitive priority in manufacturing strategy.

Browne et al. (1984) defined eight dimensions of flexibility, which are machine flexibility, process flexibility, product flexibility, routing flexibility, volume flexibility, expansion flexibility, operation flexibility, and production flexibility. Atkinson (1984), using the flexible firm model, debated the implications for manpower, work and employment. He identifies three dimensions of flexibility which are functional flexibility, numerical flexibility and financial flexibility. Upton (1995) acknowledged the important role of flexibility in today's competitive environment. Vokurka and O'Leary-Kelly (2000) have defined five dimensions of flexibility. The following dimensions as proposed by Upton (1994) seem to be

ISSN:2348-4098

relevant in Indian manufacturing environment.

i) Product customization: customize products to customer needs

ii) Product mix changes: make rapid product mix changes

iii) Design changes: make rapid design changes.

iv) Volume changes: make rapid volume changes

v) New product introduction: Introduce new products quickly

Narwal et al (2006, 2008, and 2009) studied various industries situated northern India and concluded that the competitive priority in Indian scenario varies sector to sector to manage the competition.

From all these studies it is observed that manufacturing is considered merely as a support activity for marketing and finance in most of the organization. Thus, till very recently, manufacturing have got little top management attention. Many firms are not even practicing well tested efficiency methodologies of Scientific School of Management that provides the foundation for further development as it happens in western industrialized countries. The competition is in terms of reduced cost, improved quality, product with higher performance, flexibility better service, innovation and all delivered simultaneously. So, to compete effectively and to survive in turbulent competitive environment the firms are in real need to make effective manufacturing strategy by adopting new manufacturing management philosophies from holistic view point.

3. RESEARCH METHODOLOGY

The research methodology is based on empirical data collected through a questionnaire survey. The main objective of this survey is to examine the status of manufacturing strategy issues in Indian manufacturing companies. The questionnaire was administered in 110 manufacturing companies from three major sectors i.e. automobile, tractor and general manufacturing industries in the northern India. A database of 110 companies had been created and a structured questionnaire was administered. These companies were pooled in from the database of industrial

ISSN:2348-4098

directories and located mostly in northern India. Selection criterion was based on two parameters i.e. number of employees (more than 100) and annual sales (more than Rs.1.25 crore). After reminders, phone calls, e-mails and re-reminders, 44 filled responses have been received, which gives response rate of 40%. Out of the 44 respondents, 25 (57%) were from the top management level i.e. CEO/General Manager/President having 20 to 30 years experience. The hierarchical level of the respondents in their respective organization has shown in Figure 1.1. Vital statistics of respondents is given in Table 1.1. The process through which the collected data has been analyzed discussed in the next section.

Industry sector	Questionnaire sent	Responses received (%)
Automobile	40	17(43)
Tractor	25	10(40)
General	45	17(38)
Total	110	44(40)

Table 1.1 Vital statistics of survey

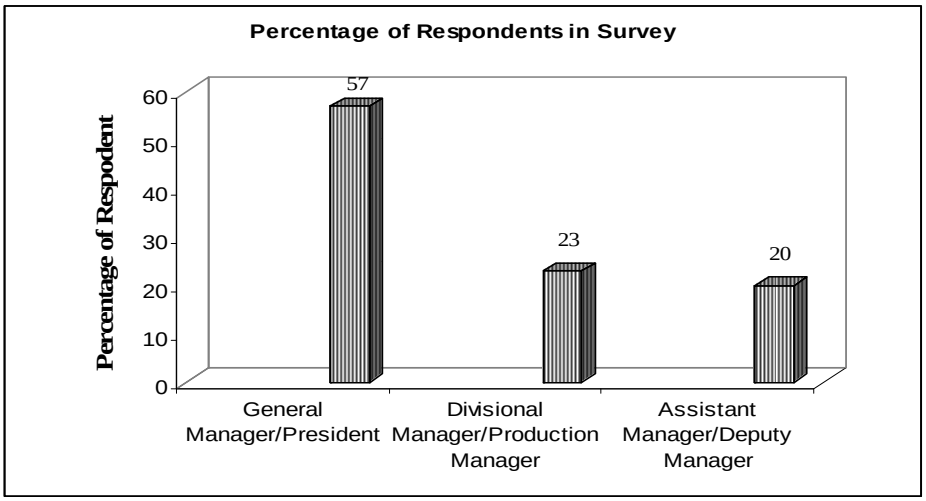

Figure 1.1 Percentage of various respondents during the survey

ISSN:2348-4098

4. ANALYSIS AND OBSERVATIONS

The overall and the sector wise values of mean and standard deviation of competitive priorities such as quality, cost, delivery, and flexibility have been considered for the analysis. The quality is having the four dimensions. But, cost and delivery are having one and two dimensions respectively, whereas the flexibility is having five dimensions. For each competitive priority, respondents were asked to indicate the degree of importance on a five point Likert scale (1-least important, 5 -most important). The basic four competitive priorities identified by various researchers were expanded into twelve dimensions i.e. conformance quality, product durability, product reliability, product performance, low cost, delivery speed, dependable delivery, product customization, product mix changes, design changes, volume changes, and new products. Table 1.2 shows the overall and sector wise value of mean and standard deviation of the four competitive priorities including the individual values of twelve dimensions.

The top most competitive priority for automobile (especially two-wheeler industry), tractor, and general manufacturing sector can now be determined from Table 1.2. Most competitive priority for tractor is quality. However, for automobile sector and general manufacturing sector it is low cost. Flexibility is the least preferred competitive priority for tractor, and general manufacturing sectors. One interesting observation can be made from table 1.2 is that highest mean score (4.71) of tractor sector is for product durability, product reliability and product performance, whereas the highest mean score (4.50) of automobile sector is for conformance quality. However, in general manufacturing sector, the highest mean value {4.66) go to delivery speed. But, in overall sector statistics highest mean score (4.32) goes to low cost. It has been observed from the above results that in overall manufacturing companies emphasize on various competitive priorities depending upon sector specific strategies and market needs.

Figure 2.1 shows mean score of the overall and sector specific (automobile especially two-wheeler industry, N=17,

ISSN:2348-4098

tractor N=10, and general manufacturing industry, N=17) competitive priorities. Sector wise mean score of 12 items of competitive priorities are represented in figure 22 (a) to (d). Table 1.3 shows the correlation between 12-items of competitive priorities. All competitive priorities except product customization (F1), product mix changes (F2) and new product (F5), are significantly correlated with other competitive priorities. The competitive priorities, which are not significantly correlated, are under the category of flexibility. The correlations imply that the manufacturing companies in the survey are strongly emphasizing on these competitive priorities. The Cronbach's alpha for the 12-item scale is 0.83, which indicates a high level of internal consistency among competitive priorities items (Nunally, 1978).

 ISSN:2348-4098

Competitive Priorities	Auto		Tractor		General		Overall	
	Mean(R)	SD	Mean(R)	SD	Mean (R)	SD	Mean	SD
Quality(Q)								
Product durability (PD)	4.08(5)	1.08	**4.71(1)**	0.48	3.41 (8)	1.08	4.06	0.88
Product reliability (PR)	4.16(4)	1.11	4.71(2)	0.48	3.50 (6)	1.08	4.12	0.89
Conformance quality (CQ)	**4.50(1)**	0.79	4.57(4)	0.53	4.50 (2)	0.67	**4.52**	0.66
Product performance (PP)	4.33(3)	1.30	4.71(3)	0.48	4.08 (4)	1.16	4.37	0.98
Sector statistics	4.26	1.07	4.68	0.49	3.87	0.99	4.27	0.85
Low cost (LC)	4.41(2)	1.48	4.14(8)	0.89	4.41(3)	0.51	4.32	0.96
Sector statistics	4.41	1.48	4.14	0.89	4.41	0.51	4.32	0.96
Delivery (D)								
Delivery Speed(DS)	3.75(8)	1.48	4.42(5)	0.53	**4.66**	0.49	4.27	0.83
Dependable delivery (DD)	3.58(10)	1.50	4.28(6)	0.50	**(1)**	1.16	3.64	1.05
Sector statistics	3.66	1.49	4.35	0.51	3.08(10)	0.82	3.96	0.94
					3.87			
Flexibility (F)								
Product customization(PC)	3.91(7)	1.50	4.28(7)	0.75	3.33 (9)	1.15	3.84	1.13
Product mix change (PM)	4.08(6)	0.90	3.29(11)	1.38	3.58 (5)	0.99	3.65	1.09
Design change (DC)	3.41(12)	1.08	3.00(12)	1.29	2.66(12)	1.07	3.02	1.14
Volume change (VC)	3.50(11)	1.24	3.57(9)	0.97	3.50 (7)	0.52	3.52	0.91
New Product (NP)	3.66(9)	1.37	3.57(10)	1.13	2.91(11)	1.24	3.38	1.24
Sector statistics	3.71	1.21	3.54	1.10	3.19	0.99	3.48	1.10

Table 1.2 Sector wise competitive priorities

 ISSN:2348-4098

Auto-Two Wheeler industry, Tractor-Tractor industry, General – General manufacturing industry, SD-Standard deviation, R-Rank (on five point Likert scale: 1-least important, 5-most important), Value in bold represent the highest mean score

	Competitive priorities	Q1 (PD)	Q2 (PR)	Q3 (CQ)	Q4 (PP)	C1 (LC)	D1 (DS)	D2 (DD)	F1 (PC)	F2 (PM)	F3 (DC)	F4 (VC)	F5 (NP)
1	Q1 (PD)	1.000	.973**	.024	.734**	.350	.298	.541**	.240	.107	.461**	.317	.322
2	Q2 (PR)		1.000	.068	.772**	.393**	.196	.491**	.227	.095	.460**	.383*	.305
3	Q3 (CQ)			1.000	.171	-.144	.272	.047	.298	.260	.021	.093	-.065
4	Q4 (PP)				1.000	.377**	.323	.386*	.341	.138	.361*	.450*	.152
5	C1 (LC)					1.000	.280	.226	.188	.245	.372*	.445*	.202
6	D1 (DS)						1.000	.283	.319	.068	.048	.165	.053
7	D2 (DD)							1.000	.203	.071	.078	.230	.020
8	F1 (PC)								1.000	.470*	.424*	.590**	.238
9	F2 (PM)									1.000	.664**	.559**	.321
10	F3 (DC)										1.000	.520**	.335
11	F4 (VC)											1.000	.234
12	F5 (NP)												1.000

Table 1.3 Correlations among competitive priorities (N=44)

Pearson's correlation coefficient calculated with SPSS for windows (version 7.5)

** Correlation is significant at the 0.01 level (2-tailed)

* Correlation is significant at the 0.05 level (2-tailed)

ISSN:2348-4098

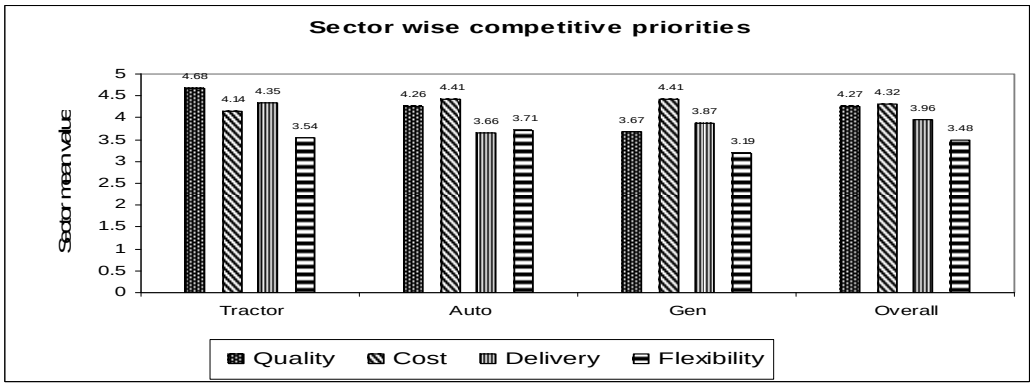

Figure 2.1 Mean score value of the overall and sector specific competitive priorities

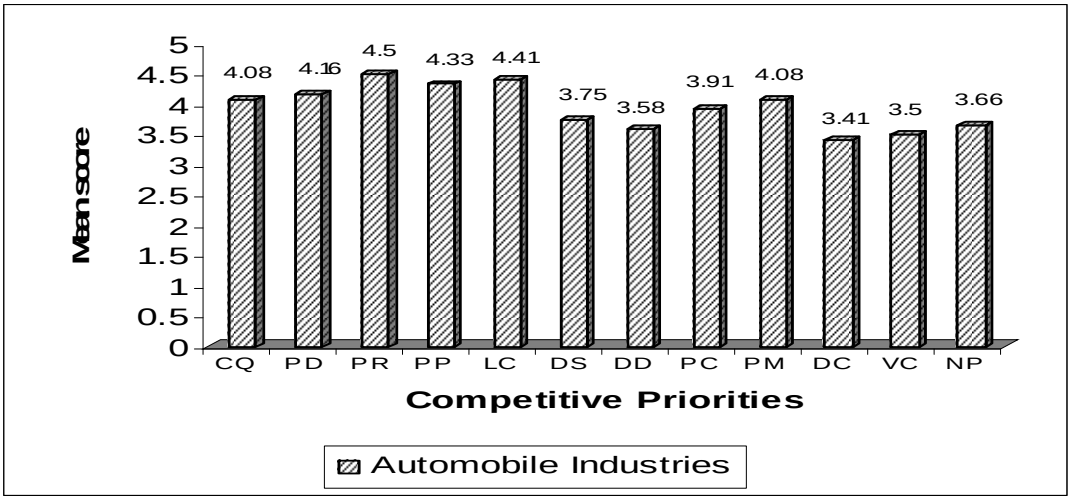

Figure 2.2 (a) Competitive priorities of Automobile sector

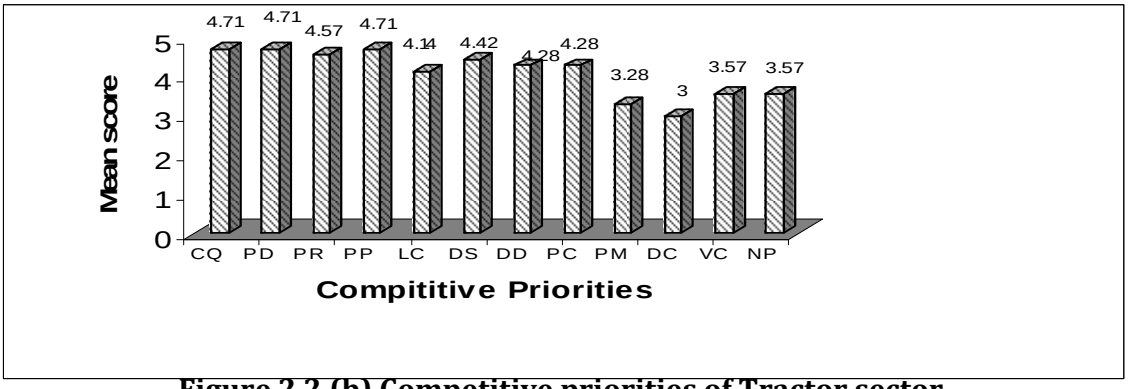

Figure 2.2 (b) Competitive priorities of Tractor sector

ISSN:2348-4098

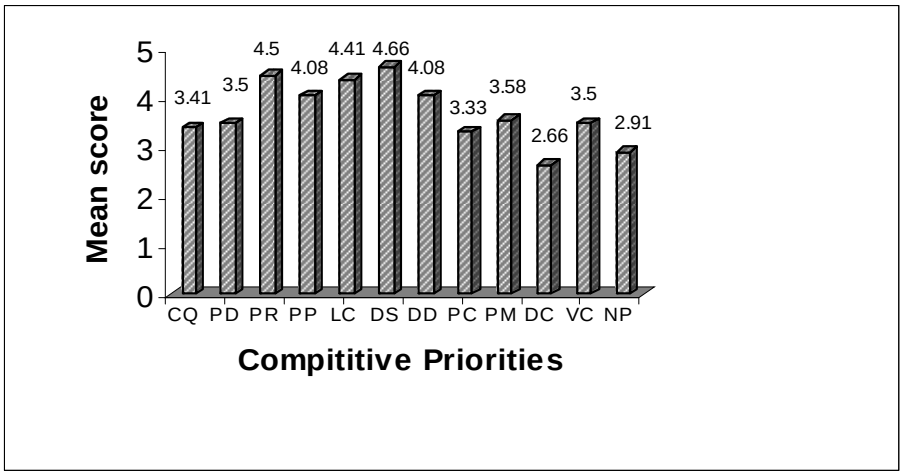

Figure 2.2 (c) Competitive priorities of General manufacturing sector

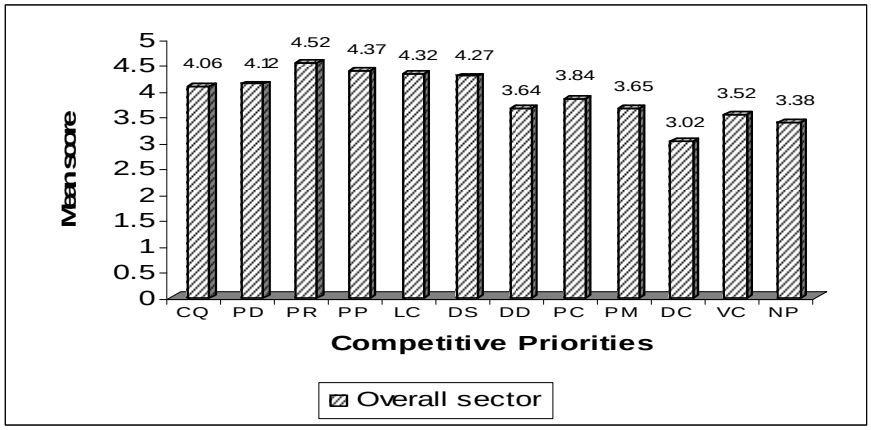

Figure 2.2 (d) Competitive priorities of Overall sector

5. CONCLUDING REMARKS

The studies have been conducted for deeper understanding of various manufacturing competitive priorities of three sector of Indian manufacturing industries viz. automobile (especially two-wheeler), tractor, and general manufacturing. The top five competitive priorities for each sector in descending order of importance are given in Table 1.3. It is observed that product durability is the top most competitive priority for tractor sector. However, conformance quality is the most important competitive priorities in automobile sector companies. On the other hand, general

ISSN:2348-4098

manufacturing sector companies give high importance to delivery speed.

Sr.No.	Automobile	Tractor	General
1	Conformance quality	Product durability	Delivery Speed
2	Low cost	Product reliability	Conformance quality
3	Product performance	Product performance	Low cost
4	Product reliability	Conformance quality	Product performance
5	Product durability	Delivery Speed	Product mix change

Table 1.3 Top five competitive priorities

It is observed that all forty four manufacturing companies of three sectors which have been surveyed are giving importance to cost(C), quality (Q), delivery (D) and flexibility (F) in descending order. In overall sector, mean score of cost and quality is more than 4.25 and also the difference between mean score of these values is very less (0.05) as compared to delivery and flexibility. This reveals that the overall sectors are emphasizing on cost and quality both, simultaneously. This supports the competitive progression theory proposed by Roth (1996). The finding of Dangayach and Deshmukh (2000, 2001 and 2003) in Indian context also matches well with this observation.

It is also observed that there is an urgent need for the Indian manufacturing firms to evolve the competitive strategy framework for its survival in the domestic competition provided by the both Indian as well as foreign multinational firms. Despite few Indian firms being awarded with Deming prize, the Indian manufacturing industries in general remains indifferent towards the issues related to competitive priorities. India has a great potential to play a significant role in this new strategy of manufacturing business. The critical success factors for potentialities depends upon the abilities of the Indian firms to link manufacturing strategy with the corporate business strategy through the achievements on various manufacturing performance objectives. Manufacturing strategy must be in terms of the whole range of interconnected policy decisions involved

ISSN:2348-4098

in its total value chain of any product from engineering design through customer service giving due consideration to competitive priorities of that industry to which the firm belongs.

REFERENCES

[1] ATKINSON, J., 1984, Manpower strategy for flexible organizations, Personnel Management, August.

[2] BROWNE, J., DUBOIS, D., RATHMILL, K., SETHI, S.P., and STECKE, K.E., 1984, Classification of flexible manufacturing systems, The FMS Magazine, April, 114-117.

[3] BUFFA, E.S. (1984), Meeting the Competitive Challenge, Dow Jones-Irwin.

[4] CORBETT, C., and WASSENHOVE, L.V., 1993, Trade-offs? What trade-offs? Competence and competitiveness in manufacturing strategy, California Management Review, summer, 107-121.

[5] DANGAYACH, G.S., and DESHMUKH, S.G., 2000, Manufacturing strategy: experiences from select Indian organizations, Journal of Manufacturing Systems, 19, 2,134-148

[6] DANGAYACH, G.S., and DESHMUKH, S.G., 2001, Implementation of manufacturing strategy: a select study of Indian process companies, Production Planning and Control, 12, 1, 89-105.

[7] DANGAYACH, G.S., and DESHMUKH, S.G., 2003, Evidence of Manufacturing Strategies in Indian industry: A survey, International Journal of Production Economic, 83 279-298

[8] FERDOWS, K., and DE MEYER, A., 1990, Lasting improvements in manufacturing performance: in search of a new theory, Journal of Operations Management, 9, 2,168 - 184.

[9] FINE, C.H., and HAX, A.C., 1985, Manufacturing strategy: a methodology and an illustration, Interfaces, 15, 6, 28-46.

[10] GARVIN, D.A., 1987, Competing on the eight dimensions of quality,

ISSN:2348-4098

Harvard Business Review, 65, 6, 104-108.

[11] GERWIN, D., 1993, Manufacturing flexibility: a strategic perspective, Management Science, 39, 4, 395-410

[12] GUPTA, Y.P., and LONIAL, S.C., 1998, Exploring linkages between manufacturing strategy, business strategy and organizational strategy, Production and Operations Management, 7, 3, 243-264.

[13] HAYES, R.H., and WHEELWRIGHT, S.C., 1979, Link manufacturing process and product life cycles, Harvard Business Review, 57, 1,133-140.

[14] HAYES, R.H., and WHEELWRIGHT, S.C., 1984, Restoring our competitive edge, competing through manufacturing, John Wiley and Sons, NY, 3-24.

[15] HART, B.H.L., 1967, Strategy, Basic Books, NY.

[16] Hill, T.J., 1989, Manufacturing Strategy: Text and Cases, Homewood IL

[17] KATHURIA, R., PORTH, S., and JOSHI, M.P., 1999, Manufacturing priorities: do general managers and manufacturing managers agree?, International Journal of Production Research, 37, 9, 2077-2092.

[18] KIM, J.S. and ARNOLD, P., 1996, Operationalising manufacturing strategy: an exploratory study of constructs and linkage, International Journal of Operations and Production Management, 16, 12, 45-73.

[19] NOBLE, M.A., 1995, Manufacturing strategy: testing the cumulative model in a multiple country context, Decision Sciences, 26, 5, 693-720.

[20] PORTER, M.E., 1986, Competitive Strategy, Harvard Business School Press, USA.

[21] ROTH, A. V., 1996, Competitive progression theory: explanation and empirical evidence, in Manufacturing Strategy: Operations Strategy in a Global Context, (C. Voss, Ed.), London Business School, 309-314.

ISSN:2348-4098

[22] SINGH, MAHENDER, BASAK, P.C., and SINGH RAJBIR, 2006, Manufacturing Strategy for Indian Corporate Success, Productivity Promotion, 9, 9, 4-11.

[23] SINGH, MAHENDER, BASAK, P.C., and SINGH RAJBIR, 2009, Strategic Management of manufacturing and some issues, Journal of Business Management, 1, 1-2, 143-151

[24] SINGH, MAHENDER, BASAK, P.C., and SINGH RAJBIR, 2008, 3rd Conference on Global Competition and competitiveness of Indian Corporates at IIM, Lucknow.

[25] SKINNER, W., 1969, Manufacturing- missing link in corporate strategy, Harvard Business Review, 47, 3, 136-144.

[26] Skinner, W., (1985), "Manufacturing: The Formidable Competitive Weapon", Johan Wiley

[27] STEINER, G., 1979, Strategic Planning, Free Press, NY.

[28] SWAMIDASS, P.M., and NEWELL, W.T., 1987, Manufacturing strategy, environmental uncertainty and performance: a path analytic model, Management Science, 33, 4, 509-524.

[29] UPTON, D.M., 1994, The management of manufacturing flexibility, California Management Review, Winter, 72-100.

[30] UPTON, D.M., 1995, Flexibility as process mobility: the management of plant capabilities for quick response manufacturing, Journal of Operations Management, 12, 205-224.

[31] VOKURKA, R.J., and O'LEARY-KELLY, S., 2000, A review of empirical research on manufacturing flexibility. Journal of Operations Management, 18, 485-501

[32] WARD, P.T., MC CREERY, J.K., RITZMAN, L.P., and SHARMA, D., 1998, Competitive priorities in operations management, Decision Sciences, 29, 4, 1035-1046.

[33] WHEELWRIGHT, S.C., 1984, Manufacturing strategy: defining the missing link, Strategic Management Journal, 5, 1, 77-91.

ISSN:2348-4098

BIOGRAPHIES

	M.S. Narwal is working as an Associate Professor in the Department of Mechanical Engineering at D.C.R. University of Science & Technology Murthal, Sonepat (Haryana), India. He has received his B.Tech degree in Mechanical Engineering from Kurukshetra (Now NIT Kurukshetra). He has received his Ph.D degree from M.D.U Rohtak (India). He is life member of ISTE, Institution of Engineers and Indian Institution of Industrial Engineering. He has published more than 20 research papers in journals & conferences at national and international level. He has more than 18 years teaching experience in Mechanical Engineering.

ISSN:2348-4098

SLIDING WEAR BEHAVIOR OF AL BASED ALLOYS FOR EQUIPMENT AND MACHINERIES

[1]ANIL KUMAR RAJAK, [2]PRAKASH KUMAR

Assistant Professor, Department of Metallurgical Engineering, BIT, Sindri – 828 123, India
E-mail: anilraj1234@gmail.com

Assistant Professor, Department of Production Engineering, BIT, Sindri – 828 123, India,
E-mail: kprakash_71@yahoo.co.in

ABSTRACT

The aim of the present paper is to understand the sliding wear behavior of Al-Mg alloys. Among various Al based alloys, Al-Mg alloys are extensively used because of its unique properties such as excellent corrosion resistance good weldability and better ductility. It is known that the microstructure and properties of aluminium alloys are strongly affected by the addition few present of Mg. In the present work, Mg was added to liquid Al in wt% of 1,2,3 and 5 wt% in a pit type electrical resistance furnace. The Mg addition in Al-Mg alloys has not only responsible for improved hardness values but also responsible for improved tensile properties. Sliding wear studies on Al-Mg alloys suggest that Mg was responsible for improved wear resistance properties as the Mg content is increase from 1 to 5wt% in the pure Al. The presence of Mg_2Si, Al_4Mg and in all the above alloys was responsible for various wear resistance results. The wear resistance of Al-5mg alloy exhibit superior wear results as coppered to Al-1mg alloys. A continuous improvement in wear resistance was noticed as the mg content was increased. The results were discussed thoroughly in the light of microstructures and wear track studies.

KEW WORDS: *Sliding wear, wear resistance, Aluminium Magnesium alloys.*

1. INTRODUCTION

Aluminium is perhaps the youngest among the large group of metallic elements. It was first commercially produced in the year 1886 and the rose in prominence meteorically to occupy today

ISSN:2348-4098

the second position in the total weight produced, next only to steel. It is deformable, easily alloyed and strengthened significantly. Add to this, the low density of the metal gives it a very high specific modules and strength. Pure aluminium is the soft metal with the modulus value of 70 GPa and the yield strength of about 40 MPa. It has the density of 2.7g/cc so that it compares favorably with several other metals and alloys in terms of specific strength and modulus. Aluminium production is highly beneficial to us as consumers, providing strong but lightweight commodities for use in building and construction, transport, consumer durables, packaging, electrical, machinery and equipment [1-2]. Addition of Mg not only increases the strength properties but is also responsible for resistance to marine corrosion, weldability and hardness. An effective alternative method to increase the strength of aluminium alloys (including Al–Mg alloys), first proposed by Willey in 1971 [3], In addition to strength, these alloys posses good corrosion resistance and weldability combined with formability [4-5]. It is well known that the addition of Mg influences the stacking-fault energy and thus the strength, the recovery and the recrystallisation characteristics of Al [6-7]. Alloys containing more than 5% Mg are seldom used in the cold worked condition because they may be susceptible to stress corrosion. A stabilizing (stress relief) treatment is used, which has little effect on properties but substantially reduces susceptibility to stress corrosion.

2. SLIDING WEAR OF AL ALLOYS

Abrasive Wear of Alumnium- Base Alloy : When a hard body slides over a soft surface, the applied normal stress ploughs a series of grooves in the latter and this is referred to as two-body abrasive wear (8) . Alloying elements such as iron, manganese and copper increase the volume fraction and that of the intermetallic silicon-bearing phases, contributing to increased wear resistance compared to binary silicon alloys In addition, magnesium and copper are also provide additional strengthening by producing submicroscopic precipitates within the matrix through an age hardening process (9). When a tangential motion is imposed, the harder surface will move, ploughing and removing the softer material (10).

ISSN:2348-4098

B. K. Prasad and co-workers (11) have reported three different stages of wear in aluminium alloy composites that contain 20% SiC particles, when sliding against a steel counterface. They observed (i) formation of steel filings (steel debris) on the test pin, caused by microcutting of the counterface by SiC particles, (ii) packing of the fillings on the sliding pin and (iii) surface deformation with loss of SiC particle (10).

2.1 WEAR MECHANISM

Wear by abrasion and erosion is forms of wear caused by contact between a particle and solid material. Abrasive wear is the loss of material by the passage of hard particle over a surface. Erosive wear is caused by the impact of particles against a solid surface. Two types of wear mechanism are (1) Abrasive wear, (2) Adhesive wear. Abrasive wear occurs whenever a solid object is loaded against particle of a material that has equal or greater hardness. Adhesive wear is a very serious from a wear characterized by high wear rates and a large unstable friction coefficient. Sliding contacts can rapidly be destroyed by adhesive wear and, in extreme cases; sliding motion may be prevented by very large coefficient of friction seizure. Metals are particularly prone to adhesive wear hence its practical significance. Most lubricant failures in sliding metal contacts results in adhesive wear since this relates to a breakdown in the lubricant's basic function of providing some degree of separation between the sliding surfaces.

Direction of Abrasion ----------→

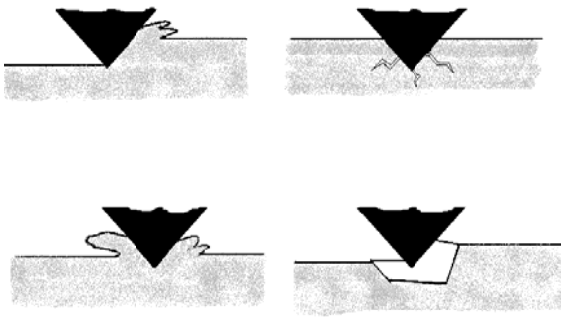

Fig- 1: Schematic diagram of abrasive wear

3. EXPERIMENTAL DETAILS

The basic raw material used for the present work is, Magnesium, and Hexochloroethane (C_2Cl_6). Commercially pure Aluminium has been used to prepare Al-Mg alloys. The alloys were prepared by controlled melting of commercially pure aluminium, Mg . (Al–1% Mg , Al–2%

ISSN:2348-4098

Mg , Al–3% Mg , Al–5% Mg) alloys in a graphite crucible using a electrically resistance furnace and cast in graphite mould Required quantities of Mg is taken and wrapped in Al foil and added to the liquid Al at 720^{0}C in an electric resistance furnace.

The liquid melt is degassed with 1% hexachloethane (C_2Cl_6) is poured in a cast iron permanent mould of different sizes.

3.1 FRICTION AND WEAR BEHAVIOR

A pin on disc type wear monitor with data acquisition system was used to evaluate the wear friction behavior of aluminium alloys against hardened ground steel (En-31) disc having hardness of RC60, a Schematic diagram of pin on disc wear and friction monitor are shown in fig 2. Pin on disc machine is shown in fig 3.Metallographical sample were prepared for optical and SEM test.

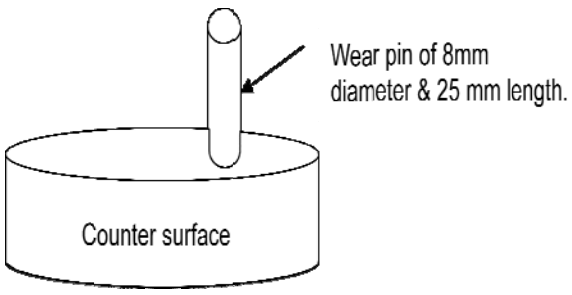

Figure 2: Schematic diagram of pin on disc wear

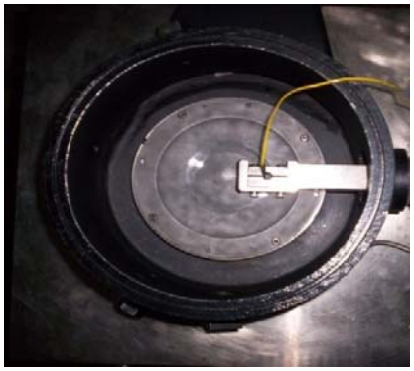

Figure 3: Shows that holding of pin on disc

4. RESULTS AND DISCUSSION

4.1 INTRODUCTION

The importance of Mg additions to Al and its alloys. Al-Mg alloys has been briefly discussed in Sec2 Addition of Mg to Al not only increases the strength properties but is also responsible for resistance to marine corrosion, weldability and hardness.

4.2 PHYSICAL AND MECHANICAL CHARACTERIZATION OF AL-MG

In order to characterize the staring material microstructure, commercial purity Al is examined and is shown in Fig.4 It is very clear from the image that the grains are columnar in nature and average size of these grains measured from the image analysis system of optical microscope, it is having ~850µm. The columnar structure is more favorable for plastic deformation and the Al has very

ISSN:2348-4098

good formability. However, the strength levels are low. To overcome the melting losses, 10% additional quantities have been added. The optical images of Al-Mg alloys are shown in Fig.5 a-b respectively.

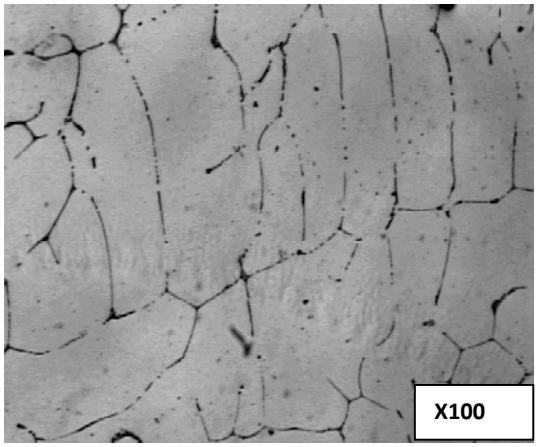

Figure 4: microstructure of pure Al

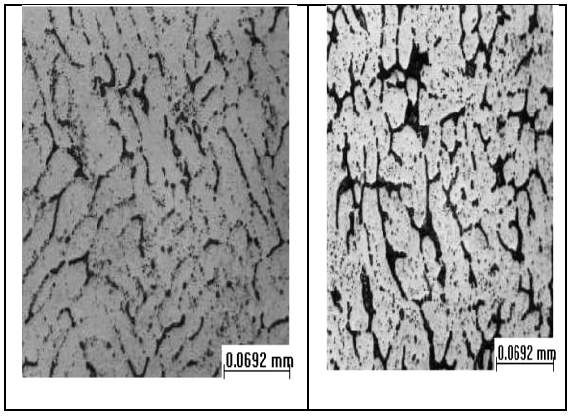

Figure 5: microstructure of Mg added Al-Mg alloys.

The micro structural details suggest that increasing the Mg content, the grain size is substantially reduced. Al-1Mg has ~95µm and drastically reduced from 850 µm that is observed for CP-Al. Further improvement in Mg content, Al-5Mg alloys exhibited a grain size of 65 µm .Fig 6 indicates that the hardness value increases by increasing percentage of Mg in Al.

Table-1: Hardness value of Al-Mg alloys

Aluminum Composition	Hardness (VHN)
Al	25
Al-1Mg	35
Al-2Mg	42
Al-3Mg	47
Al-5Mg	55

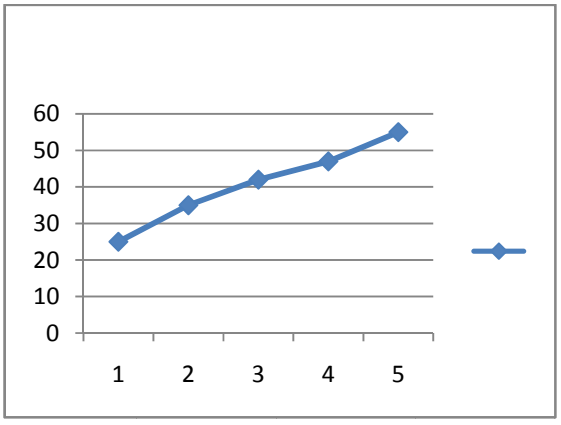

Figure 6: Variation of hardness value by addition of Mg in Al.

ISSN:2348-4098

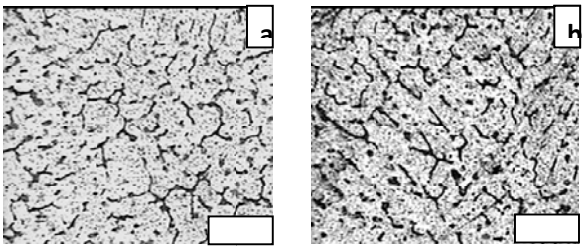

Figure 7: SEM images of Al-Mg alloys

4.3 SLIDING WEAR BEHAVIOR OF AL-MG ALLOYS

The sliding wearer response of Al-Mg alloys at 1 and 2kg loads is shown in Fig.8 and Fig.9 respectively. It can be seen from both the figures that as the Mg content is increased from1 to 5wt%, the wear loss is increased continuously. The trend is in contrast the hardness values where the hardness is increased as the Mg content is increased. Referring to the Fig.8a and Fig 8.b sudden increase in the initial stage is observed which is due to the adhesion of the sample to the sliding disc. A close observation of Fig.8 and fig 8.b.clearly suggest that at higher loads, higher wear loss is observed, as expected. Al-5Mg alloy exhibited a wear loss of 110µm for 1kg load whereas the Al-1Mg alloy exhibited ~30µm wear loss at 1khg load. At higher load like 2kg, Al-1Mg and Al-5Mg alloys exhibited ~60µm and ~140µm wear loss respectively suggesting that higher load is responsible for higher wear loss.

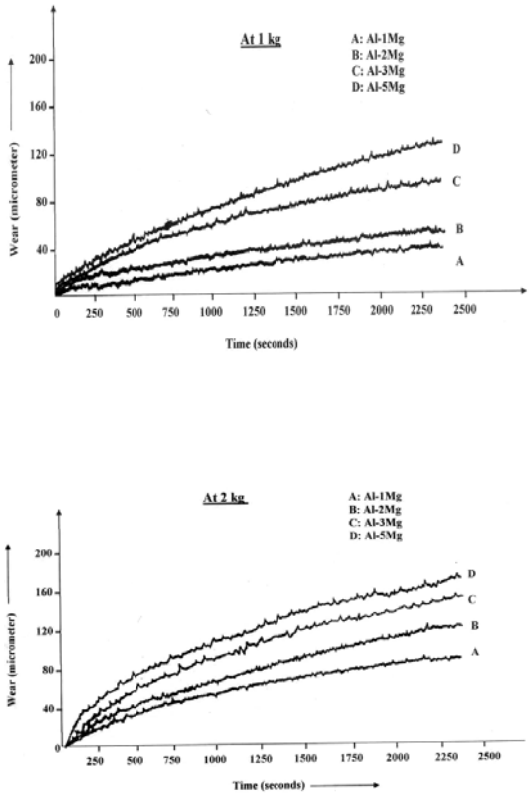

Figure 8: Sliding wear plot at various sliding distance for Al-Mg alloys at loads of a) 1kg, and b)2kg

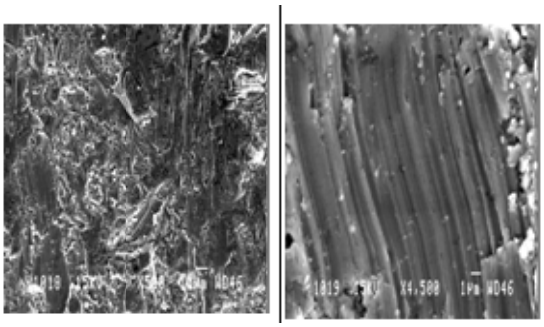

Figure 9: SEM images of wear tracs of Al-Mg alloys.

ISSN:2348-4098

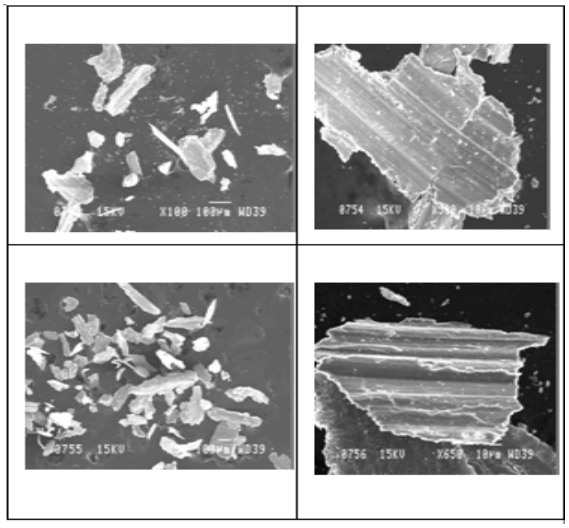

Figure 10: SEM images of debris for Al-1Mgalloy at a,b) 1kg load, c,d) 2kg load

Table- 2: Abrasive results for Al-Mg alloys at 3kg load

Sample	Initial wt (gm)	Final wt (gm)	Difference In wt. (gm)
Al-1Mg	34.14982	33.98324	0.16658
Al-2Mg	34.12234	33.96108	0.16126
Al-3Mg	32.56571	32.41465	0.15106
Al-4Mg	31.34070	31.19099	0.14971

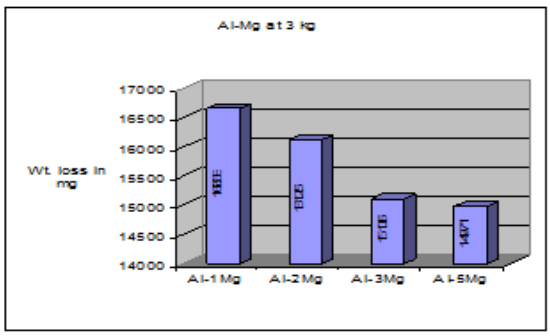

Figure 11: Abrasion behavior of Al-Mg alloys

The abrasive performance of Al-Mg alloys have shown interesting results as compared to sliding results. The Al-5mg alloys exhibited better wear performance as compared to other alloys. In other words, increasing Mg content was responsible for better abrasion results (Fig.11). The increase in hardness of alloys played significant role on the abrasion performance. Fig, 11 shows that as the percentage of Al is increased the hardness value of alloy is also increased but wear debries is decreased, it indicates that the wear resistance of Al Mg alloy is increased.

ACKNOWLEDGEMENT

The authors wish to express their sincere thanks to Dr. K. Venkatswarlu, Scientist, NAL Bengaluru, India .

CONCLUSION

Following conclusion have been drawn from the above results

1. Addition of 1wt% Mg is responsible for converting the columnar grain size that has been observed for CP-Al.
2. Increasing the Mg content is responsible for improved hardness

ISSN:2348-4098

(due to solid solution strengthening) and decreased grain size values.

3. Sliding wear behavior of Al-Mg alloys (by increasing the Mg content) is increases . Load bearing capacity of precipitates played an important role while the hardness has not much effect. The results further suggest that there must be an optimum combination of hardness and strength in the materials to achieve higher wear resistance.
4. Abrasive performance of Al-Mg alloys showed better wear resistance properties. In this case, hardness played an important role.

REFERENCES

[1] I J Polmeer, text book of Light alloys, Edward Arnold Publsihers, UK, chapter 2, 3, 4

[2]Aluminum and Al alloys, ASM International, 1993 Chapter 2, 4, 5

[3] Willey, L.A., US Patent No. 3619181; 1971

[4] Polmear IJ. Light alloys—metallurgy of the light metals., 3rd ed. London: Arnold, a division of Hodder Headline, PLC, 1995.

[5] ASM metals handbook, properties and selection: nonferrous alloys and special-purpose materials. vol. 2, 10th ed. Ohio, USA: ASM International; 1990.

[6] F.J. Humphreys, M. Hatherly, Recrystallization and Related Annealing Phenomena, Pergamon, Oxford, UK, 1995.

[7] M. Verdier, M. Janecek, Y. Bréchet, P. Guyot, Mater. Sci. Eng. A248 (1998) 187.

[8] B.K. Prasad *et al.*., Mater. Trans, JIM 36, (1995) 1048-1052

[9] B.K. Prasad, K. Venkateswarlu, S. Das, A.k. jha, R. Das gupta, JMS Lett 16 (1997) 1113-115

[10] A. Banerjee *et al.*., wear 83 (1992) 41-146

[11] B.K. Prasad, K. Venkateswarlu, O.P. Modi, A.K. Jha, S. Das, , R. Das Gupta, A.H. Yegneswaran, Met and mater trans A, 29A (1998) 2651-2660

ISSN:2348-4098

EXPERIMENTAL ANALYSIS OF FABRICATED MAGNETORHEOLOGICAL DAMPER

[1]VIJAY TRIPATHI, [2]PROF. U.K.JOSHI

[1]Research scholar, Fourth Semester, M. E. (Machine design) Jabalpur Engineering College, Jabalpur (MP)-482011, India
[2]Associate Professor, Department of Mechanical Engineering Jabalpur Engineering College, Jabalpur (MP)-482011, India

ABSTRACT

Magnetorheological (MR) fluid damper are semi active control device that have been applied a wide range of practical vibration control application. In this study, the methodology adopted to get a control structure is based on the experimental results. An Experiment has been conducted to establish the behavior of the MR damper. In this paper, the behavior of MR damper is studied and used in implementing vibration control. The force displacement and force-velocity response with varying current has been established for the MR damper. In this paper we investigated theoretically at fabricated Magnetorheological damper by using different Magnetorheological fluid. Here two types of MR fluid developed first by mixing of prepared nano size (fe3o4) iron particle by co precipitation method, second by separation of magnetic tape. And a comparative study had done between these iron particles prepared MR fluid. Here an experimental performed on fabricated MR damper and discussed the behavior of MR damper.

KEYWORDS: Magnetorheological (MR) fluids; Magnetorheological dampers; Semi-active damper; nano particle; Magnetic field intensity.

1. INTRODUCTION

The suppression of mechanical and structural vibration using semi-active control method has been actively worked by many researchers in last two decades [21]. Recently, various semi-active suspension systems featuring MR fluid damper have been proposed and

ISSN:2348-4098

successfully applied in the real field, especially in vehicle suspension[3] systems Magnetorheological damper is becoming the most promising vibration controller in the intelligent suspension presently and it wins the favors of vehicle manufactures, because it takes the advantageous of high strength, good controllability, wide dynamic range, fast response rate, low energy consumption and simple structure[2]. Conventional damper has constant setting throughout their lifetime, and hence will not be able to operate satisfactorily in a wide range of road conditions. It is for these reasons that semi-active systems like MR dampers have attracted the attention of suspension designers and researchers [2]. Models that can accurately represent the behavior of MR dampers are essential in understanding the operation and working principles of the device. Such models can eliminate a great deal of uncertainties during the design process, which can subsequently enable control strategies for the damper to be developed efficiently and reliably. A mathematical model is derived from their physical features like geometry and construction can provide insights into the way various parameters affect the performance of the device [4].

In this paper, the fundamental design method of the MR damper is investigated theoretically. A mathematical model is used to characterize the constitutive behavior of the MR fluids subject to an external magnetic field strength. Here I introduced a new concept for generating a magnetic field inside the piston cylinder by use of circular armature core. Then a theoretical method is developed for analyzing the shear stress by the MR fluid within the MR Damper.

1.1 PROBLEM STATEMENT AND OBJECTIVE

The previous studies on MR dampers have shown that the MR dampers either in passive-on or semi-active controlled modes could be more efficient as compared with systems with conventional viscous dampers. The goal of this research is to investigate the characteristics of the MR damper and a single-degree-of freedom (SDOF) system with the MR damper through experimental studies and analyses under harmonic excitation of the base. In particular, it will be explained why the frequency shift of the peak transmissibility for the MR damper system is different from that with the viscous damper. The transmissibility will

ISSN:2348-4098

also be quantified and compared with that of the conventional viscous damper through updating the equivalent damping coefficient with changing driving frequency. Here the main problem for fabrication of MR Damper is generation of magnetic field inside of cylinder piston. [14]

2. PHYSICAL STUDY OF MAGNETORHEOLOGICAL DAMPER

2.1 MR FLUID

A magneto-rheological-fluid is a fluid with rheological behavior which depends on the strength of a magnetic field. The rheological status changes reversibly from liquid to the solid. The Greek word ‘‘rheos’’ means flowing and rheology is the science of deformation behavior of materials which are able to flow. Normally the rheological property of viscosity changes with other physical properties, such as chemical composition, shear stress and temperature. These features are not easily controlled in most applications because they are fixed by the environment in a particular situation. In the case of MR the fluid viscosity becomes intelligently controllable using the magnetic field. This change of viscosity up to the solid condition is reversible and is the basic feature of MRF technology. The MRF effect is the difference in rheological properties with and without a magnetic field. [11]

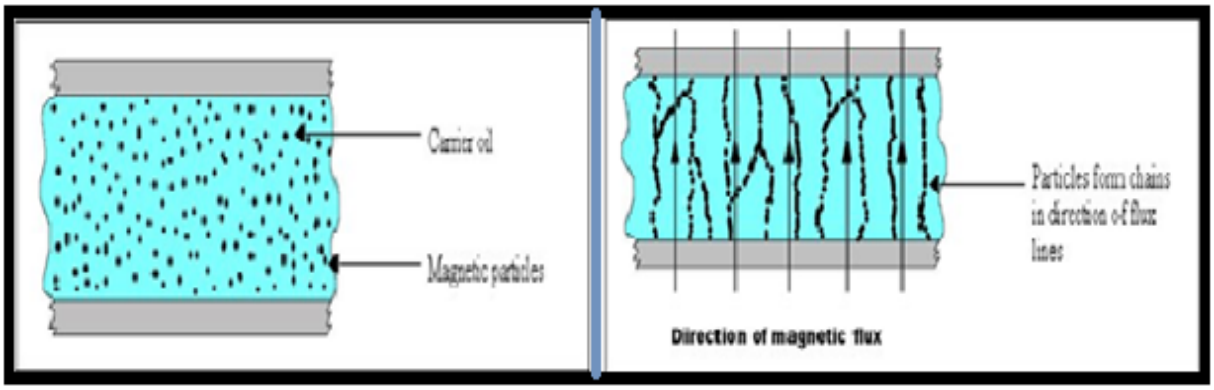

Figure 1: Behavior of MR fluid (a) Without magnetic field (b) With magnetic field

There are basically three components in an MR fluid: basic fluid, metal particles and stabilizing additives. The base fluid has the function of the carrier and naturally combines

 ISSN:2348-4098

lubrication (in combination with additives) and damping features. For the highest MRF effect the viscosity of the fluid should be small and almost independent of temperature.

The MR fluid used in this research is prepared in the applied chemistry laboratory of Jabalpur engineering collage University of (RGTU) (m.p.) India. Here I prepared two types of magnetizable iron particles first FeO, Fe_2O_3 ferric oxide particles separate from magnetic tape. Acetone is use for melt and separates this Ferric oxide. Here I use old music or video records tape it's a low cost simple process for making a magnetizable iron oxide particles in micro meter range. Second Fe_3o_4 magnetizable iron oxide particles made by co precipitation method. In this method, by adding a 1M Sodium Hydroxide (NaOH > 99%) solution into a mixed solution of 1.28M Ferric chloride hexa-hydrate (FeCl3.6H2O > 99%) and 0.64M ferrous sulphate tetra hydrate (FeSO4.7H2O > 99%) solution (molar ratio 2:1) these solution proper mixed on mechanical stirring (500rpm)at room temperature and then heat up at 80°C in 3hour's after that washed properly then dry with use of oven and finally Fe_3o_4 particle sample is prepared. The size of magnetizable particles is nano and micrometers in average diameter and the carrier fluid is 1000 cps (1Pa·s=1N·s/m2=1000cps) of veedol front frok oil. So the appearance of this MR fluid is even dark gray and sensitive to the magnetic field. Poiseuille was derived a formula for coefficient of the viscosity, for determined the viscosity of MR fluid glycerin is used as a reference fluid of the known properties.

$$\eta = \frac{(\rho.t)}{(\rho g.tg)}\eta g$$

Where: ρ is Density of the magneto-rheological fluid, t is out flow time of the magneto-rheological fluid from the capillary, ρ_g is density of the reference fluid, tg is outflow time of the reference fluid from the capillary, η_g is viscosity coefficient of the reference fluid.

2.2 MR FLUID DAMPER

A Magneto-Rheological (MR) damper is very similar to the traditional damper. The difference lies on the use of a magneto-rheological fluid, which typically consists of micron sized, magnetically polarizable particles dispersed in a carrier medium such as mineral or silicone oil (Bombard et al., 2002). When a magnetic field is applied to the fluid, particle

ISSN:2348-4098

chains are formed, and the fluid becomes semi-solid, exhibiting plastic behavior, changing the flow properties of the fluid. A MR damper could be build using a traditional damper body with magnetic valves able to act over the MR fluid property. The peak power required to fluid control is less than 30 watts, which could allow the damper to operate continuously for more than an hour on a small batter.

Figure 2: Schematic diagram of fabricated Magnetorheological Damper

2.3 MAGNETIC FIELD

The magnetic field in the MR damper can be generated with coils wound around the piston by use of circular armature core. Circular armature core is a main part for generation of magnetic field on MR Damper, The dimension of these circular armature fins are outer diameter D_O=38MM, inner diameter D_I=12MM, height H=1MM. The supply wire connecting this electromagnet is then lead out through the hallow piston shaft. Maximum current supply of this coil is 2amp (0 to 2amp). And the temperature range is (0 to 70°C)

3. EXPERIMENTAL PROGRAM

Typically, a fabricated MR damper consists of a hydraulic cylinder, magnetic coils and MR fluid offering design simplicity as soon is fig.2. This MR damper has a conventional cylindrical body configuration filled with 100 ml of MR fluid and comprising the piston, the magnetic circuit with a coil resistance of 20 Ω and the accumulator. The enclosing cylinder

ISSN:2348-4098

is 41.4 mm in diameter and the damper is 208 mm long in its extended position with ±25 mm stroke. The device can operate within a current range from 0.0 A up to 2.0 A with a recommended input value of 1.0 A for continuous operation and can deliver a peak force of 1000 N at a velocity of 50 mm/s with a continuous operating current level of 1.0 A. The MR damper can reach at least 90% of maximum level during a 0.0 amp to 1.0 amp step input in less than 25 milliseconds. [4]

Table.1: Sinusoidal excitation parameters fabricated MR damper

Parameter	Values
Frequencies (Hz)	(1.00, 2.00,3.00,3.50,4.00,4.50,5.00)
Amplitudes (mm)	(1.0,2.0, 4.0, 6.0, 8.0, 10.0)
Current supplies (A)	(0.00, 0.10, 0.20, 0.25, 0.50, 0.75, 1.00)

4. THEORETICAL CONSIDERATION FOR DESIGN OF FABRICATED MR DAMPER

The damper design was done based on the following facts. The mechanical energy required for yielding increases with increase in applied magnetic field intensity which in turn increases yield shear stress. In the presence of magnetic field, the shear stress associated with the flow of MR fluid can be predicted by the Bingham equations. [23]

$$\tau = \eta\dot{\gamma} + \tau_Y(H)$$

$$\tau > \tau_Y \quad \ldots\ldots (1)$$

Here τ is the fluid shear stress, τ_y is the fluid's yield stress at a given magnetic flux density B, η is the plastic viscosity(i.e. viscosity at B=0), and $\dot{\gamma}$ is the fluid shear rate. The above equation is used to design a device which works on the basis of MR fluid.

MR dampers generally use the pressure driven by flow (valve) mode of the fluid. The total pressure drop in the MR Damper is evaluated by summing the pressure drop through viscous component and yield stress component. [16]

 ISSN:2348-4098

$\Delta P = \Delta P_n + \Delta P_Y$

$\Delta P = \frac{12\eta QL}{g^3 w} + \frac{C\tau_Y L}{g}$ ..... (2)

Here ΔP is the total pressure drop, ΔP_η is the viscous pressure loss, ΔP_Y is the field dependent yield stress pressure loss, η is the fluid viscosity, Q is the flow rate, L is the pole length, w is the pole width, g is the fluid gap, and τ_y is the field yield stress.

The design of MR fluid damper is to establish the relation between the damper and the parameters of the structure and magnetic field strength. As the magnetic field is applied, the damping force F by MR fluid can be calculated by [8].

$F_{damper} = P_{reb}(A_{piston} - A_{rod}).P_{com}A_{piston} + frictionSgn(\dot{x})$

$F = \frac{12\eta L\pi r^2}{\pi R h^3} v + \left(\frac{k_0 L\tau_B \pi r^2}{h}\right) sgn(v)$ ..... (3)

Where v is the speed of piston; f is friction of piston and cylinder; K_0 is a coefficient (0.8–1.0); h is the thickness of the annular MR fluid between the piston and outer cylinder. The value of h can be given by

$h = R - r$ ..... (4)

If it is assumed that the value of f is much smaller, Eq. (1) and (2) can be mathematically manipulated to yield

$F = 2\pi\tau_B Lr^2 + \frac{2\pi\eta v Lr^3}{h}$ ..... (5)

Eqn. (3) shows that the damping developed in the cylindrical MR fluid damper can be divided into a magnetic field dependent induced yield stress component F_Y and a viscous component F_η.

The total damping F is the sum of F_B and F_η.

$F_Y = 2\pi\tau_B Lr^2$, $F_\eta = \frac{2\pi\eta v Lr^3}{h}$

ISSN:2348-4098

The active volume of annular MR fluid in the cylindrical MR damper can be obtained through the integration the radius of annular MR fluid as follows.

$V = 2\pi L\int_r^R rdr$ ..... (6)

Therefore, $v = 2\pi rLh$

Here we also find out the electric power consumption of the device is

$J = i^2 R + \beta \frac{L}{R}$ ..... (7)

Where R is resistance, L is inductance, i is current, β is weighting coefficient and J is objective function.

5. MODELING OF FABRICATED MR DAMPER

The Cantilever structure with attached mass is the most widely used configuration for spring mass device. The stiffness of the structure depends on the loading condition, material, and cross-sectional area perpendicular to the direction of vibration. The governing equation of motion for the system shown in Fig. 3 can be obtained from energy balance equation or D'Alembert's principle.

The schematic diagram of the mechanical model proposed in this work is shown in the Fig. 2. In this picture, the variable x means the displacement of damper rod and F is the reaction force of damper rod under θ displacement and$\dot{\theta}$ Velocity, the parameters k and c are respectively the spring stiffness of the accumulator and the damping coefficient of the viscosity.

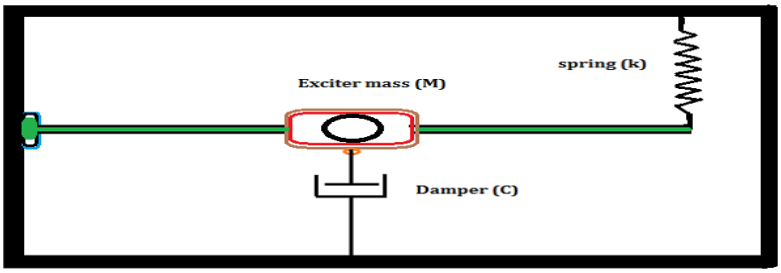

Figure 3: Mechanical model for cantilever beam structure

 ISSN:2348-4098

The governing equation of motion of a lumped spring mass system can be written as:

$I\ddot{\theta} + ca^2\dot{\theta} + kb^2\theta = 0$ ..... (i)

The natural frequency of a spring mass system is defined by

$$\omega_n = \sqrt{\frac{kb^2}{ma^2}} = \frac{b}{a}\sqrt{\frac{k}{m}}$$ ..... (ii)

The stiffness K for each loading condition should be initially calculated. Here for the case of a cantilever beam, the stiffness K is given by $K = 3EI/L^3$, where E is the modulus of elasticity, I is the moment of inertia, and L is the length of beam. The moment of inertia for a rectangular cross-sectional can be obtained from expression, $I = \frac{1}{12}bh^3$, where b and h are the width and thickness of the beam in transverse direction, respectively.

A damping factor ξ, is a dimensionless number defined as the ratio of system damping to critical damping as: We know that the condition of critical damping value of damping factor $\xi = 1$,

$$\omega = \omega_n, \quad c = c_c, \quad = \frac{2b}{a}\sqrt{k\,m}$$ ..... (iii)

5.1 SDOF SYSTEM WITH MR DAMPER

Considering the SDOF system with a MR damper (figure), assume the base of the system undergoes harmonic motion, i.e.

$x_b(t) = X_b \sin \omega t$.

Then the system response can be expressed as

$x_s(t) = X_s \sin(\omega t - \varphi)$.

Here consider the equation of motion of an under damped system is

$x = Xe^{-\xi\omega n.t} \sin(\omega_{d.}t - \phi)$

The displacement transmissibility amplitude Xs/Xb

 ISSN:2348-4098

$$\frac{Xs}{Xb} = \left[\frac{k2 + (c\omega)2}{k - ms\omega 2) 2 + (c\omega)2}\right]^{1/2} = \left[\frac{1+(2\zeta r)2}{(1 - r2)2+(2\zeta r)2}\right]^{1/2}$$

The phase angle φ can be obtained as

$$\varphi = \tan{-1}\left[\frac{2\zeta r3}{1+(4\zeta 2\ -\ 1)r2}\right]$$

6. EXPERIMENTAL SET-UP DETAILS

The experimental set-up consists of (see Figure 4):

1. Vib-lab instrument it's a vibration lab instrument manufacture by ARE Educational Equipment pvt. Ltd. Industrial area miraj Maharashtra, that equipment are used for measure system vibration. It's a vibration measuring device which mesure all type of vibration like free, forced etc.

2. Variable voltmeter it's a control device here i used for control the current supply on MR damper with variable range (0 to 270v)

3. Speed controller it's also a control device used for control the speed of DC motor which are generate vibration on system Range (0-1500 rpm)

4. Exciter (DC motor) is used for generate the vibration on system, manufacturer by patil electric co. pvt. Ltd. Its maximum speed is 1500 rpm and supply of current maximum is 0.7amp range (0 to 0.7amp).

5. Multimeter is used for show the exact value of supply current which give on armature coil for generate the magnetic field inside the MR Damper.

6. MR Damper it's a main component of our experiment all analysis is perform on these mechanical system here I used a prototype of fabricated MR Damper.

7. Recorder it's a mechanical recording device which is record the amplitude vibration of system, speed of strip chart recorder is 33mm/sec.

8. LVDT linear variable differential transducer is a one type of transducer which is measuring linear variable displacement in between the range (0 to 25 mm).

ISSN:2348-4098

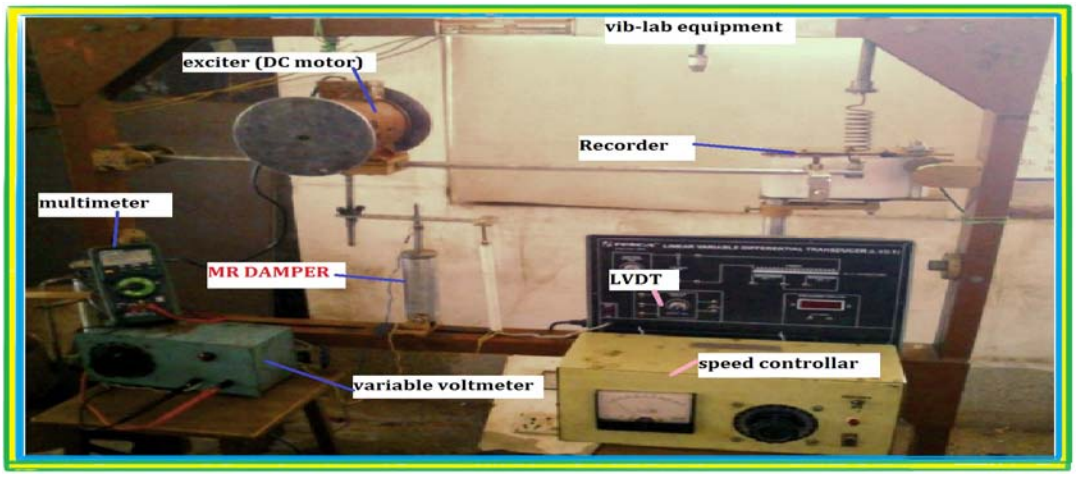

Figure 4: Experimental set up for testing of MR damper

7. RESULT AND DISCUSSION

7.1 EFFECT OF AMPLITUDE OF VIBRATION WITH AND WITHOUT USE OF MR DAMPER AT VARIABLE LENGTH OF EXCITER

Here this graph is show effect of amplitude of vibration with changing the length of exciter with and without use of MR Damper. The variation of amplitude is 0 to 7 mm in this experiment show when the variable length of exciter is varying the amplitude of vibration also vary. At 550 mm length the amplitude of vibration is maximum.

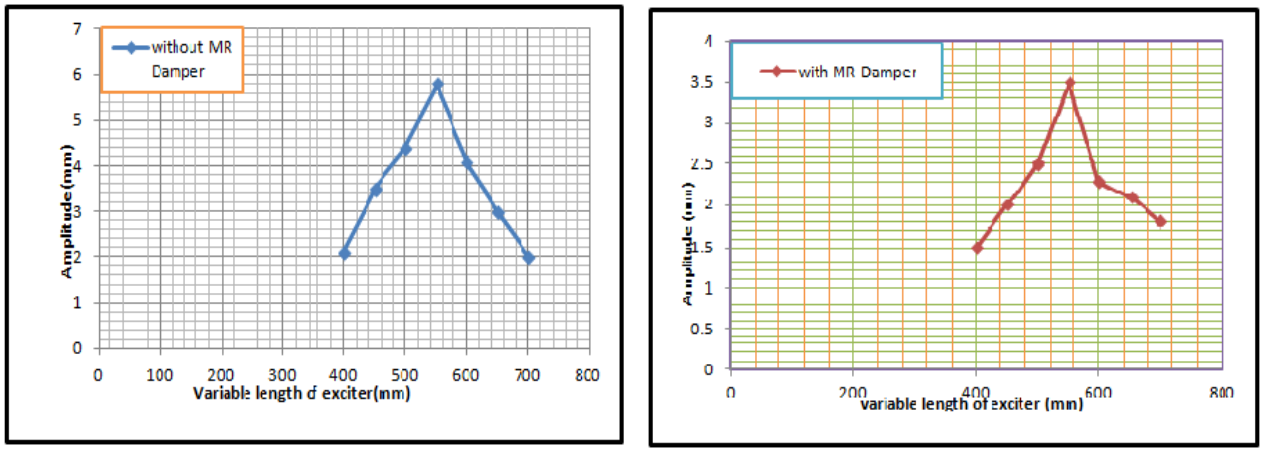

Graph 1: Show the effect of amplitude of vibration with and without use of MR damper at variable length of exciter

ISSN:2348-4098

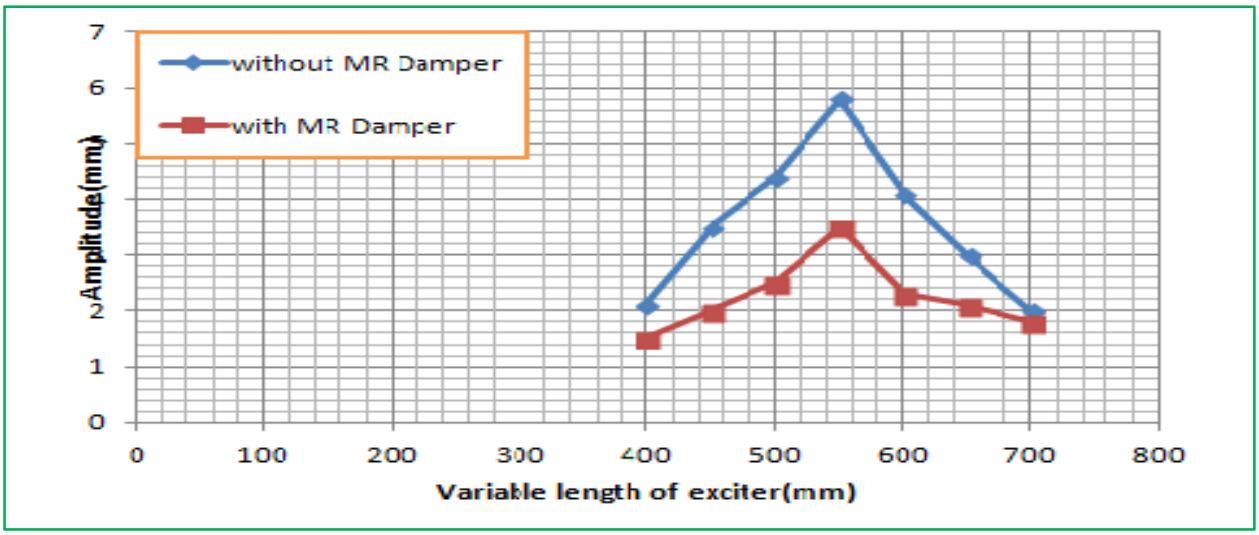

Graph 2: show the combined graph for show the effect of amplitude of vibration with and without use of MR Damper at variable length of exciter

7.2 EFFECT OF MR DAMPER PISTON DISPLECMENT BY VARRING THE SUPPLY CURRENT

This experiments test show the behavior of MR Damper piston displacement when the value of current increase the displacement of piston is decrease. It means current is the main parameter that are affected the behavior of MR Damper. Here the graph plot between the displacement and current at the variable length at the length 500 the graph show the maximum displacement.

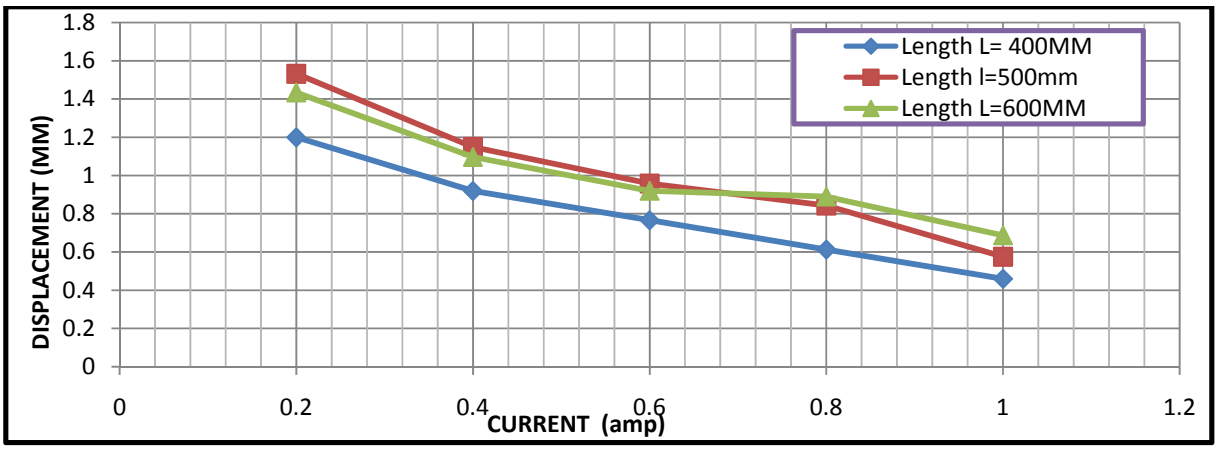

Graph 3: combined graph for show behavior of MR damper piston displacement by varying the supply current

ISSN:2348-4098

7.3 EFFECT OF AMPLITUDE OF VIBRATION ON MR DAMPER BY INCREASING THE PERCENTAGE OF IRON PARTICLE ON MR FLUID

This experiment show the behavior of MR damper by varying the percentage of iron particle here this graph show when the percentage of iron particle increases the amplitude of vibration is gradually decreases. And the(MRF1)is more efficient as campier to (MRF2) because MRF1 magnetic field intensity is high as compare to MRF2.MRF1 type fluid is prepared by mixing of feo, fe_2o_3 iron particle which are separate the magnetic tape. And MRF2 type fluid is prepared by mixing of fe_3o_4 iron particle which is prepared by chemical co precipitation method.

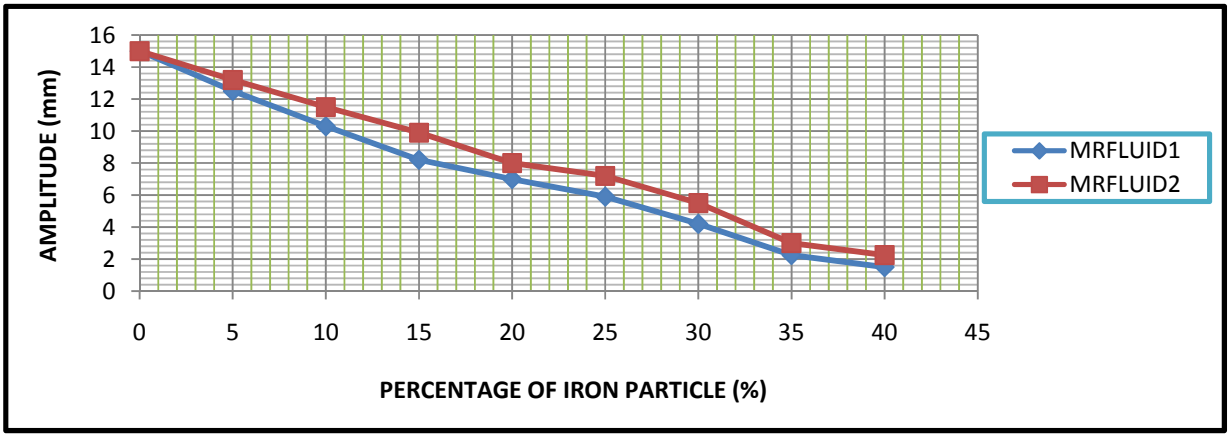

Graph 4: shows the behavior of MR damper by varying the percentage of iron particle

7.4 EFFECT OF FORCE/DISPLACEMENT CHARACTERISTIC OF MR DAMPER

Sine vibration with the frequency of 1Hz, 2Hz, and 3Hz, 4Hz was provided by vib-lab machine, and its vibration amplitude was (1 to 20mm) range. In different conditions, at the range from 0A to 1.0A direct current was inputted to MR damper. Experimental data was collected at intervals of 0.1A and the testing results were showed in graph.5. In our experiments, the MR damper showed obvious initial shear characters. With the increase of current and speed, the damping force was in an increase trend, however, it was not notable with the increase of current after 0.5A; instead a saturated performance was presented.

 ISSN:2348-4098

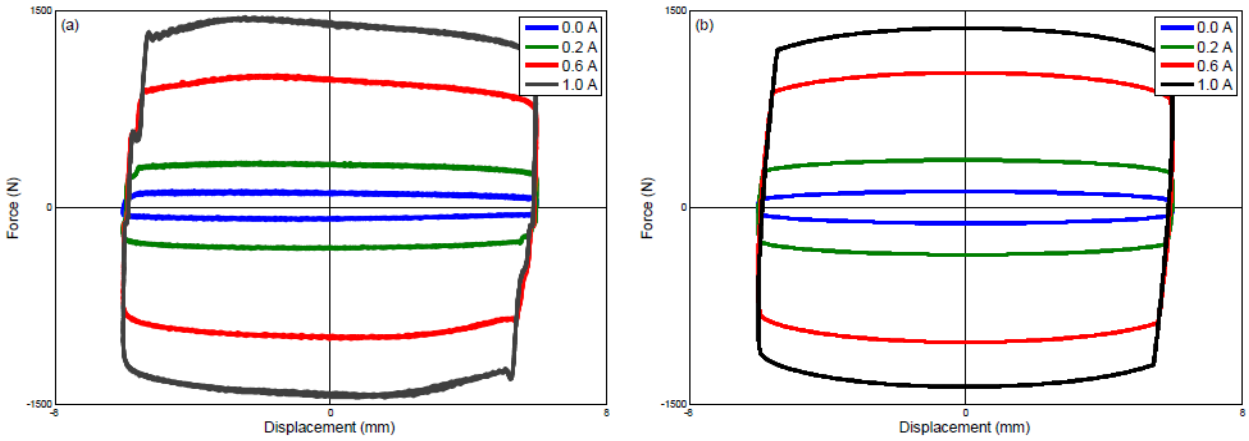

Graph 5: Force/displacement characteristic of MR damper (a) Experimental test (b) Numerical test 6mm, 2Hz sinusoidal excitation

8. CONCLUSION

Magnetorheological (MR) fluid dampers have provided technology that has enabled effective semiactive control in a number of real world applications. Because of their simplicity, low input power, scalability and inherent robustness. The design calculations of the volume, thickness and width of the annular MR fluid within the damper are derived. A mathematical model of the MR fluid damper is adopted. The equivalent damping coefficient of the MR damper in terms of input voltage, displacement amplitude and frequency are investigated. The SDOF isolation system with the MR damper is analyzed by studying its transmissibility. Also, the relative displacement with respect to the base excitation is quantified and compared with that of the without MR damper and with MR damper.

1. It was shown that, by minimizing the objective function, the yield stress force, dynamics range and conductive time constant are significantly improved at any value of applied current. The power consumption of the optimized damper was also significantly reduced.

2. The iron particle (feo, fe_2o_3) is more efficient for reduction of vibration as compare to use of fe3o4 iron particle on making of MR fluid;

3. MR Damper is mainly depended on magnetic flux density.

ISSN:2348-4098

4. AS compare to conventional damper use of MR damper plays an important role in reducing the vibrations because, for every load condition the behavior of MR damper is change positively.

5. Magnetic circuit and structure integrated optimal design of MRF damper was well completed in our work. Multiple structure parameters and magnetic circuit parameters were simultaneously designed at the same time and it was with highly efficiency.

REFERENCES

[1] Nitin Ambhore, Shyamsundar Hivarale, Dr. D. R. Pangavhane. "A Study of Bouc-Wen Model of Magnetorheological Fluid Damper for Vibration Control". (IJERT) ISSN: 2278-0181 Volume 2 Issue 2, February- 2013

[2] Meng-Gang Yang, Chun-Yang Li, Zheng-Qing Chen. "A new simple non-linear hysteretic model for MR damper and verification of seismic response reduction experiment". Engineering Structures 52 (2013) 434–445.

[3] Francesc Pozoa, MauricioZapateiro, LeonardoAcho, Yolanda Vidala, Ningsu Luob. "Experimental study of semi active VSC techniques for vehicle vibration reduction". Journal of the Franklin Institute 350 (2013) 1–18. www.elsevier.com/locate/jfranklin.

[4] M.T. Braz-Cesar, R.C. Barros. "Experimental Behaviour and Numerical Analysis of MR Dampers".15 WCEE LISBOA (2012)

[5] Fengchen Tu, Quan Yang, Caichun He, Lida Wang." Experimental Study and Design on Automobile Suspension Made of Magneto-Rheological Damper" Sciverse science direct Energy Procedia 16 (2011) 417-425. www.sciencedirect.com

[6] S-evki C- es-meci, Tahsin Engin. "Modeling and testing of a field-controllable magnetorheological fluid damper". International Journal of Mechanical Sciences 52 (2010) 1036–1046.

[7] Zekeriya Parlak, TahsinEngin "Time-dependent CFD and quasi-static analysis of magnetorheological fluid dampers with experimental validation". International Journal of Mechanical Sciences 64 (2012) 22–31

[8] Mukund A. Patil, Swapnil Sapkale, Sagar Soni.et al.(2012) "Theoretical and experimental studies on magnetorheological damper with DC input". ISSN 0976 – 6359 (Online) Volume 3, Issue 2, May-August (2012), pp. 610-619 © IAEME:

[9] Hamid Reza Karimi." A Semi-active Vibration Control Design for Suspension Systems with MR Dampers". ISBN: 978-953-307-433-7, (2011)

[10] K.H. Lama, Z.H. Chen, Y.Q. Ni, H.L.W. Chan." A magnetorheological damper capable of force and displacement sensing". ELSEVIER Sensors and Actuators A 158 (2010) 51–59

[11] A.G. Olabi, A. Grunwald "Technical Report on Design and application of magneto-rheological fluid" ELSEVIER Science Direct Materials and Design 28 (2007) 2658–2664.

[12] Andrzej Milecki "Investigation and control of magneto–rheological fluid dampers" PERGAMON International Journal of Machine Tools & Manufacture 41 (2001) 379–391

[13] Jeong-Hoi Koo, Fernando D Goncalves and Mehdi Ahmadian "A comprehensive analysis of the response time of MR dampers" Smart Mater. Struct. 15 (2006) 351–358 doi:10.1088/0964-1726/15/2/015

[14] W H Liao and C Y Lai "Harmonic analysis of a magnetorheological damperfor vibration control" SMART MATERIALS AND STRUCTURES 11 (2002) 288-296. PII: S0964-1726(02)34308-8

[15] Zekeriya Parlak, Tahsin Engin, Ismail Call "Optimal design of MR damper via finite element analyses of fluid dynamic and magnetic field" mechatronics 22(2012)890-903.

[16] Md. Sadak Ali Khan, A. Suresh, N. Seetha Ramaiah "Investigation on the Performance of MR Damper with various Piston configurationsInternational Journal of Scientific and Research Publications, Volume 2, Issue 12, December 2012 ,ISSN 2250-3153

[17] A. Ashfak, K.K Abdul Rasheed, J. Abdul Jaleel " Modeling, Simulation and Experimental validation of Magneto-Rheological Damper" (ICANMEET-2013). "International Conference on Advanced Nanomaterials & Emerging Engineering Technologies, 24' -26, July, 2013.

[18] A. Rodr´ıguez, F. Ikhouane, J. Rodellar, N. Luo "Identification of a magnetorheological damper: Theory and experiments". 17th World Congress The International Federation of Automatic Control Seoul, Korea, July 6-11, 2008.

[19] Weng W. Chooi, S. Olutunde Oyadiji "Design, modelling and testing of magnetorheological (MR) dampers using analytical flow solutions. ELSEVIER science direct Computers and Structures 86 (2008) 473–482.

[20] Mehdi Ahmadian , James A. Norris "Experimental analysis of magnetorheological dampers when subjected to impact and shock loading" ELSEVIER science direct Communications in Nonlinear Science and Numerical Simulation 13 (2008) 1978–1985.

[21] Q H Nguyen, S B Choi and K S Kim "Geometric Optimal Design of MR Damper Considering Damping Force, Control Energy and Time Constant" Journal of Physics: Conference Series 149 (2009) 012076.

[22] S. Kciuk a, R. Turczyn b, M. Kciuk " Experimental and numerical studies of MR damper with prototype magnetorheological fluid**".** JAMME volume 39 issue 1 march 2010.

[23] Md. Sadak Ali Khan, A.Suresh, N.Seetha Ramaiah "Performance evaluation of Magnetic circuit for MR Fluid Damper using F.E.M" AMAE Int. J. on Production and Industrial Engineering, Vol. 4, No. 1, June 2013.

[24] G.Z. Yao, F.F. Yap, G. Chen, W.H. Li, S.H. Yeo "MR damper and its application for semi-active control of vehicle suspension system". Mechatronics 12 (2002) 963–973

[25] Tamizharasi.g, ajit kamath, kaustav sen gupta and umesh. G "Magnetorheological Dampers – An overview". International journal of earth science and engineering ISSN 0974-5904, Volume 05, No. 04 (02) August 2012, P.P. 1068-1072.

[26] E. Świtoński, A. Mężyk, S. Duda, S. Kciuk "Prototype magnetorheological fluid damper for active vibration control system". Journal of Achievements in Materials and Manufacturing Engineering (JAMME) VOLUME 21 ; ISSUE 1 March 2007

[27] K. Hudha, H. Jamaluddin, P.M. Samin and R.A. Rahman "Effects of control techniques and damper constraint on the performance of a semi-active magnetorheological damper" Int. J. Vehicle Autonomous Systems, Vol. 3, Nos. 2/3/4, 2005.

[28] A. Ashfak, A. Saheed, K. K. Abdul Rasheed, and J. Abdul Jaleel "Design, Fabrication and Evaluation of MR Damper" International Journal of Aerospace and Mechanical Engineering 5:1 2011

[29] M. Zapateiro, N. Luo, J. Rodellar, A. Rodríguez "MODELING AND IDENTIFICATION OF HYSTERETIC DYNAMICS OF MR DAMPERS AND APPLICATION TO SEMIACTIVE VIBRATION CONTROL OF SMART STRUCTURES" The 14th World Conference on Earthquake Engineering October 12-17, 2008, Beijing, China

[30] Butz, T.; von Stryk, O." Modelling and Simulation of Electro- and Magnetorheological Fluid Dampers" ZAMM · Z. angew. Math. Mech. 78 (1998) 0, 1–22

ISSN:2348-4098

COMPUTATIONAL CHARACTERIZATION OF POROUS AND MECHANICAL PROPERTIES OF 3D SCAFFOLDS FOR POTENTIAL TISSUE ENGINEERING APPLICATIONS

[1]M. ENAMUL HOQUE, [1]LOK WENG LUM, [2]Y. LENG CHUAN,[3]M. N. M. ANSARI

[1]Department of Mechanical, Materials and Manufacturing Engineering; University of Nottingham Malaysia Campus

[2]Department of Mechanical Engineering, Taylor's University, Lakeside Campus, Malaysia

[3]Department of Mechanical Engineering, Universiti Tenaga Nasional, Malaysia

*Corresponding Author's E-mail: enamul.hoque@nottingham.edu.my

ABSTRACT

In developing 3D tissue engineering (TE) scaffolds via rapid prototyping system, the design parameters such as filament gap, filament diameter and lay down angle which play significant roles in controlling porous and mechanical characteristics can be modulated. This study focuses on developing a computational model to simulate porous and mechanical characteristics of 3D tissue engineering scaffolds. The simulation is performed by manipulating the design inputs and analyzing the influences of change of the parameters on porous and mechanical characteristics of the scaffolds. With a constant filament gap, the increase of filament diameter decreases porosity and thus increases the mechanical properties of the scaffolds. However, with a constant filament diameter, the increase of filament gap increases the porosity and consequently, decreases the scaffolds' mechanical properties. Increasing lay down angle also increases the porosity that also influences the mechanical properties of the scaffolds. The actual mechanical properties of scaffolds are always obtained through physical experiments. The computational model provides predictive insight to the mechanical properties of the scaffold with specific design to be fabricated. Also, by superimposing the graphs of similar porous and mechanical characteristics from the computational model, the desired porous and/or mechanical properties can be obtained to design scaffolds as required. Utilizing the information obtained from the predictive model, the rapid

ISSN:2348-4098

prototyping technique could be employed to develop scaffolds with customized architecture and properties for any particular application.

Keywords: Computational Characterization, Design Parameters, Porous and Mechanical Properties, Tissue Engineering, Scaffold, Rapid Prototyping

1. INTRODUCTION

Tissue Engineering (TE) scaffold serves as a template to facilitate cell adhesion and proliferation providing temporary mechanical support to newly grown tissue, while maintaining a 3D-structure. Tissue engineering aims to produce patient-specific biological substitutes to overcome the limitations of conventional clinical therapies. By transplanting cells onto scaffolds, experimental manipulation at three levels to achieve optimal construct is required. These levels are at the cells, the polymeric scaffolds and the construction method (Marler et al., 1998; Leong et al., 2003).

With the technological advancements, there is a paradigm shift of interest from conventional scaffold fabrication techniques to RP techniques. It is difficult to produce scaffolds with great accuracy and reproducibility using conventional fabrication techniques. Scaffolds produced by conventional techniques such as fiber bonding, phase separation and solvent casting, tend to possess random and disordered micro-architectures and lack of mechanical strength (Bergman and West, 2008). Besides, the conventional techniques are associated with shape limitations as they have to be fabricated using molds and also being inconsistent and inflexible, rendering reproducibility of similar scaffolds extremely difficult (Bergman and West, 2008). The architecture, mechanical and porous characteristics of scaffolds produced by conventional techniques are often very difficult to predict and model.

Rapid prototyping (RP) is an automated process that can develop 3D scaffolds by sequential delivery of energy and/or material to points on the plane (Chua et al, 2003). There is no need for any tooling or skilled craft model makers. An initial computer-aided design (CAD) model is input into a computer system. The model is then virtually sliced into multiple layers to lay out the fabrication work path by an RP software and lastly the designed model is fabricated in an additive manner layer by layer from the bottom (Wang et al., 2010; Almeida and Bártolo, 2010).

ISSN:2348-4098

Precise parameters can be set up for advanced RP techniques, while the accuracy can be monitored by a computer program. As such, the growth rate of cells that are seeded in vitro or in vivo, and degradation of the scaffolds can be predicted more accurately. This is because the parameters of the scaffolds produced by RP techniques can be precisely quantified compared to scaffolds produce by conventional techniques. RP system is highly beneficial as it provides control over selecting the optimal scaffold design for optimal cell growth, while maintaining structural integrity upon application.

There are number of RP techniques that are widely used for commercial and research purposes such as stereolithography (SLA), fused deposition modeling (FDM), laminated object manufacturing (LOM) and many others. However, the growth of science in the RP field has led to the development of more contemporary techniques. These techniques include multi-nozzle deposition manufacturing (MDM), robocasting, pressure-assisted microsyringe etc. which are innovative improvements from its predeceasing technologies (Almeida and Bártolo, 2010).

Predictive computational models are used to bridge gaps between the supply and demand of the scaffold design. In order to develop an optimal scaffold for a particular application, the scaffold has to possess appropriate mechanical and porous characteristics. Computational models provide quick means to obtain and cross reference the scaffold design output data with specific porous and mechanical requirements for a particular TE application.

In essence, with an appropriate incorporation of computational model and RP technology, tailored scaffolds could be developed. This would provide innovative solutions to real life problems allowing customization of treatment to patients suffering from diseased or damaged organs. As such, this study mainly focuses on the development of computational models to assist building scaffolds using extrusion-based rapid prototyping technique.

2. MATHEMATICAL MODELS FOR SCAFFOLD CHARACTERISTICS

2.1 POROUS AND MECHANICAL CHARACTERISTICS

2.1.1 POROSITY

Scaffold porosity can be defined as empty space, which is argued to influence the mechanical strength and permeability of scaffolds. It is usually measured in a form of fraction or percentage. Armillotta and Pelzer (2007) define porosity as the ratio of scaffold voids to its total volume as stated below:

$$P = 1 - \frac{V_{solid}}{V_{cubic}} \quad (1)$$

Where,

P = Porosity

V_{solid} = Volume of solid in scaffold

V_{cubic} = Gross volume of a scaffold cube

This mathematical formula (in terms of volume) is too generic to be considered in CAD data to hold proper control over the overall scaffold fabrication. It can be better illustrated in terms of unit cells within the scaffold. Depending on the scaffold volume, the number of cells within a scaffold is determined by the filament gap and filament diameter which when combined, controls the volume. Thus by decomposing the formula in terms of filament gap and filament diameter, a quadratic regression model (Montgomery, 1996) was derived empirically through experiments by (Ang et al., 2006) to further relate the scaffold's porosity to the filament diameter and filament gap.

$$P = 54.1 + 66.5F_{gap} - 58.9F_{diameter} - 20.2F_{gap}^2 + 23.3F_{diameter}^2 - 13.1F_{gap}F_{diameter} \quad (2)$$

Where,

F_{gap} = Filament Gap

$F_{diameter}$ = Filament Diameter

This model defines the filament gap as the centre to centre distance between adjacent filaments. Upon analysis using the pore size theory modelled by Naing et al. (2005) the filament gap creates voids that can essentially be modelled to the pore size for greater mathematical flexibility. The pore diameter is assumed to be equivalent to the largest circle that can be manifested within the geometry of a cubic or triangular pore. Combining both theories, Ang and co-researcher's (2006) model can possibly be more

 ISSN:2348-4098

accurate by substituting the filament gap with the actual scaffolds' pore size. Therefore, the regression model replaces the filament gap with pore diameter, P_{gap} as shown in the modified regression model below:

$$P = 54.1 + 66.5P_{gap} - 58.9F_{diameter} - 20.2P_{gap}^2 + 23.3F_{diameter}^2 - 13.1P_{gap}F_{diameter} \quad (3)$$

Where,

P_{gap}= Pore Diameter

2.1.2 YOUNG'S MODULUS

The Young's modulus, E also known as modulus of elasticity or elastic modulus is a measure of rate of change of stress over strain (Hutchings, 1996) that can be stated as:

$$E = \frac{\text{tensile strength}}{\text{tensile strain}} = \frac{\sigma}{\varepsilon} \quad (4)$$

The Young's modulus for a scaffold however, can be modelled by assuming the scaffold to take a cubic or isotropic form (Hollister, 2005; Hollister and Lin, 2007).

For a cubic scaffold with a base material, Ecubic, upper can be modelled as:

$$E_{cubic,upper} = \frac{2E\rho(2-v)}{\rho(3v^2+v-2)-3v^2-3v+6} \quad (5)$$

On the other hand, for a general isotropic scaffold, Eisotropic, upper can be modelled as:

$$E_{isotropic,upper} = \frac{2E\rho(7-5v)}{\rho(3v^2+v-2)-3v^2-3v+6} \quad (6)$$

Where,

Ecubic, upper = Young's Modulus for Cubic Scaffold

Eisotropic, upper = Young's Modulus for Isotropic Scaffold

ρ = Volume fraction of Solid Material

v = Poisson's Ratio

 ISSN:2348-4098

The equations essentially take into consideration the material's bulk properties which would affect the mechanical characteristics of the scaffold. The mathematical model selected to better represent a wider variation of scaffold design is presented in Eq. (6).

2.1.3 YIELD STRENGTH

Yield strength is defined as the stress at which a material or structure begins to deform plastically. It is typically the stress at the yield point of which often occurs with a plastic strain of 0.2%. Ang et al. (2006) have carried out experiments to determine the relationship between the scaffold design and its mechanical properties. The analysis strongly suggests that the porosity directly influences the yield strength of the scaffold and is modelled as:

$$\sigma_c = -25.8 \ln P + 116.9 \quad (7)$$

Where,

σ_c = Yield Strength

Eq. (7) is used to model yield strength as it uses the modified porosity model shown in Eq. (3), which is now able to establish data for a wider range of scaffold designs. Eq. (7) also simplifies the correlation between design inputs and the yield strength of the scaffold that is only to be affected by porosity.

2.2 ASSUMPTIONS FOR THE COMPUTATIONAL MODEL

2.2.1 SCAFFOLD ASSUMPTIONS

Several assumptions are made while modeling the scaffold's properties based on its mechanical characteristics. The assumptions for the layout of the scaffold's design parameters are shown in Fig. 1a. As the mathematical models are formulated under ideal circumstances, the parameters should also match ideal conditions as closely as possible.

Firstly, the extruded filament diameter is assumed to have square cross-section. This is to maximize the contact area between the interlayer filaments. As can be seen from Fig. 1b, a filament diameter with a circular cross-section will have least contact area among the layers. This induces high stress at the contact points between the filaments. Hence, the filaments are modelled with a square cross section to maximize the contact area

 ISSN:2348-4098

between the interlayer filaments. As such, ideally there will be no stress concentration effect in the system.

2.3. UNIT CELL CHARACTERIZATION

Fig. 1a also illustrates that the filaments are laid exactly over each other so that the junction behaves as a load bearing column under compression. As a result, the stress applied onto the scaffold can be supported by the "columns" and consequently be redistributed into the scaffold structure.

2.3.1 0°/90° LAY DOWN PATTERN

A typical scaffold with a 0°/90° lay down pattern can be seen in Fig. 2a. Unit cell models were generated using Pro/Engineer as illustrated in Fig. 2b-2c. The scaffold with a 0°/90° lay down pattern is modelled as an ideal cube as shown in Fig. 2b. On top of that, Fig. 2c represents the solid entities contained in a single unit cell volume, which is used to determine the solid volume in the scaffold.

2.3.2 0°< Θ < 90° LAY DOWN PATTERN

A typical scaffold with a 0°< θ <90° lay down pattern can be seen in Fig. 3a. The triangular unit cell models were also generated (Fig. 3) using Pro/Engineer and the scaffold with triangular pore architecture is modelled to represent a triangular column based on previous assumptions. Fig. 3c represents the solid entities contained in a single unit cell of a scaffold with triangular pore architecture. This is used to determine the solid volume of the scaffold.

2.4 COMPUTER MODEL FLOW CHART

The computer model flow chart is presented in Fig. 4. Initially the lay down angle is input along with other design parameters of the scaffold (filament gap, filament diameter, scaffold dimensions, material properties). Depending on the lay down angle input, either the cubic or triangular equation path will be activated, providing the necessary details and predictive results for the selected scaffold design. Finally, it will be prompted to further continue running the simulation before going through the whole process again or ending the simulation process.

2.5 COMPUTATIONAL SIMULATION METHODOLOGY

ISSN:2348-4098

To better identify the design constraints and trends based on manipulation of the filament gap, filament diameter and lay down angle, the material properties are assumed to be fixed. Hypothetical data of material properties are used to analyze the mechanical and porous characteristics of the scaffold in detail. The scaffold is modelled considering the width, length and height of 5 cm each, while the hypothetical Young's modulus and Poisson ratio of the material were assumed to be 2 GPa and 0.4, respectively.

The filament gap is first kept constant, while slowly increasing the filament diameter from 0.1 – 0.5 mm with 0.1 mm increment. It produces the data (graph) that investigates the influence of filament diameter on the porous and mechanical characteristics. Likewise, the filament gap is increased with similar values, while keeping the filament diameter constant to investigate the influence of filament gap on the porous and mechanical characteristics. These graphs can then be superimposed to obtain a logical solution for designing a scaffold with required porous and mechanical characteristics.

3. COMPUTATIONAL RESULTS AND DISCUSSIONS

3.1 POROUS CHARACTERISTICS

The influences of user-defined design parameters namely, filament diameter, filament gap and lay down angle are studied to modulate the scaffold characteristics for various applications as required. It is observed that the variations of these parameters induce the scaffold's porous characteristics as demonstrated by Fig. 5 and 6. By keeping the filament gap constant and increasing the filament diameter, the porosity is found to decrease as shown in Fig. 5. Likewise, the increase of filament gap, while the filament diameter is kept constant results in increase of porosity as presented in Fig. 6. This is because of the fact that when the filaments are laid further from each other the bulk scaffold contains less deposited solid material, which makes more empty spaces in the scaffold resulting in higher porosity. On the other hand, when the filaments are laid closely there results in an increased deposition of solid material and thus accordingly, decreases the pore volume (Moroni et al., 2006; Sun et al., 2005; Hutmacher et al., 2004). The change of lay down angle also influences the scaffold's porous characteristic. For example, an increase of lay down angle from 30° to 60° increases the porosity by

ISSN:2348-4098

about 0.8-1% while the filament diameter varies and filament gap remains constant as demonstrated in Fig. 5. However, the porosity increases by approximately 15% when the lay down angle increases from 30° to 90° with the same conditions of filament diameter and gap. Similarly, the increase of lay down angle from 30° to 60° increases the porosity by about 1.4-2.2% while the filament diameter remains constant and filament gap varies as demonstrated in Fig. 6. However, the porosity increases by approximately 20% when the lay down angle increases from 30° to 90° with the same conditions of filament diameter and gap. Interestingly, in Fig. 6, as the filament gap decreases towards zero the porosity curves tend to converge to a single point. This indicates that with zero filament gaps all the scaffolds will produce zero porosity irrespective of lay down angle. In Fig. 5 & 6, it is shown that the porosity changes significantly with the change of filament diameter and filament gap. Besides, different RP techniques have different levels of accuracy that might affect the scaffold characteristics as well. Therefore, there has to be stringent control over the filament diameter, filament gap, lay down angle and the manufacturing accuracy while designing a scaffold to obtain desired characteristics.

3.2 MECHANICAL CHARACTERISTICS

The influences of filament diameter, filament gap and lay down angle on the mechanical characteristics of the scaffolds are thoroughly investigated. The mechanical characteristics (Young's modulus and yield strength) of the scaffolds with varying filament diameter, filament gap and lay down angle are presented in Fig. 7 - 10. The scaffold porosity decreases with the increase of filament diameter while the filament gap remains constant. The decrease in porosity increases the scaffold's mechanical properties (Young's modulus & yield strength) as observed in Fig. 7 and 8. On the other hand, the scaffold porosity increases with the increase of filament gap while the filament diameter remains constant. The increase in porosity decreases the scaffold's mechanical properties (Young's modulus & yield strength) as observed in Fig. 9 and 10. The increase of lay down angle also increases the porosity of the scaffold and accordingly, decreases the mechanical properties as shown in Fig. 7 – 10. Therefore, with a constant filament diameter, the scaffold with smallest filament gap is found to be the stiffest and that with largest filament gap is found to be the weakest. This variation in mechanical properties due to change of filament gap can be attributed to the fact that

ISSN:2348-4098

the filament junctions mainly resist the deformation when the scaffold is compressed. Under compression, these junctions behave like columns. The scaffold with the smallest filament gap has maximum number of columns (i.e. junctions) in a given sample dimension that resist the deformation most and thus, the scaffold becomes stiffest. On the contrary, the scaffold with the largest filament gap has minimum number of columns in the same given sample dimension that resist the deformation least, rendering the scaffold weakest. Similar findings are reported in the experimental study performed by Moroni et al. (2006), which states that the dynamic stiffness and equilibrium modulus increase with decrease of fiber spacing. The observed trends are directly related to the scaffold porosity. The increase of filament diameter results in increase of solid material in the scaffold structure and accordingly, decreases the porosity and hence increases the mechanical strength (Young's modulus and yield strength) as shown in Fig. 7 and 8.

Results indicate that a customized scaffold can be designed through appropriate combination of the user-defined parameters such as filament diameter, filament gap and lay down angle for tailored tissue engineering application.

4. DEVELOPMENT OF SCAFFOLD

A systematic process can be generated to develop scaffolds by using similar characteristic graphs that can be superimposed. It can be used as a tool, like the steam table where the mechanical or porous outputs can be cross referenced and checked with design inputs and requirements to verify whether it meets the design specifications. However, the limitation of the mathematical model presented in this study is that it is only designed for the scaffolds with filament junctions that act as vertical columns perpendicular to the scaffold layers. As such, it is rigid and is only able to provide results for the fundamental designs of a scaffold. A more integrated and comprehensive algorithm has to be developed in order to obtain results from scaffolds with the basic cubic or prism unit cell designs. This computational model is designed for scaffolds with an ideal and distinct shape. Practically, the fabrication techniques are not always able to produce scaffolds with ideal resolutions due to its accuracy limitations. Thus, there might be disparities between the predicted and actual results of the scaffolds' mechanical and porous characteristics. Future study is aimed to examine the

ISSN:2348-4098

disparity between predicted and actual results of the scaffolds' mechanical and porous characteristics utilizing some available RP technologies. Also, a more comprehensive algorithm could be designed to further improve the range and dimensions of scaffold characteristic predictions.

With more detailed study (theoretical and experimental) and compilation of data, an effective scaffold library could be developed that would have an extensive database on the relationship among the scaffold materials, structures and properties. This would be an effective tool for the tissue engineers to design scaffolds for tailored tissue engineering applications. A scaffold library will allow users to easily select a scaffold's fundamental geometry and architecture as a point of reference and further modify its parameters to satisfy the requirements for a final biomedical application (Chua et al., 2003).

5. CONCLUSIONS

Based on the computational analyses, the manipulation of design parameters (filament gap, filament diameter and lay down angle) has significant influence on the porous and mechanical characteristics of the scaffold. The manipulation of filament gap has a higher order of control over the porous and mechanical characteristics of the scaffold as compared to filament diameter and lay down angle. Incorporating the data obtained from this predictive model into a suitable rapid prototyping technique, a patient-specific scaffold could be developed with customized structure and properties to satisfy wider tissue engineering applications.

ACKNOWLEDGEMENTS

The authors would like to thank the Faculty of Engineering, University of Nottingham Malaysia Campus for providing the fund to carry out this research.

REFERENCES

Almeida HdA, Bártolo PJ. Virtual topological optimisation of scaffolds for rapid prototyping. Medical Engineering & Physics, 2010, 32, 775-82.

Ang KC, Leong KF, Chua CK, Chandrasekaran M. Investigation of the Mechanical Properties and Porosity Relationships in Fused Deposition Modelling-Fabricated Porous Structure. Rapid Prototyping Journal, 2006, 12, 100 - 5.

Armillotta A, Pelzer R. Modelling of Porous Structures for Rapid Prototyping of Tissue Engineering Scaffolds. London: Springer-Verlag, 2007.

Bergman NM, West JL. Histogenesis in Three-Dimensional Scaffolds. Principles of Regenerative Medicine. San Diego: Academic Press; 2008, 686-703.

Chua CK, Leong KF, Cheah CM, Chua SW. Development of a Tissue Engineering Scaffold Structure Library for Rapid Prototyping. Part 1: Investigation and Classification. The International Journal of Advanced Manufacturing Technology, 2003, 21, 291-301.

Hollister SJ, Lin CY. Computational Design of Tissue Engineering Scaffolds. Computational Methods in Applied Mechanics and Engineering, 2007, 196, 2991-8.

Hollister SJ. Porous Scaffold Design for Tissue Engineering. Nature Materials, 2005, 4, 518-24.

Hutchings R. Physics. London: Nelson International Edition, 1996.

Hutmacher DW, Sittinger M, Risbud MV. Scaffold-based Tissue Engineering: Rationale for Computer-Aided Design and Solid Free-Form Fabrication Systems. Trends in Biotechnology, 2004, 22, 354-62.

Leong KF, Cheah CM, Chua CK. Solid Freeform Fabrication of Three-Dimensional Scaffolds for Engineering Replacement Tissues and Organs, Biomaterials, 2003, 24, 2363-78.

Marler JJ, Upton J, Langer R, Vacanti JP. Transplantation of Cells in Matrices for Tissue Regeneration. Advanced Drug Delivery Reviews, 1998, 33, 165-82.

Montgomery DC. Design and Analysis of Experiments. 4th Edition ed. New York: Wiley, 1996.

Moroni L., Wijn J. R. and Blitterswijk Van. 3D fiber-deposited scaffolds for tissue engineering: Influence of pores geometry and architecture on dynamic mechanical properties. Biomaterials, 2006, 27, 974-785.

Niang MW, Chua CK, Leong KF, Wang Y. Fabrication of Customised Scaffolds Using Computer-Aided Design and Rapid Prototyping Techniques. Rapid Prototyping Journal, 2005, 11, 249-59.

Sun W, Starly B, Nam J, Darling A. Bio-CAD Modelling and its Applications in Computer-Aided Tissue Engineering. Computer-Aided Design & Applications, 2005, 37, 1097-114.

Wang C-S, Wang W-HA, Lin M-C. STL rapid prototyping bio-CAD model for CT medical image segmentation. Computers in Industry, 2010, 61, 187-97.

ISSN:2348-4098

FIGURE CAPTIONS

Figure 1. a) Cross sectional view of ideal scaffold layout; b) Filament cross section variation & c) Plan view of scaffold lay down pattern angle (Moroni et al., 2006)

Figure 2. a) Microscopic image of a scaffold with internal architecture of a 0°/90° lay down pattern (Chua et al., 2003), b) Unit cell interpretation 0°/90° unit cell model, c) solid entities contained in a single unit cell volume

Figure 3. a) Microscopic image of a scaffold with a triangular internal architecture (Sun et al., 2005), b) Triangular unit cell interpretation triangle unit cell model, c) solid entities contained in a single unit cell volume

Figure 4. Flow chart dictating the process flow of the computer model used

Figure 5. Influence of change in filament diameter on porosity while the filament gap remains constant at 0.2 mm.

Figure 6. Influence of change in filament gap on porosity while the filament diameter remains constant at 0.2 mm.

Figure 7. Influence of change in filament diameter on Young's modulus while the filament gap remains constant at 0.2 mm.

Figure 8. Influence of change in filament diameter on yield strength while the filament gap remains constant at 0.2 mm.

Figure 9. Influence of change in filament gap on Young's modulus while the filament diameter remains constant at 0.2 mm.

Figure 10. Influence of change in filament gap on yield strength while the filament diameter remains constant at 0.2 mm.

ISSN:2348-4098

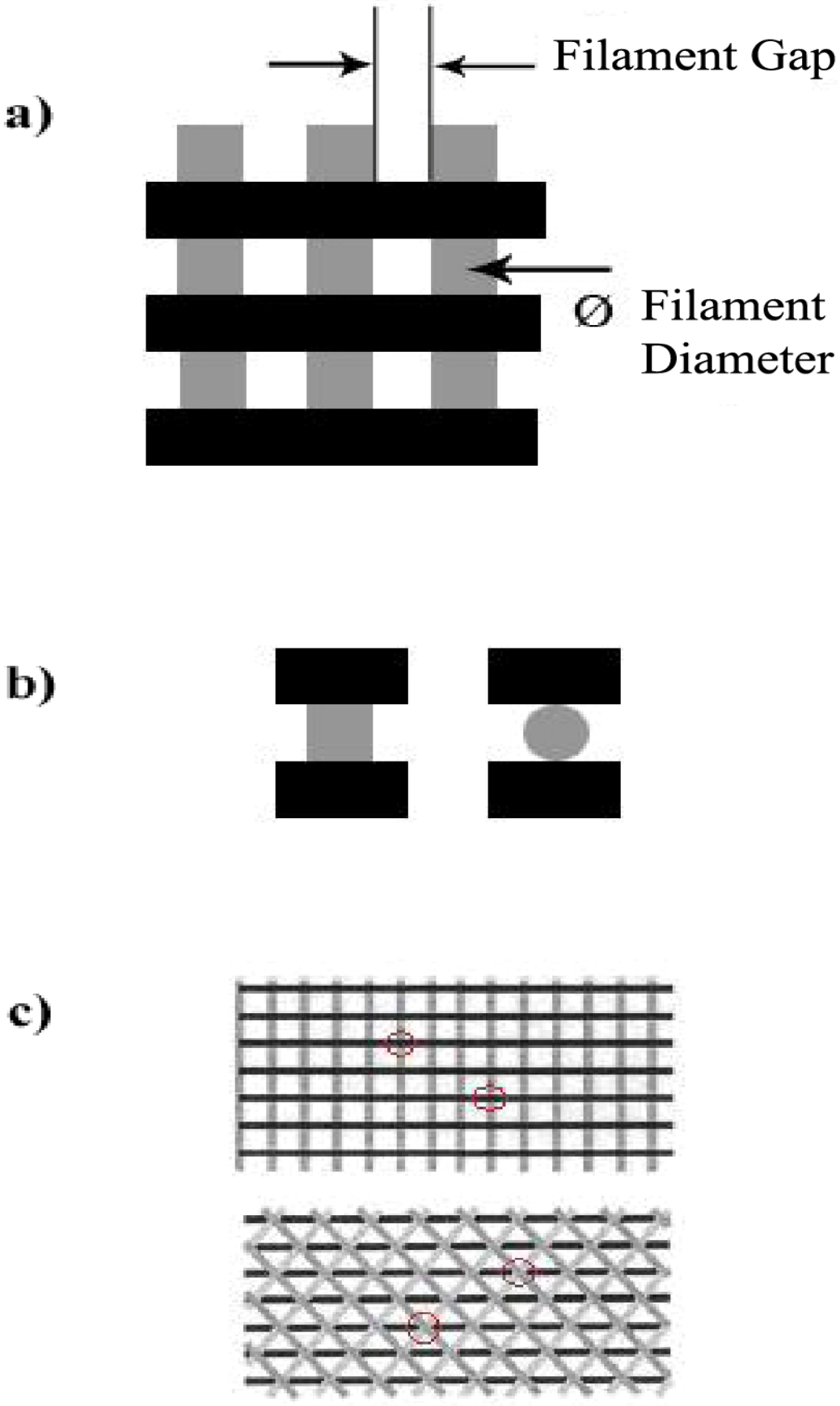

Figure 1

ISSN:2348-4098

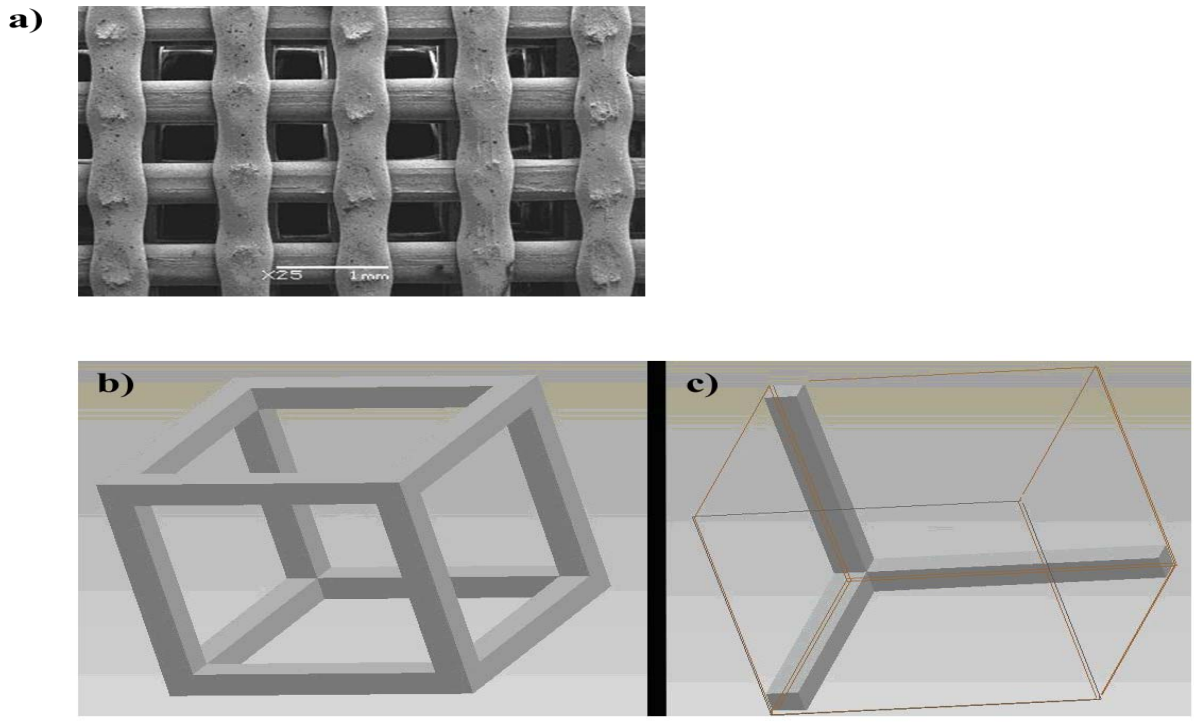

Figure 2

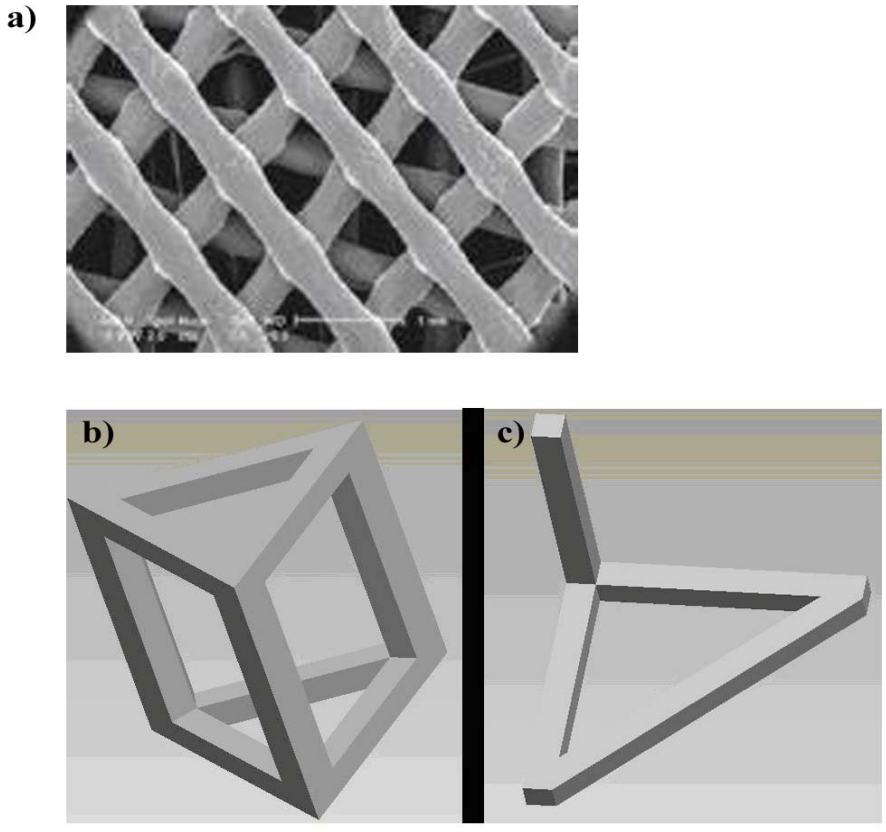

Figure 3

ISSN:2348-4098

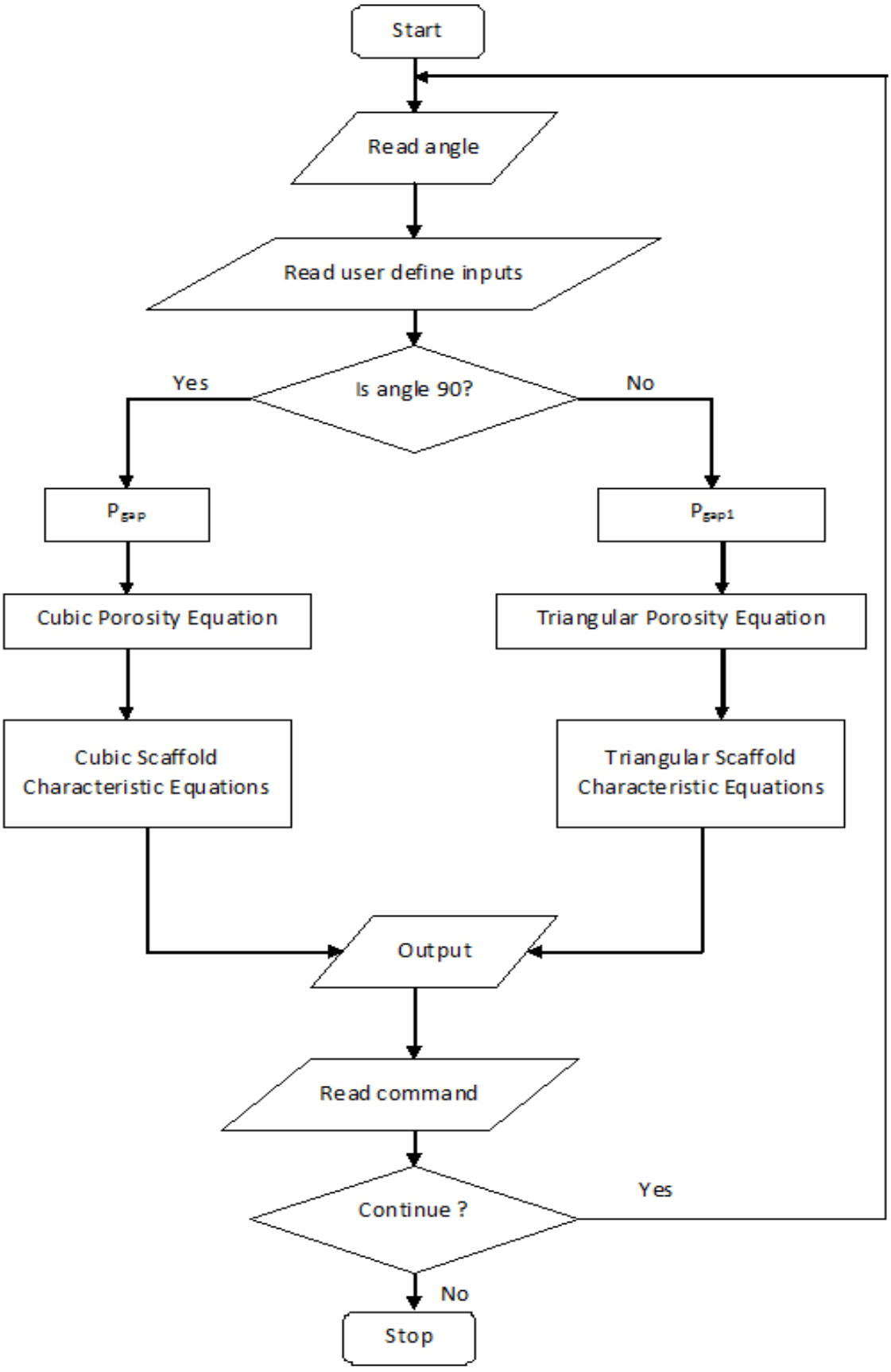

Figure 4

ISSN:2348-4098

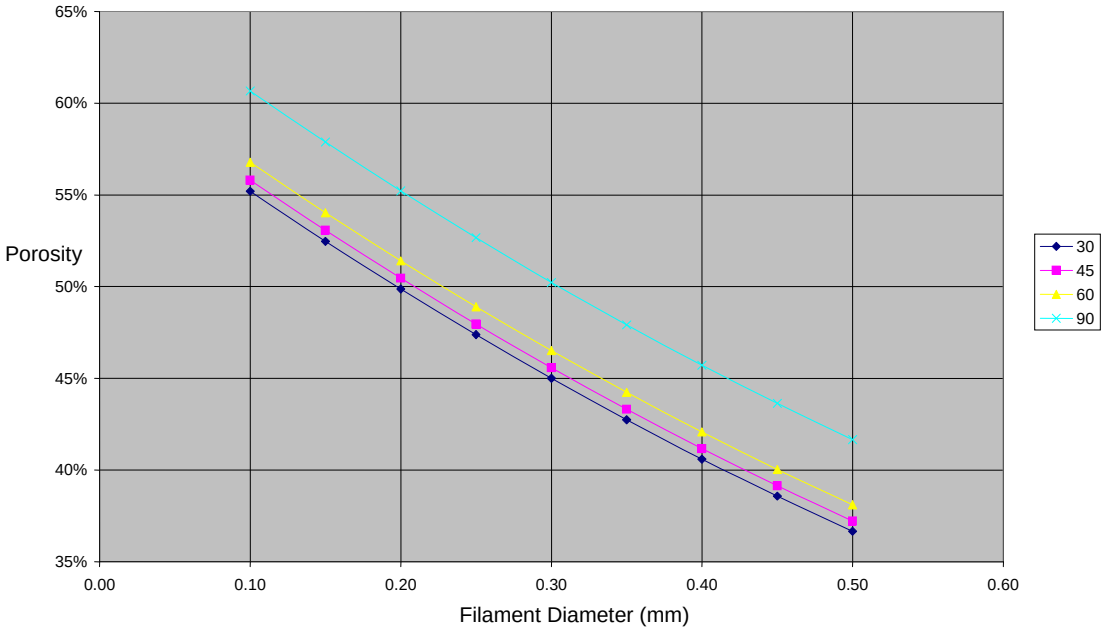

Figure 5

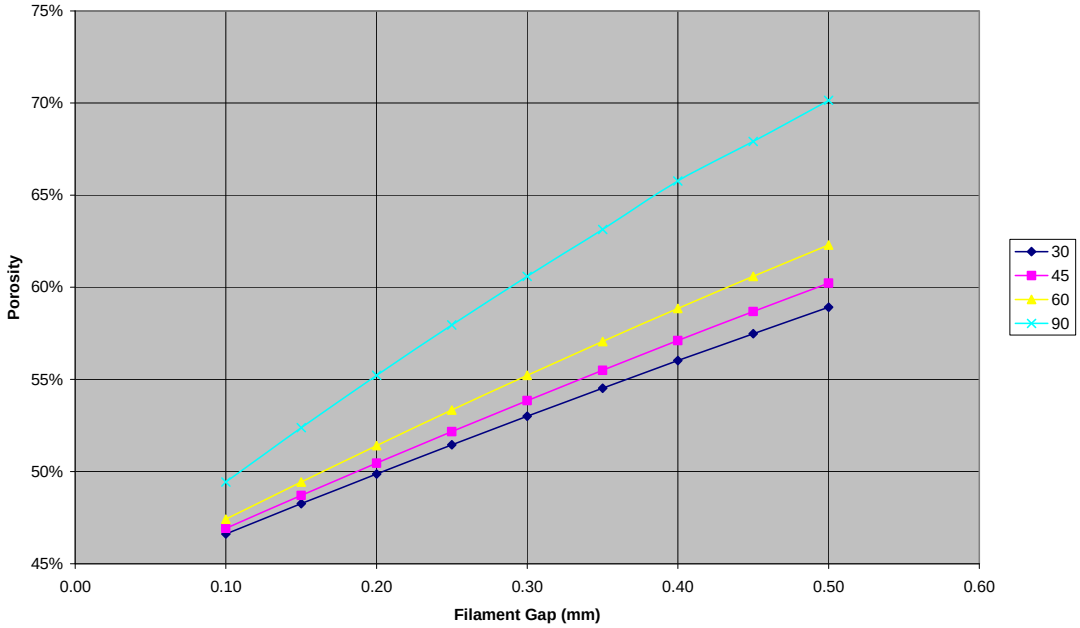

Figure 6

ISSN:2348-4098

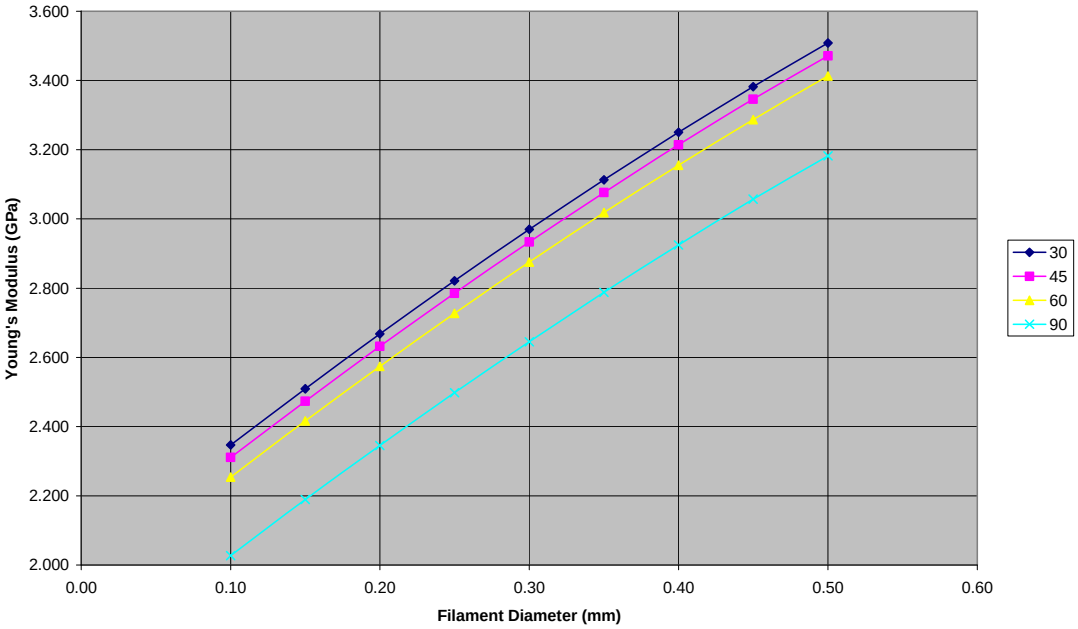

Figure 7

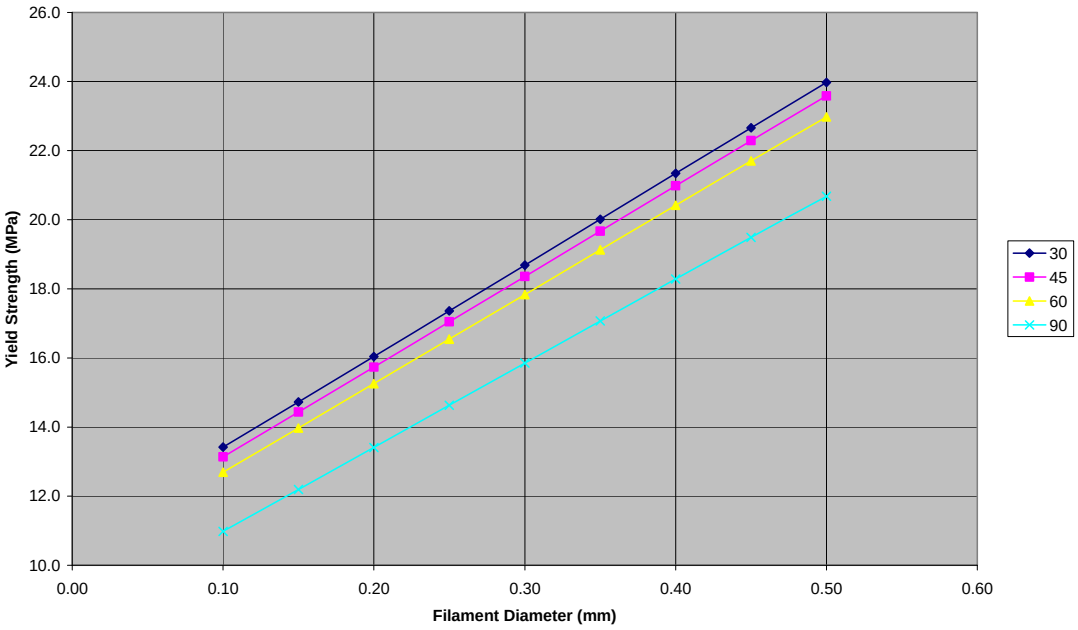

Figure 8

ISSN:2348-4098

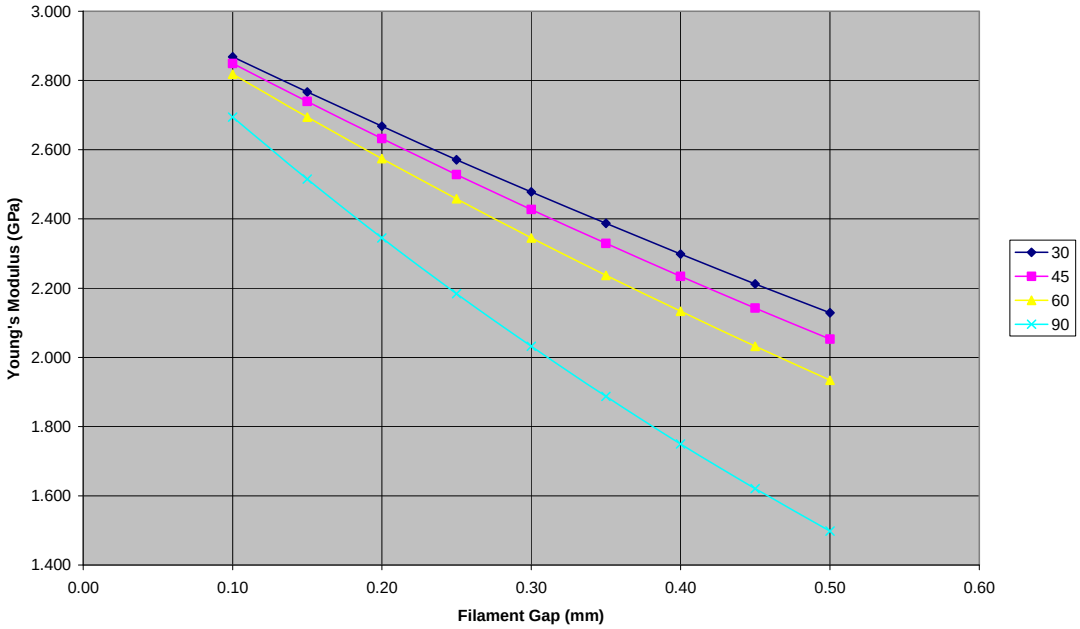

Figure 9

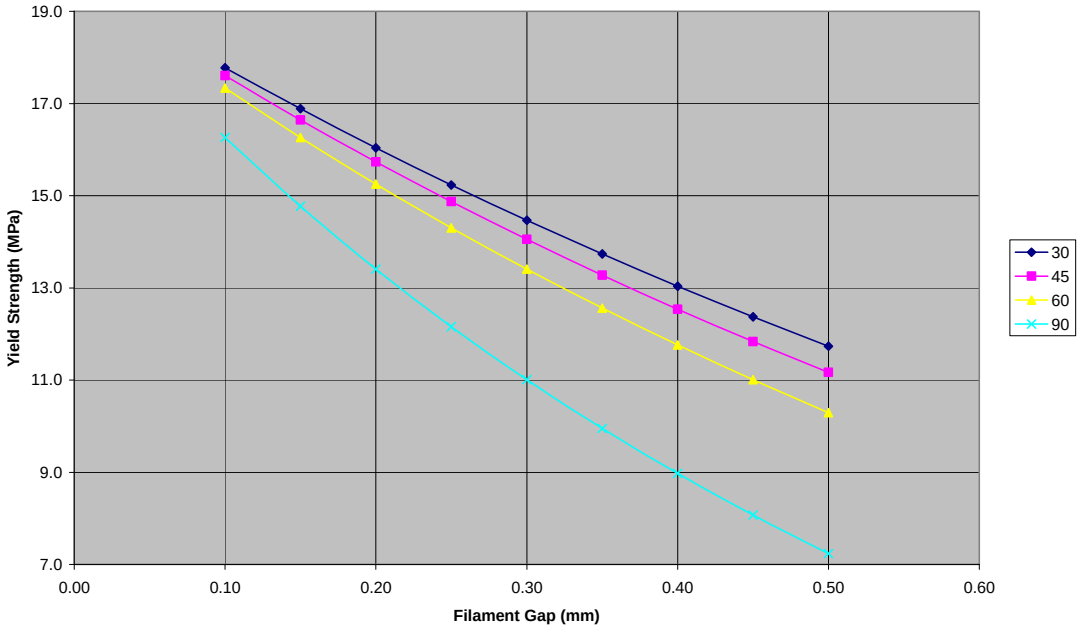

Figure 10

ISSN:2348-4098

EFFICIENT USER REVOCATION AND MULTIOWNER DATASHARING SCHEME FOR CLOUD BASED DYNAMIC GROUPS

G. L. SARANYA
M.E. SCHOLAR
DEPT OF COMPUTER SCIENCE, ARASU ENGINEERING COLLEGE, KUMBAKONAM
Email: sweetsarancse@gmail.com

ABSTRACT

Cloud computing provides an economical and efficient solution for sharing group resource among cloud users. Unfortunately, sharing data in a multi-owner manner while preserving data and identity privacy from an untrusted cloud is still a challenging issue. In this paper, we propose a secure multi- owner data sharing scheme, named Mona, for dynamic groups in the cloud. By leveraging group signature and dynamic broadcast encryption techniques, any cloud user can anonymously share data with others. Meanwhile, the storage overhead and encryption computation cost of our scheme are independent with the number of revoked users.Groupsignature will provide security to cloud users.We are providing blocked list,, revoked list to the cloud. In addition, we analyze the security of our scheme with rigorous proofs, and demonstrate the efficiency of our scheme in experiments.

KEYWORDS- *Cloud computing, data sharing, privacy-preserving, access control, Group Signature, dynamic groups.*

1. INTRODUCTION

CLOUD computing is recognized as an alternative to traditional information technology [1] due to its intrinsic resource-sharing and low-maintenance characteristics.In cloud computing, the cloud service providers (CSPs), such as Amazon, are able to deliver various services to cloud users with the help of powerful datacenters. By migrating the local data management systems into cloud servers, users can enjoy high-quality services and save significant investments on their local infrastructures. One of the most fundamental services offered by cloud providers is data storage

ISSN:2348-4098

.First, identity privacy is one of the most significant obstacles for the wide deployment of cloud computing.Without the guarantee of identity privacy. Compared with the single-owner manner [3], where only the group manager can store and modify data in the cloud, the multiple-owner manner is more flexible in practical applications. More concretely, each user in the group is able to not only read data, but also modify his/her part of data in the entire data file shared by the company. Last but not least, groups are normally dynamic in practice, e.g., new staff participation and current employee revocation in a company. The changes membership makes secure data sharing extremely difficult. On one hand, the anonymous system challenges new granted users to learn the content of data files stored before their participation, because it is impossible for new granted users to contact with anonymous data owners, and obtain the corresponding decryption keys. On the other hand, an efficient membership revocation mechanism without updating the secret keys of the remaining users is also desired to minimize the complexity of key management. However, the complexities of user participation and revocation in these schemes are linearly increasing with the number of data owners and the number of revoked users, respectively. By setting a group with a single attribute, Lu etal. [7] proposed a secure provenance scheme based on the ciphertext-policy attribute-based encryption technique [8], which allows any member in a group to share data with others.

1.1 OUR CONTRIBUTIONS

To solve the challenges presented above, we propose Mona, a secure multi-owner datasharing scheme for dynamic groups in the cloud. The main contributions of this paper include:

1. We propose a secure multi-owner data sharing scheme. It implies that any user in the group can securely share data with others by the untrustedcloud.

2. Our proposed scheme is able to support dynamic groups efficiently. Specifically, new granted users can directly decrypt data files uploaded before their participation without contacting with data owners. User revocation can be easily achieved through a novel revocation list without updating the secret keys of the remaining users. The size and computation overhead of encryption are constant and independent with the number of revoked users.

ISSN:2348-4098

3. We provide secure and privacy-preserving access control to users, which guarantees any member in a group anonymously utilize the cloud resource. Moreover, the real identities of data owners can be revealed by the group manager when disputes occur.

4. We provide rigorous security analysis, and perform extensive simulations to demonstrate the efficiency of our scheme in terms of storage and computation overhead.

2. RELATED WORKS

In [4], Kallahalla et al. proposed a cryptographic storage system that enables secure file sharing on untrusted servers, named Plutus. By dividing files into file groups and encrypting each file group with a unique file-block key, the data owner can share the file groups with others through delivering the corresponding lockbox key, where the lockbox key is used to encrypt the file-block keys. However, it brings about a heavy key distribution overhead for large-scale file sharing. Additionally, the file-block key needs to be updated and distributed again for a user revocation. In [5], files stored on the untrusted server include two parts: file metadata and file data. The file metadata implies the access control information including a series of encrypted key blocks, each of which is encrypted under the public key of authorized users. Thus, the size of the file metadata is proportional to the number of authorized users. The user revocation in the scheme is an intractable issue especially for large-scale sharing, since the file metadata needs to be updated. In their extension version, the NNL construction [10] is used for efficient key revocation. However, when a new user joins the group, the private key of each user in an NNL system needs to be recomputed, which may limit the application for dynamic groups. Another concern is that the computation overhead of encryption linearly increases with the sharing scale.Ateniese et al. [6] leveraged proxy encryptions to secure distributed storage. Specifically, the data owner encrypts blocks of content with unique and symmetric content keys, which are further encrypted under a master public key. For access control, the server uses proxy cryptography to directly re encrypt the appropriate content key(s) from the master public key to a granted user's public key. Unfortunately, a collusion attack between the untrusted server and

ISSN:2348-4098

any revoked malicious user can be launched, which enables them to learn the decryption keys of all the encrypted Then, the group manager assigns an access structure and the corresponding secret key to authorized users, such that a user can only decrypt a ciphertext if and only if the data file attributes satisfy the access structure. To achieve user revocation, the manager delegate's tasks of data file re encryption and user secret key update to cloud servers. However, the single owner manner may hinder the implementation of applications with the scenario, where any member in a group should be allowed to store and share data files with others. From the above analysis, we can observe that how to securely share data files in a multiple-owner manner for dynamic groups while preserving identity privacy from an untrusted cloud remains to be a challenging issue. In this paper, we propose a novel Mona protocol for secure data sharing in cloud computing. Compared with the existing works, Mona offers unique features as follows:

1. Any user in the group can store and share data files with others by the cloud.
2. The encryption complexity and size of cipher texts are independent with the number of revoked users in the system.
3. User revocation can be achieved without updating the private keys of the remaining users.
4. A new user can directly decrypt the files stored in the cloud before his participation.

3. PRELIMINARIES

3.1 BILINEAR MAPS

Let G1 and G2 be an additive cyclic group and a multiplicative cyclic group of the same prime order q, respectively [11]. Let e: G1 *G1 -≥G2 denote a bilinear map constructed with the following properties:

1. Bilinear: For all $a, b \in Z_q^*$ and $P, Q \in G_1$, $e(aP, bQ) = e(P, Q)^{ab}$.
2. Nondegenerate: There exists a point P such that $e(P, P) \neq 1$.
3. Computable: There is an efficient algorithm to compute $e(P, Q)$ for any $P, Q \in G_1$.

3.2 Complexity Assumptions

Definition 1 (q-strong Diffie-Hellman (q-SDH) Assumption [12]). *Given $(P_1, P_2, \gamma P_2, \gamma^2 P_2, \ldots, \gamma^q P_2)$, it is infeasible to compute $\frac{1}{\gamma+x} P_1$, where $x \in Z_q^*$.*

Definition 2 (Decision linear (DL) Assumption [12]). *Given $P_1, P_2, P_3, aP_1, bP_2, cP_3$, it is infeasible to decide whether $a + b = c \bmod q$.*

Definition 3 (Weak Bilinear Diffie-Hellman Exponent (WBDHE) Assumption [13]). *For unknown $a \in Z_q^*$, given $Y, aY, a^2Y, .., a^lY, P \in G_1$, it is infeasible to compute $e(Y, P)^{\frac{1}{a}}$.*

Definition 4 ((t,n)-general Diffie-Hellman Exponent (GDHE) Assumption [14]). *Let $f(X) = \Pi_{i=1}^{r}(X + x_i)$ and $g(X) = \Pi_{i=1}^{n-r}(X + x_i')$ be the two random univariate polynomials. For unknown $k, \gamma \in Z_q^*$, given*

$G_0, \gamma G_0, ..., \gamma^{t-1} G_0, \gamma f(\gamma) G_0, P_0, ..., \gamma^{t-1} P_0, kg(\gamma) H_0 \in G_1$ and $e(G_0, H_0)^{f^2(\gamma) g(\gamma)} \in G_2$,

it is infeasible to compute $e(G_0, H_0)^{kf(\gamma)g(\gamma)} \in G_2$.

ISSN:2348-4098

3.2 GROUP SIGNATURE

The concept of group signatures was first introduced in [15] by Chaum and van Heyst. In general, a group signature scheme allows any member of the group to sign messages while keeping the identity secret from verifiers denoted. In this paper, a variant of the short group signature scheme [12] will be used to achieve anonymous access control, as it supports efficient membership revocation.

3.3 DYNAMIC BROADCAST ENCRYPTION

Broadcast encryption [16] enables a broadcaster to transmit encrypted data to a set of users so that only a privileged subset of users can decrypt the data. Besides the above characteristics, dynamic broadcast encryption also allows the group manager to dynamically include new members while preserving previously computed information, i.e., user decryption keys need not be recomputed, the morphology and size of cipher texts are unchanged and the group encryption key requires no modification.

4. SYSTEM ARCHITECTURE

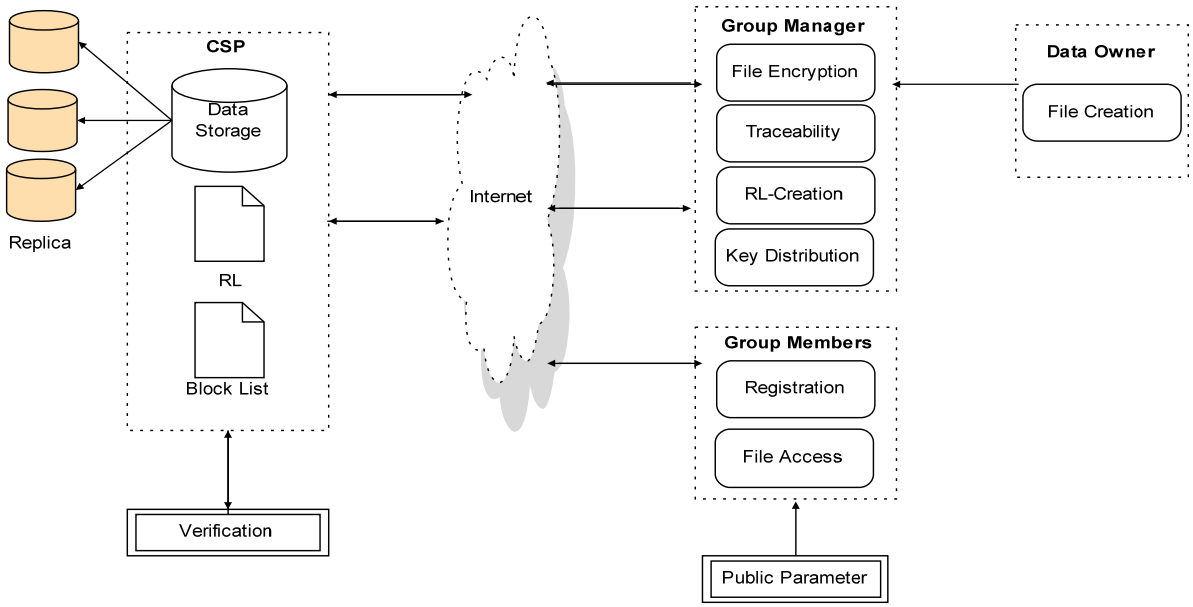

ISSN:2348-4098

4.1 SYSTEM MODEL AND DESIGN GOALS

4.1.1 SYSTEM MODEL

We consider a cloud computing architecture by combining with an example that a company uses a cloud to enable its staffs in the same group or department to share files. The system model consists of three different entities: the cloud, a group manager (i.e., the company manager), and a large number of group members (i.e., the staffs) as illustrated in Fig. 1.Cloud is operated by CSPs and provides priced abundant storage services. However, the cloud is not fully trusted by users since the CSPs are very likely to be outside of the cloud users' trusted domain. Similar to [3], [7], we assume that the cloud server is honest but curious. That is, the cloud server will not maliciously delete or modify user data due to the protection of data auditing schemes [17], [18], but will try to learn the content of the stored data and the identities of cloud users .Group members are a set of registered users that will store their private data into the cloud server and share them with others in the group. In our example, the staffs play the role of group members. Note that, the group membership is dynamically changed, due to the staff resignation and new employee participation in the company.

4.1.2 DESIGN GOALS

In this section, we describe the main design goals of the proposed scheme including access control, data confidentiality, anonymity and traceability, and efficiency as follows:

- **Access control:** The requirement of access control is twofold. First, group members are able to use the cloud resource for data operations.
- **Data confidentiality:** Data confidentiality requires that unauthorized users including the cloud are incapable of learning the content of the stored data. An important and challenging issue for data confidentiality is to maintain its availability for dynamic groups.
- **Anonymity and traceability**: Anonymity guarantees that group members can access the cloud without revealing the real identity. Although anonymity represents an effective protection for user identity, it also poses a potential inside attack risk to the system.

ISSN:2348-4098

- **Efficiency:** The efficiency is defined as follows: Any group member can store and share data files with others in the group by the cloud .User revocation can be achieved without involving the remaining.

TABLE 1
Revocation List

ID_{group}	A_1	x_1	t_1	P_1			
	A_2	x_2	t_2	P_2			
	.	.	.	.			
	A_r	x_r	t_r	P_r	Z_r	t_{RL}	$sig(RL)$

4.2 THE PROPOSED SCHEME: MONA OVERVIEW

To achieve secure data sharing for dynamic groups in the cloud, we expect to combine the group signature and dynamic broadcast encryption techniques. Specially, the group signature scheme enables users to anonymously use the cloud resources, and the dynamic broadcast encryption technique allows data owners to securely share their data files with others including new joining users.

4.2.1 Scheme Description

This section describes the details of Mona including system initialization, user registration, user revocation, file generation, file deletion, file access and traceability.

- **System Initialization**

The group manager takes charge of system initialization as follows:

- Generating a bilinear map group system
- Selecting two random elements H1,H2,H3 along with two random numbers q , and computing
- Randomly choosing two elements P;G 2 G1 and a number and computing respectively.
- Publishing the system parameters including S;P;H;H0;H1;H2; U; V ;W; Y ;Z; f; f1,

where f is a one-way hash function: f0 f1 is hash function.

function: f0; 1g,G1; and EnckðÞ is a secure symmetric encryption algorithm with secret key k.In the end, the parameter ð_; _1; _2;GÞ will be kept secret as the master key of the group manager.

- **User Registration:** For the registration of user i with identity IDi, the group manager randomly select a number q and computes. Then, the group manager adds into the group user list, which will be used in the traceability phase. After the registration, user i obtains a private key

ISSN:2348-4098

which will be used for group signature generation and file decryption.

➢ **User Revocation:** User revocation is performed by the group manager via a public available revocation list ðRLÞ, based on which group members can encrypt their data files and ensure the confidentiality against the revoked users. As illustrated in Table 1, the revocation list is characterized by a series of time stamps (t1 < t2 <; :::; tr). Let ID group denote the group identity. The tuple ðAi; xi; tiÞ represents that user i with the partial private key (Ai; xi) is revoked at time ti. P1; P2; :::; Pr and Zr are calculated by the group manager with the private secret key. Revocation list, we let the group manger update the revocation list each day even no user has being revoked in the day. In other words, the others can verify the freshness of the revocation list from the contained current date t RL.

$$\begin{cases} P_1 = \frac{1}{\gamma + x_1} \cdot P \in G_1 \\ P_2 = \frac{1}{(\gamma + x_1)(\gamma + x_2)} \cdot P \in G_1 \\ P_r = \frac{1}{(\gamma + x_1)(\gamma + x_2) \cdots (\gamma + x_r)} \cdot P \in G_1 \\ Z_r = Z^{\frac{1}{(\gamma + x_1)(\gamma + x_2) \cdots (\gamma + x_r)}} \in G_2. \end{cases}$$

➢ **File Generation:**

To store and share a data file in the cloud, a group member performs the following operations:

1. Getting the revocation list from the cloud. In this step, the member sends the group identity ID group as a request to the cloud. Then, the cloud responds the revocation list RL to the member.

2. Verifying the validity of the received revocation list. First, checking whether the marked date is fresh.

Second, verifying the contained signature. If the revocation list is invalid, the data owner stops this Revocation.

Case 1. There is no revoked user in the revocation list:

i. Selecting a unique data file identity ID data;

ii. Choosing a random number k 2 Z _q ;

iii. Computing the parameters C1; C2; K; C

➢ **File Deletion:** File stored in the cloud can be deleted by either the group manager or the data owner (i.e., the member who uploaded the file into the server). To delete a file ID data, the group manager computes a signature _f1ðIDdataÞ and sends the signature along with ID data to the cloud. The cloud will delete the file. Traceability When a data dispute occurs, the tracing operation is performed by the group manager to identify the real identity of the data

ISSN:2348-4098

owner. Given a signature a1,a2 T3; c; s_; s_; sx; s_1; s_2 Þ, the group manager employs his private key ð_1; _2Þ to compute Ai ¼ T3 _ ð_1 _ T1 þ _2 _ T2Þ. Given the parameter Ai, the group manager can look up the user list to find the corresponding identity.

➢ **Algorithm**

Parameters Computing

Input: The revoked user parameters $(P_1, x_1), \ldots, (P_r, x_r)$,

and the private key.

Output: Ar;r or NULL

begin

set temp = A

for1 to r

if x =x

return NULL

else

set temp ¼ 1

x—x

temp

return temp

end

➢ **File Access:**

To learn the content of a shared file, a member does the following actions:1. Getting the data file and the revocation list from the cloud server. In this operation, the user first adopts its private key A; x Þ to compute a signature _u on the message ID group; ID data; tÞ by using Algorithm 1, where t denote the current time, and the ID data can be obtained from the local shared file list maintained by the manager. Then, the user sends a data request containing ID group; ID data; t; _up to the cloud server. Upon receiving the request, the cloud server employs Algorithm 2 to check the validity of the signature and performs revocation verification.

➢ **Traceability:**

When a data dispute occurs, the tracing operation will be performed by the group manager. The cloud the real identity of the data owner. Given a signature _ ¼ ðT1; T2;T3; c; s_; s_; sx; s_1; s_2 Þ, the group manager employs his private key .

5. PERFORMANCE EVALUATION

In this section, we first analyze the storage cost of Mona, and then perform experiments to test its computation cost.

5.1 STORAGE:

Without loss of generality, we set q =160 and the elements in G1 and G2 to be 161 and 1,024 bit, respectively. In addition,

ISSN:2348-4098

we assume the size of the data identity is 16 bits, which yield a group capacity of 216 data files. Similarly, the size of user and group identity are also set as 16 bits. Group manager. In Mona, the master private key of the group manager is G1,G2,G3 Additionally, the user list and the shared data list should be stored at the group manager. Considering an actual system with 200 users and assuming that each user share 50 files in average, the total storage of the group manager .

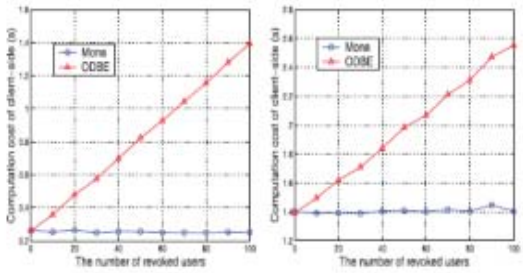

(a) Generating a 10 MB file (b) Generating a 100 MB file

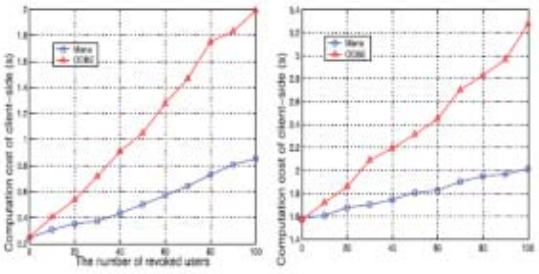

(a) Accessing a 10 MB file (b) Accessing a 100 MB file

6. CONCLUSION

In this paper, we design a secure data sharing scheme, Mona, for dynamic groups in an untrusted cloud. In Mona, a user is able to share data with others in the group without revealing identity privacy to the cloud.

Additionally, Mona supports efficient user revocation and new user joining. More specially, efficient user revocation can be achieved through a public revocation list without updating the private keys of the remaining users, and new users can directly decrypt files stored in the cloud before their participation.

Computation Cost of the Cloud (s)

Request	The number of revoked users		
	0	50	100
File generation (100 MB)	0.065	0.154	0.271
File generation (10 MB)	0.045	0.125	0.226
File access (100 MB)	0.045	0.150	0.237
File access (10 MB)	0.045	0.151	0.240
File deletion (100 MB)	0.041	0.153	0.240
File deletion (10 MB)	0.042	0.156	0.238

Cloud Computation Cost

To evaluate the performance of the cloud in Mona, we test its computation cost to respond various client operation requests including file generation, file access, and file deletion. Assuming the sizes of requested files are 100 and 10 MB, the test results are given in Table 3. It can be seen that the computation cost of the cloud is deemed acceptable, even when the number of revoked users is large. This is because the cloud only involves group signature and revocation verifications to ensure the validity of the requestor for all

ISSN:2348-4098

operations. In addition, it is worth noting that the computation cost is independent with the size of the requested file for access and deletion operations, since the size of signed message is constant, e.g., ðID group; IDdata; tÞ in file access and ðID data; _Þ in file deletion requests.

REFERENCES

[1] M. Armbrust, A. Fox, R. Griffith, A.D. Joseph, R.H. Katz, A. Konwinski, G. Lee, D.A. Patterson, A. Rabkin, I. Stoica, and M. Zaharia, "A View of Cloud Computing," Comm. ACM, vol. 53, no. 4, pp. 50-58, Apr. 2010.

[2] S. Kamara and K. Lauter, "Cryptographic Cloud Storage," Proc. Int'l Conf. Financial Cryptography and Data Security (FC), pp. 136- 149, Jan. 2010.

[3] S. Yu, C. Wang, K. Ren, and W. Lou, "Achieving Secure, Scalable, and Fine-Grained Data Access Control in Cloud Computing,"Proc. IEEE INFOCOM, pp. 534-542, 2010.

[4] M. Kallahalla, E. Riedel, R. Swaminathan, Q. Wang, and K. Fu, "Plutus: Scalable Secure File Sharing on Untrusted Storage," Proc. USENIX Conf. File and Storage Technologies, pp. 29-42, 2003.

[5] E. Goh, H. Shacham, N. Modadugu, and D. Boneh, "Sirius: Securing Remote Untrusted Storage," Proc. Network and Distributed Systems Security Symp. (NDSS), pp. 131-145, 2003.

[6] G. Ateniese, K. Fu, M. Green, and S. Hohenberger, "Improved Proxy Re-Encryption Schemes with Applications to Secure
Distributed Storage," Proc. Network and Distributed Systems SecuritySymp. (NDSS), pp. 29-43, 2005.

[7] R. Lu, X. Lin, X. Liang, and X. Shen, "Secure Provenance: The Essential of Bread and Butter of Data Forensics Cloud Computing," , pp. 282-292, 2010Proc. ACM Symp. Information, Computer and Comm. Security pp. 29-43, 2006

ISSN:2348-4098

WEBVIEW VULNERABILITIES IN ANDROID

[1]SANDEEP JAIN, [2]PREETI KHANNA

[1]Associate Professor, Department, Doon Valley Institute of Engineering & Technology

[2]M. Tech. Scholar, Department, Doon Valley Institute of Engineering & Technology

ABSTRACT

WebView is an essential component in Android, enabling tablet apps and Smartphone to embed a simple but powerful browser inside them. In order to achieve a better interaction b/w the apps and their embedded “browsers", WebView provides a no. of APIs, allowing app’s code to invoke and be invoked by the JavaScript code within the web pages and intercept and modify their events. Using such features, apps act like customized “browsers" for their intended web applications. Currently, according to a survey more than 80% of the most downloaded apps in the Android market in 10 diverse categories use WebView.

The landscape of the Web is changed by the design of WebView, especially from security perspective. Web's security infrastructure’s two essential pieces are weakened if WebView along with its APIs are used: the sandbox protection implemented by browsers and the Trusted Computing Base (TCB) at the client side. Therefore, many attacks can be launched either against apps or websites. The paper’s objective is to present the attacks firstly, and then after analysing their fundamental causes, discuss its potential solutions.

1. INTRODUCTION

What truly makes customization possible is the APIs provided by WebView. WebView not only allows apps to display web content, through its APIs, more importantly, it apps are also enabled to interact with the web content of the loaded site. The interaction is two-way: From apps to web pages, apps can invoke JavaScript code within web pages or there is an option to insert their own JavaScript code into web pages. Not just this, apps can also monitor and intercept the events occurred within web pages, and respond to them. From web pages to apps, apps can register interfaces to WebView, so the JavaScript code in the embedded web pages can invoke these interfaces.

ISSN:2348-4098

1.1 WEBVIEW: AN OVERVIEW

To understand vulnerabilities in WebViews, we must first understand the features provided by WebViews. The WebView class allows developers to display data from web pages and files within the confines of the application, seamlessly integrating web and application content. Through the WebView, not only can developers set the content to be displayed, but they can also specify the layout and behaviour of the WebView. Essentially, the WebView class allows a developer to create their own custom, embedded web browser.

Alternatively, web content can be displayed by sending a request to a browser application to load the content. We will focus on the WebView approach as WebView can lead to security problems, while browsers are separate applications outside of an application's security boundary.

What makes WebView exciting is not just the fact that it simply serves as an embedded browser, but also because it enables Android applications to interact with web pages and web applications, making web applications and Android applications tightly integrated.

1.2 THREATS IN WEBVIEW

The attacks discussed here are categorized based on two threat models, depicted in Figure 1. We are giving a high-level overview of these models in this section, leaving the attack details. It should be noted that we have not discussed the attacks that are common in the Web, such as cross-site scripting, cross-site request forgery, SQL injection, etc., because these attacks are not specific to WebView. It is like, WebView is neither immune to them, nor does it make the situation worse.

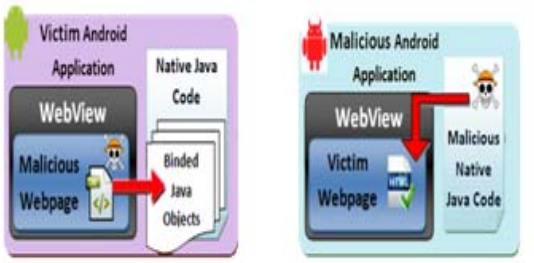

Figure 1: Threats in Web View

1.3 ATTACKS FROM MALICIOUS WEB PAGES

Here we study how malicious web pages can attack Android applications. In this attack model, we assume that apps are benign, and they are intended to serve a web application, such as Facebook. These apps can be either first-party (i.e. owned by the intended web application) or third-party (i.e. owned by an independent entity). The objective of attackers is to compromise the apps and

ISSN:2348-4098

their intended web application. To achieve this, the attackers need to trick the victim to load their web pages into the apps, so that they could launch attacks on their target WebView.

The attack is depicted in Figure 1(a). Getting the victim to load attacker's web pages is not as difficult as it sound, as it could be done through a lot of means, such as emails, advertisements, social networks, etc. A few attacks from malicious web pages are as follows:

- Attacks through Holes on the Sandbox
- Attacks through Frame Confusion

1.4 ATTACKS FROM MALICIOUS APPS

Now, we study how malicious apps can attack web applications. In this threat model, we already assume that an attacker owns a malicious app, specifically designed for a web application such as Facebook. The goal of the attacker is to directly launch attacks on the web application. The attack is depicted in Figure 1(b). It is quite obvious that these attacks only make sense for third-party apps. In order to prepare a victim for such attacks, the attacker first of all needs to fascinate users to use their apps for the intended web application.

Although it sounds difficult but the above goal is not difficult to achieve at all, and many apps from the Android market have already achieved that, although none of them is malicious to the best of our knowledge. For example, one of the most popular Facebook apps for Android is called Friend-Caster for Facebook, which is developed by Handmark, not Facebook; it has been downloaded for 500,000 times. The application uses the android's WebView component to browse Facebook. A few attacks from malicious apps are:

- JavaScript Injection
- Event Sniffing and Hijacking

2. PROBLEM FORMULATION

The persistent use of WebView and mobile devices has actually changed the security landscape of the Web. For the past many years rather almost a decade, we were accustomed to browse the Web from a handful of familiar browsers, such as Google Chrome, IE, Firefox and many more, all of which are developed by well-recognized companies, and we trust them very well. Such a paradigm has changed in the case of Smartphone's and tablets: thanks to Android's WebView, apps could now act much like browsers, giving us hundreds of thousand "browsers". Most of them are

ISSN:2348-4098

not developed by well-recognized companies, because of which their trustworthiness is not guaranteed.

A Browser is a critical component in the Trusted Computing Base (TCB) of the Web: Web applications rely on browsers on the client side to secure their web contents, cookies, JavaScript code, and HTTP requests. The reason for using those selected browsers is that we have a feeling of trust that they can serve as a TCB, and that their developers have put a lot of time into the security testing. When shifting to those unknown “browsers", the faith is gone, and so is the TCB. We do not know whether these “browsers" are trustworthy, if they have been passed through rigorous security testing, or even if the developers have adequate security expertise or not. Therefore, in reality WebView has weakened the TCB of the Web infrastructure.

Another important security feature of browsers is sandbox, which contains the behaviors of web pages inside the browsers, preventing them from accessing the system resources or pages from other origins. Unfortunately, to support better interactions between apps and web pages, WebView allows apps to punch “holes" on the sandbox, creating a whole lot of opportunities for attacks.

3. RELATED WORK

IDENTIFY PRIME ADVERTISING LOCATIONS

Kirandeep, Anu Garg in **Implementing Security on Android Application[7]** stated that there are some advanced features in android Smartphone, with which user can easily share applications via online market store i.e. Google market store. But, there are attacks and threats included in this platform, like malware applications are also attack on Android actual applications. Because malware on device can create number of risks, which creates problem while connectivity because of security issues. In this paper, they described that how security can be improved of Android Operating System so that users can safely use the android smart phones.

Tiwari Mohini, Srivastava Ashish Kumar and Gupta Nitesh stated in their paper **Review on Android and Smartphone Security[10]** that Android has very few restrictions for developer which increases the security risk for end users. In this paper they have reviewed android security model, application

ISSN:2348-4098

level security and security issues in the Android based Smartphone.

Would You Mind Forking This Process? A Denial of Service attack on Android (and Some Countermeasures)[14] by **Alessandro Armando, Alessio Merlo, Mauro Migliardi and Luca Verderame** presented a previously undisclosed vulnerability of Android OS which can be exploited by mounting a Denial-of-Service attack that makes devices become totally unresponsive. It discuss the characteristics of the vulnerability – which affects all versions of Android – and propose two different fixes, each involving little patching implementing a few architectural countermeasures.

William Enck, Machigar Ongtang and Patrick Mcdaniel in **Understanding Android Security[13]** shared experiences working with the Android security policy revealed that it begins with a relatively easy-to-understand MAC enforcement model, but the number and subtlety of refinements make it difficult for someone to discover an application's policy simply by looking at it. Some refinements push policy into the application code. Others add delegation, which mixes discretionary controls into the otherwise typical MAC model. This situation makes gathering a firm grasp on Android's security model nontrivial.

Another research, **Mobile Application Security on Android [8]** by **Jesse Burns** suggested that if you are exposing your application for programmatic access by others, make sure you enforce permissions so that unauthorized applications can't get the user's private data or abuse your program. Make your applications security as simple and clear as possible. When communicating with other programs, think clearly about how much you can trust your input, and validate the identity of services you call.

Perakovic Dragan, Husnjak Sinisa & Remenar Vladimir in their paper **Research Of Security Threats In The Use Of Modern Terminal Devices[9]** stated that the research of their paper focused on defining forms of security threats and possible attacks on smartphones and a brief description of possibilities for protecting smartphones.

As stated by **Vaibhav Rastogi, Yan Chen, and Xuxian Jiang** in their paper **Evaluating Android Anti-malware**

ISSN:2348-4098

against Transformation Attacks[6] that they evaluated the state-of-the-art commercial mobile anti-malware products for Android and test how resistant they are against various common obfuscation techniques (even with known malware). They also developed DroidChameleon, a systematic framework with various transformation techniques, and used it for their study. Their results were worrisome: as none of the tools is resistant against common malware transformation techniques. Finally, in the light of their results, they propose possible remedies for improving the current state of malware detection on mobile devices.

A Study of Android Application Security [2] by **William Enck, Damien Octeau, Patrick McDaniel, and Swarat Chaudhuri** stated that their paper seeks to better understand smartphone application security by studying 1,100 popular free Android applications. They introduced the ded decompiler, which recovers Android application source code directly from its installation image. They designed and executed a horizontal study of smartphone applications based on static analysis of 21 million lines of recovered code. Their analysis uncovered pervasive use/misuse of personal/phone identifiers, and deep penetration of advertising and analytics networks. They concluded by considering the implications of these preliminary findings and offer directions for future analysis.

The research titled **Auditing Enterprise Class Applications And Secure Containers On Android - The Limitations of Mobile Security in the Enterprise[5]** by **Marc Blanchou** stated that their paper covers research into the threats, with a focus on mobile devices running Android. By understanding the different attack vectors and the current mobile security models, this research paper aims to determine what should be protected, when it should be protected, and how commercial security solutions fit into the mix. The paper also discusses design concerns in popular Android security products and techniques used to assess them.

Lastly, **A Brief Guide to Android Security[1]** by **Ryan Farmer** can be summarized as - a malicious user or malware on the device can create a number of risks for an organisation, and

ISSN:2348-4098

so the fact that these devices are not necessarily connected does not translate to a lack of security risks. This paper discussed why it is important to secure an Android device, what some of the potential vulnerabilities are, and security measures that can be introduced to provide a baseline of security on Google's mobile OS.

4. PROPOSED WORK

Our work would be the systematic study on the WebView security problems. The objective of this work is to conduct a systematic study of WebView's impact on web security, with a particular focus on identifying its fundamental causes. Through our systematic studies, we will classify some existing concerns that have been raised by the community and the new attacks that are discovered by us, based on the cause of the vulnerabilities. These attacks reveal a fundamental problem caused by the weakening of the TCB and sandbox in the WebView infrastructure. Attacks are possible if the apps themselves are malicious, or if they are non-malicious but vulnerable. Android applications and web applications may become victim if they use WebView or are loaded into WebView.

In this work, we would also detail various WebView based attacks and present our vulnerability identification tool, SmartphoneCop, which closely examines two aspects of WebView interaction, the application and the web content, to automatically identify WebView vulnerabilities in Android applications.

Our **intended method of work** would be as follows:

We would firstly demonstrate the attacks from malicious web pages which include attacks through holes on the sandbox and attacks through frame confusion. Attacks through frame confusion would comprise the demonstration of the attacks from child frame & the attacks from main frame.

After that we would be demonstrating the other type of attacks that are attacks from malicious apps such as JavaScript injection and event sniffing and hijacking.

And then a tool, SmartphoneCop, would be introduced which would identify the existing WebView vulnerabilities in Android.

And finally we would recommend modifications to address these risks.

We would make the following contributions:

ISSN:2348-4098

–We will demonstrate the vulnerabilities in WebViews.
–We will build a tool to identify vulnerable WebViews.
–We will suggest and evaluate solutions to mitigate these vulnerabilities.

5. CONCLUSION AND FUTURE WORK

The WebView technology in the Android system enables apps to bring a much richer experience to users, but unfortunately, at the cost of security. In this paper, we have discussed a number of attacks on WebView, either by malicious apps or against non-malicious apps. Two fundamental causes of the attacks have been identified by us: weakening of the TCB and sandbox. While WebViews facilitate the creation of rich, interactive applications, they also introduce the potential for attack if developers are not careful. We examine vulnerabilities of WebViews and present SmartphoneCop, which analyzes both Android applications and web content to identify vulnerabilities in applications. We also propose changes to WebViews to grant code access based on the domain and not the WebView, thereby limiting the opportunity for exposure to malicious JavaScript.

In our future work, we would be developing more intense solutions to secure WebView. Our goal is to defend against the attacks on WebView by building desirable security features in WebView.

REFERENCES

[1] Ryan Farmer, “A Brief Guide to Android Security”, White Paper

[2] William Enck, Damien Octeau, Patrick McDaniel, and Swarat Chaudhuri, “A Study of Android Application Security”

[3] Wei-Meng Lee, “Android Application Development Cookbook”, John Wiley & Sons, Inc., First Edition- 2013, ISBN: 978-1-118-17767-9

[4] Rafael Fedler, Christian Banse, Christoph Krauss, and Volker Fusenig, “Android OS Security: Risks and Limitations”, AISEC Technical Reports, May 2012

[5] Marc Blanchou, “Auditing Enterprise Class Applications And Secure Containers On Android - The Limitations of Mobile Security in the Enterprise”, iSEC Partners, Dec 2012

[6] Vaibhav Rastogi, Yan Chen, and Xuxian Jiang, “Evaluating Android Anti-malware against Transformation Attacks”, March 2013

ISSN:2348-4098

[7] Kirandeep, Anu Garg, "Implementing Security on Android Application", The International Journal of Engineering And Science (IJES), Volume-2 ||Issue-3 ||Pages 56-59 ||2013

[8] Jesse Burns, "Mobile Application Security on Android", Black Hat USA talk

[9] Perakovic Dragan, Husnjak Sinisa & Remenar Vladimir, "Research Of Security Threats In The Use Of Modern Terminal Devices", Annals of DAAAM for 2012 & Proceedings of the 23rd International DAAAM Symposium, Volume 23, No. 1, ISSN 2304-1382, ISBN 987-3-901509-91-9

[10] Tiwari Mohini, Srivastava Ashish Kumar and Gupta Nitesh, "Review on Android and Smartphone Security", Research Journal of Computer and Information Technology Sciences, Vol. 1(6) ||Pages 12-19 ||November (2013), ISSN 2320 – 6527

[11] Stephen Smalley and Robert Craig, "Security Enhanced (SE) Android: Bringing Flexible MAC to Android", Trusted Systems Research National Security Agency

[12] Lei Wu, Michael Grace, Yajin Zhou, Chiachih Wu and Xuxian Jiang, "The Impact of Vendor Customizations on Android Security"

[13] William Enck, Machigar Ongtang and Patrick Mcdaniel, "Understanding Android Security", IEEE Security & Privacy, January/February 2009

[14] Alessandro Armando, Alessio Merlo, Mauro Migliardi and Luca Verderame, "Would You Mind Forking This Process? A Denial of Service attack on Android (and Some Countermeasures)"

ISSN:2348-4098

A SURVEY ON CLUSTERING PROBLEM WITH OPTIMIZED K- MEDOID ALGORITHM

[1]SUNITA KUMARI, [2]ABHA KAUSHIK

[1]M.Tech, Computer Science & Engineering, Galgotia's University, Gr. Noida, UP, India ,
E-mail: sunita.rao86@gmail.com
[2]M.Tech, Computer Science & Engineering, Galgotia's University, Gr. Noida, UP, India ,
E-mail: abha15.1990@gmail.com

ABSTRACT

Clustering is the division of data into groups of similar objects. It disregards some details in exchange for data simplification. Informally, clustering can be viewed as data modeling concisely summarizing the data, therefore, it relates to many disciplines from statistics to numerical analysis. Such applications usually deal with large datasets and many attributes. Searching of such data is a subject of data mining. This survey based on clustering algorithms from a data mining viewpoint. The goal of this survey is to provide a comprehensive review of different clustering techniques in data mining. Clustering is a partition of data into groups of similar objects. Each and every group, called a cluster, consists of various objects that are similar to one another and dissimilar to objects of other groups.

KEYWORDS: K Means, K Medoid, Clustering, Partitional Algorithm,

1. INTRODUCTION

The goal of this survey is to provide a comprehensive review of different clustering techniques in data mining. Clustering, which aims at dividing a dataset into groups or clusters containing similar data, is a fundamental problem in unsupervised Learning and has many applications in various domains. In recent years, there has been significant interest in developing clustering algorithms to massive datasets. Clustering is useful technique for discover some or the entire hidden patterns. The discovery of data sharing and patterns in the underlying data. Cluster is a collection of data objects

- Similar to one another in similar cluster

ISSN:2348-4098

- Different to the objects in other clusters
- A good clustering method will produce better quality clusters with
  - High intra class relationship
  - Low inter class relationship

The value of clustering result based on both the similarity measure used by the method and its implementation.

The value of clustering method is also measured by its capability to

DATA CLUSTERING ALGORITHMS: Data clustering algorithms can be divided into following categories. Some of these algorithms are given as follows:

PARTITIONING ALGORITHMS:

Build various partitions and then evaluate them by some measure.

HIERARCHY ALGORITHMS:

Create a hierarchical breakdown of the set of data (or objects) using some criterion.

DENSITY-BASED: built on connectivity and density functions.

GRID-BASED: Grid based clustering is depending on a multiple-level granularity structure.

MODEL-BASED: A model is offered for each of the clusters and the idea is to find the best fit of that model to each other.

2. PARTITIONING METHODS

2.1 K-Means Method

2.2 K –Medoids Method

2.3 CLARA

2.4 CLARANS

2.1 K-MEANS ALGORITHM

K-means is a widely used partitioned clustering method. While there are considerable exploration efforts to characterize the key features of K-means clustering, further exploration is needed to reveal whether the optimal number of clusters can be found on the run based on the cluster quality measure. It classifies a given set of n data objects in k clusters, where k is the number of preferred clusters and it is required in advance. A centroid is defined for all clusters. Each data objects are positioned in a cluster having centroid nearby to that data object. Later handling all data objects, k-means, or centroids, are rearranged, and the whole process is repeated. All data objects are certain to the clusters depend on the new centroids. In each repetition centroids change their location step by step. In other words, centroids move in each repetition. This process is sustained until no any centroid move. As a result, k clusters are found signifying a set of n

ISSN:2348-4098

data objects. An algorithm for k-means method is given below.

Algorithm Input: 'k', is the number of clusters to be divided; 'n', is the number of objects. **Output**: A set of 'k' clusters based on given similarity function.

Steps:

i) Arbitrarily choose 'k' objects as the initial cluster centers;

ii) Repeat,

a. Reassign each object to the cluster to which the object is the most similar; based on the given similarity function;

b. Update the centroid (mean value of cluster), i.e., calculate the mean value of the objects for each cluster;

iii) Until no change.

Limitations and problems: K-means attempts to minimize the squared or absolute error of points with respect to their cluster centroids. Although this is sometimes a reasonable criterion and leads to a simple algorithm, K-means has a number of limitations and problems.

Handling Empty Clusters: One of the problems with the basic K-means algorithm given earlier is that empty clusters can be obtained if no points are allocated to a cluster during the assignment step. If this happens, then an approach is needed to choose a replacement centroid, since otherwise, the squared error will be larger than necessary.

Reducing the SSE with Post processing: In k-means to get better clustering we have to reduce the SSE that is most difficult task. There are various types of clustering methods available which reduces the SSE [16].

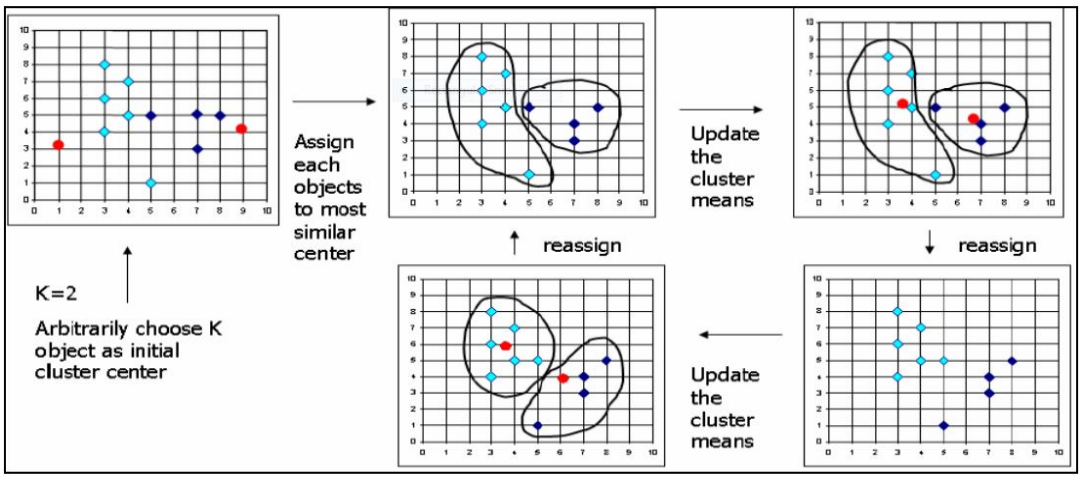

Figure1. Working of k means algorithm

ISSN:2348-4098

2.2 K-MEDOID ALGORITHMS

The k-means method uses centroid to represent the cluster and it is sensitive to outliers. This means, a data object with an extremely large value may disrupt the distribution of data. K-Medoids method overcomes this problem by using Medoids to represent the cluster rather than centroid. A Medoids is the centrally positioned data object in a cluster. Here, k data objects are selected randomly as Medoid to represent k cluster and remaining all data objects are placed in a cluster having Medoids nearest (or most similar) to that data object. After handling all data objects, new Medoids is determined which can represent cluster in a better way and the whole process is repeated. Again all data objects are bound to the clusters depend on the new Medoids. In each repetition, Medoids change their location step by step. In other words, Medoids move in each repetition. This process is continued until no any Medoids change. [2]

Algorithm:

Input: 'k', is the number of clusters to be divided; 'n', the number of objects.

Output: A is the set of 'k' clusters that reduces the sum of the dissimilarities of all the objects to their neighboring Medoid.

Steps:

(i) Arbitrarily choose 'k' objects as the initial Medoid;

(ii) Repeat,

(a). Allot each remaining object to the cluster with the neighboring Medoid;

(b). Randomly select a non-Medoid object;

(c). Compute the total cost of swapping old Medoid object with a new selected non- Medoid object

(d). If the total cost of swapping is less than zero (< 0), then perform that swap operation to form the new set of k-Medoid.

(iii) Until no change.

ISSN:2348-4098

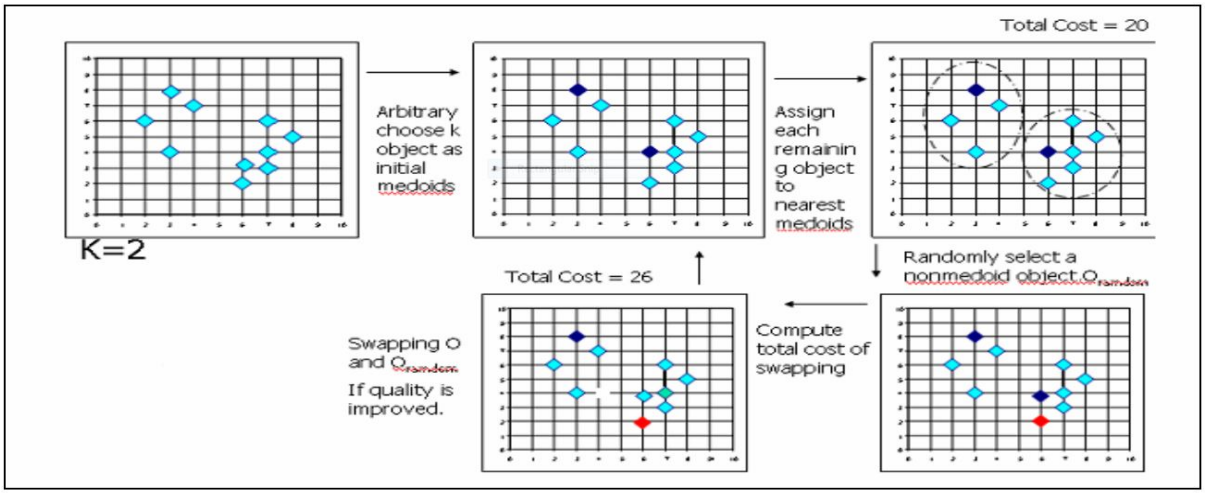

Figure2. Working of k- Medoid algorithm

Features of K-Medoid Algorithm

K-Medoid works on the dissimilarity matrix of the given data set or when it is offered with data matrix, the algorithm first computes a dissimilarity matrix. It is more robust; because it minimizes a sum of dissimilarities instead of a sum of squared Euclidean distances it provides a novel graphical representation, the outline plot, which permits the user to select the optimal number of clusters. However, PAM lacks in scalability for very large databases and it present high time and space complexity It is understood that the average time for normal distribution is greater than the average time for the uniform distribution. This is true for both the algorithms K-Means and K-Medoids. When the number of data points is less than the K-Means algorithm takes less execution time as compare to k-Medoid algorithm. But when the data points are increased to maximum the K-Means algorithm takes maximum time and the K-Medoids algorithm performs reasonably better than the K-Means algorithm. The specific feature of k-Medoid algorithm is that it needs the distance among every pair of objects only once and uses this distance at every stage of repetition.[3]

2.3 CLARA

CLARA (Clustering large Applications) algorithm is designed by Kaufman and Rousseeuw to handle large data sets, It depend on sampling. Instead of finding representative objects for the whole data set, CLARA draws a model of the data set,

ISSN:2348-4098

applies PAM on the model, and finds the Medoid of the sample. The point is that, if the model is drawn in a sufficiently random way, the Medoid of the model would approximate the Medoid of the whole data set. For finding the better approximations, CLARA draws several models and provides the best clustering as the result. Here, for perfection, the quality of a clustering is measured based on the average dissimilarity of all objects in the whole data set, and not only of those objects in the models. [4]

2.4 CLARANS

CLARANS is very efficient and effective. Second, we study how CLARANS can handle not only point's objects, but also polygon objects efficiently. One of the approaches measured, called the IR-approximation, is very efficient in clustering convex and nonconvex polygon objects. CLARANS is a main-memory clustering technique, while many of the above-mentioned techniques are designed for out-of-core clustering applications. We admit that whenever wide I/O operations are difficult, CLARANS is not effective as the others. However, we argue that CLARANS still has considerable applicability.

CLARANS uses a randomized search approach to improve on both CLARA and PAM. Conceptually CLARANS does the following.

1) Randomly pick K candidate Medoids.

2) Randomly consider a swap of one of the selected points for a non-selected point.

3) If the new configuration is better, i.e., has lower cost, then repeat step 2 with the new configuration.

4) Otherwise, repeat step 2 with the current configuration unless a parameterized limit has been exceeded. (This limit was set to max (250, K *(m - K)).

5) Compare the current solution with any previous solutions and keep track of the best.

6) Return to step 1 unless a parameterized limit has been exceeded. (This limit was set to 2.)

3. CONCLUSION

This survey starts with a brief introduction about clustering in data mining. Since measuring similarity between data objects is simpler than mapping data objects to data points in feature space, these pairwise similarity

ISSN:2348-4098

based clustering algorithms can greatly reduce the difficulty in developing clustering based pattern recognition applications. The advantage of the K means algorithm is its favorable execution time. Its disadvantage is that the user has to know in advance how many Clusters are searched for. It is observed that K means algorithm is efficient for smaller data sets and K-Medoids seems to perform better for large datasets. [3]

REFERENCES

[1] Weiguo Fan, Linda Wallace, Stephanie Rich, Zhongju Zhang "Tapping into the Power of Text Mining" February 16, 2005.

[2] Singh s s , Chauhan N C " K-means v/s K-medoids: A Comparative Study" National Conference on Recent Trends in Engineering & Technology, 13-14 May 2011.

[3] Batra A. " Analysis and Approach: K-Means and K-Medoids Data Mining Algorithms" 5th IEEE International Conference on Advanced Computing & Communication Technologies [ICACCT-2011] ISBN 81-87885-03-3

[4] Raymond T. Ng and Jiawei H. "CLARANS: A Method for Clustering Objects for Spatial Data Mining" IEEE TRANSACTIONS ON KNOWLEDGE AND DATA ENGINEERING, VOL. 14, NO.5, SEPTEMBER/OCTOBER 2002

[5] An Introduction to Cluster Analysis for Data Mining (ebook).

[6] Soni T. M. "AN OVERVIEW ON CLUSTERING METHODS" IOSR Journal of Engineering Apr. 2012, Vol. 2(4) pp: 719-725

[7] Berkhin P. "Survey of Clustering Data Mining Techniques" Accrue Software, 1045 Forest Knoll Dr., San Jose, CA, 95129

[8] STEFANOWSKI J. delivered Lecturer on "Data Mining-Clustering" at Institute of Computing Sciences Poznan University of Technology Poznan, Poland Lecture 7 SE Master Course 2008/2009

[9] Han J. and Kamber M. "Data Mining: Concepts and Techniques"

[10] Alsabti K., Ranka S., and Singh V." An Efficient K-Means Clustering Algorithm.", 1997

[11] Das S., Abraham A. and Konar A. "Document Clustering Using Differential Evolution" link.springer.com/content/pdf/bfm%3A978-3-540-93964-1%2F1.pdf

[12] Das S., Abraham A . and konar A., " Automatic Clustering Using an Improved

ISSN:2348-4098

Differential Evolution Algorithm" IEEE VOL. 38, NO. 1, JANUARY 2008.

[13] Jusoh Shaidah and Hejab M. Alfawareh "Techniques, Applications and Challenging Issue in Text Mining" IJCSI International Journal of Computer Science Issues, Vol. 9, Issue 6, No 2, November 2012 ISSN.

[14] Xindong Wu, Kumar V. J. Ross Quinlan, Ghosh J, Yang. Q ,"Top 10 algorithms in data mining",Knowl Inf Syst (2008) 14:1–37 DOI 10.1007/s10115-007-0114,December 2007

[15] Malik. S. , Sharma N ., and Singh S. , "Evolving limitations in K-means algorithm in data mining and their removal" IJCEM (International Journal of Computational Engineering & Management), Vol. 12, April 2011

[16] Monz.C, "Delivered a lecture on Machine Learning for Data Mining", Week 6: Clustering at Queen mary university of London.

[17] Velmurugan T. and Santhanam T. "Computational Complexity between K-Means and K-Medoids Clustering Algorithms for Normal and Uniform Distributions of Data Points" Journal of Computer Science 6 (3): 363-368, 2010 ISSN 1549-3636 © 2010 Science Publications.

[18] Pratap A ,R, Suvarna V.K., Devi R.J, Rao N.K. " An Efficient Density based Improved K- Medoids Clustering algorithm" International Journal of Advanced Computer Science and Applications, Vol. 2, No. 6, 2011.

[19] Polinati S.G, Babu V., Satapathy C. S, Pradhan G. "Effective Image clustering with Differential Evolution Technique", International Journal of computer and communication Technology, Vol. 2,No. 1.2010.

ISSN:2348-4098

A COMPARATIVE STUDY AND VALIDATION OF MATHEMATICAL DRYING MODELS FOR INFRARED (IR) DRYING OF RAW AND BLANCHED CARROT (DAUCUS CAROTA)

[1]SUDIPTA DAS, [2]SAIKAT MAZUMDER

[1,2]Department of Food Technology, Techno India University, Kolkata, West Bengal, India

ABSTRACT

In this study, we have evaluated infrared (IR) drying characteristics of fresh and blanched carrot slices dried with an IR moisture analyzer. IR drying tests were conducted on the basis of 3^2 full factorial designs, at three range of temperatures (60^0C, 90^0C, and 105^0C) and three blanching time (2, 3, and 5 minutes) to evaluate the color changes and shrinkage volume of the finished product. The experimental data of moisture changes during IR drying were modeled with eight different models, including Page, modified Page, Thompson, Newton, Wang and Singh, and Henderson and Pabis, regression model-1, regression model-2. The Wang & Singh model shows a very good fit (R^2- 0.99, χ^2- 0.000533, RMSE- 0.019867 for raw carrot slices, R^2- 0.99, χ^2- 0.002711, RMSE- 0.036833 for blanched carrot slices) for raw and blanched carrot slices, page model also fit well (R^2- 0.98, χ^2- 0.000957, RMSE- 0.027567) for the blanched carrot slices. The best combination of blanching time and drying temperature was found as 2 minutes, 90^0C respectively. The shrinkage volume was more than 86% for drying at 105^0C and the best shrinkage volume was 90% for 2 minutes blanching and drying at 90^0C.

KEY WORDS: Carrot slices, Blanching, IR drying, mathematical modeling, shrinkage volume, colorimeter analysis.

1. INTRODUCTION

The carrot (Daucus carota) is a root vegetable, usually orange, purple, red, white or yellow in color, with a crisp texture when fresh. Carrot is considered as one of the most important crops in many countries. India has a production

ISSN:2348-4098

of 5-25 Mt, ranking second to China. In India, the convective drying technique is in use in the dehydration of carrot, at a commercial level. Convective drying usually extends over a long period and causes many undesirable changes in the material (1). Infrared radiation (IR) drying is fundamentally different from convective drying where material is dried directly by the absorption of IR energy rather than the transfer of heat from the air (2). When IR is used to heat or to dry moist materials, the radiation impinges on the exposed materials surface, penetrates it and the energy of radiation converts into heat (3). Infrared (IR) drying has been studied for achieving fast drying and reducing quality loss of fruits and vegetables (4).

Compared with hot air drying, IR heating offers many advantages such as greater energy efficiency, heat transfer rate, and heat flux, which results in reduced drying time and higher drying rate. It has been investigated as a potential method for increasing heating efficiency and obtaining high quality of dried foodstuffs, including peaches (5), carrots (6), onions (7), rice (8), and many other fruits and vegetables (9).

Mathematical modeling of mass transfer is a very useful tool in investigating the intrinsic kinetics of a drying process. Empirical models can derive a direct relationship between moisture ratio (MR) and drying time. Various mathematical models have been proposed to describe the IR drying characteristics of many products like onions (10, 11, 12, and 7), eggplants (7), and rice (13, 14), carrot (15, 16). The models are usually semi theoretical models with assumption of mass transfer obeying Fick's law (17).

In this study so called "desi carrot" (orange in colour) has been considered as a raw material. Drying of carrot is as a function of heating temperature. In this study, raw slices and slices of carrot blanched in sodium chloride (NaCl) for different time are used for IR drying. The objectives of this study were a comparative investigation and validation of several mathematical modeling as well as change in colour, specific energy consumption, and drying efficiency for raw and blanched carrot slices. Three parameters several statistical tool like coefficient of determination (R^2), reduced chi-square ($\chi 2$), and root mean square error (RMSE) were used to evaluate the fit of tested models to the experimental data (18, 19, 20, 12, 7, 21).

2. MATERIAL AND METHODS

ISSN:2348-4098

2.1 RAW MATERIAL

Carrot of orange in colour (so called "desi carrot" in Kolkata) was used as raw material, was collected from local market of Kolkata. The carrots were washed with running tap water followed by distilled water and after wards the excess surface water of was removing by muslin cloth. Then these were peeled and cut into small cubes (1.587±0.79 cm^3) with the help of a knife. These cubes were used for farther experiments.

2.2 METHODS

2.2.1 Experimental Procedure of Drying

The whole experiment was divided into two categories. In the first categories the cubes of carrot slices was directly subjected to drying at different temperature, and in other categories first blanching with sodium chloride (NaCl) for different time, followed by drying at different temperature. The drying was carried out in an IR moisture meter analyzer (Model No. MA45C-000230V1, SARTORIUS). The initial moisture content of the carrot was 87±0.82 %.

2.2.1.1 Design of Experiments

The factorial design with three levels treatment of temperature and blanching time was assigned for 3^3 full factorial designs which lead to 9 sets of experiments. The factorial design was applied to estimate the functional relationship between the drying time and blanching time on drying behaviour of carrot. The three level ranges of factors are 60^0C, 90^0C, 105^0C for drying temperature (-1, 0, +1 level respectively) and 2minutes, 3 minutes, and 5 minutes for blanching time ((-1, 0, +1 level respectively). In other sets of drying where blanching is not involved the slices was dried at 60^0C, 90^0C, 105^0C (-1, 0, +1 level respectively) which leads to 3sets of experiments.

2.2.2 Determination of Moisture Ratio (MR)

Moisture ratio of samples during drying was determined using following equation:

$MR= (M_t-M_e)/ (M_o-M_e)$

Here, M_t is moisture content at any specific time, M_e is the equilibrium moisture content and M_o is the initial moisture content.

2.2.3 Mathematical Modeling

During convective drying of raw and blanched carrot slices with IR heat source, two transport mechanisms simultaneously occur: a heat transfer to carrot slices and a moisture transfer from carrot to the surrounding

ISSN:2348-4098

environment. Heat is transferred by conduction and moisture transfer is governed by diffusion (16). Eight mathematical models successfully used in our research studies to evaluate the relationship between moisture ratio and drying time of raw and blanched (Table 1). Three parameters, coefficient of determination (R^2), reduced chi-square (χ^2), and root mean square error (RMSE) were used to evaluate the fit of tested models to the experimental data (19, 20, 12, 7, and 21). The lowest $\chi 2$ and RMSE values and the highest R^2 value (7) describe the fitness of model for the drying. Statistical values were defined with equations

$$\chi^2 = \sum_{i=1}^{n} (MR_{exp,i} - MR_{pre,i})^2 / (N-n)$$

$$RMSE = \sqrt{\sum_{i=1}^{n} (MR_{pre,i} - MR_{exp,i})^2 / N}$$

Where MRexp,i and MRpre,i are experimental and predicted moisture ratios respectively. N is the number of observations, and n is the number of drying constants.

Table 1: Mathematical Model of Raw and Blanched Carrot Slices

Model No.	Model Equation	Model Name
1	MR = a exp(-kt)	Henderson and Pabis (22)
2	MR= at^2+ bt + 1	Wang and Singh (23)
3	MR= exp(-kt)	Newton (24)
4	MR= exp(-kt^n)	Page (25, 26)
5	MR= exp[-$(kt)^n$]	Modified Page (27, 28)
6	t= a[ln(MR)]^2 +bln(MR)	Thompson (29)
7	MR= exp[-(at^2+ bt)]	Regression model-1 (30)
8	t = aMR^2 + bMR + c	Regression model-2 (30)

2.2.4 Determination of Shrinkage volume

The shrinkage volume of the raw and blanched carrot slices determined after every condition of drying. The volume of the carrot slices were measured by venire scale. Difference in volume raw and dry carrot is the shrinkage volume

ISSN:2348-4098

in terms of shrinkage percentage is calculated by following formula

Shrinkage (%) = {(volume of raw slice-volume of dry slice) / volume of raw slice}* 100

2.2.5 Determination of Percentage Mass Loss

The percentage mass loss was determined by the following formula

Mass loss (%) = {(Initial mass of raw slices – mass of slices at any time)/initial mass} *100

2.2.6 Hunter Lab Colorimeter analysis

The colour changes of the raw and blanched carrot slices was studied using Hunter Lab Colorimeter (Color flex, 45/0 spec photometer). The color readings were expressed by CIE coordinates (L*a*b*) system. L*(varying from 0-black to 100-white), a*(varying from -60 to +60) and b*(varying from -60 to +60) indicates whiteness/darkness, redness/greenness, blueness/yellowness values, respectively.

The polar coordinate chroma or saturation (c*) is an indication of how vivid the product is (ranging from 0-60), which can be calculated from the L*a* and b* Cartesian co-ordinate by the expression

$C^* = (a^{*2}+b^{*2})^{0.5}$ ..... (1)

Total color difference (ΔE) was calculated from the following equation (31)

$\Delta E = [(L^*-L_{standard})^2 + (a^*-a_{standard})^2 + (b^*-b_{standard})^2]^{0.5}$ ..... (2)

The hue angle values of 0^0, 90^0, 180^0 and 270^0 represents the red, yellow, green and blue color respectively (32).

Hue angle (H_0) is determined by using following equations

$H_0 = \tan^{-1}(b/a)$ ..... (3)

ISSN:2348-4098

3. RESULTS & DISCUSSIONS

3.1 DETERMINATION OF MOISTURE RATIO (MR)

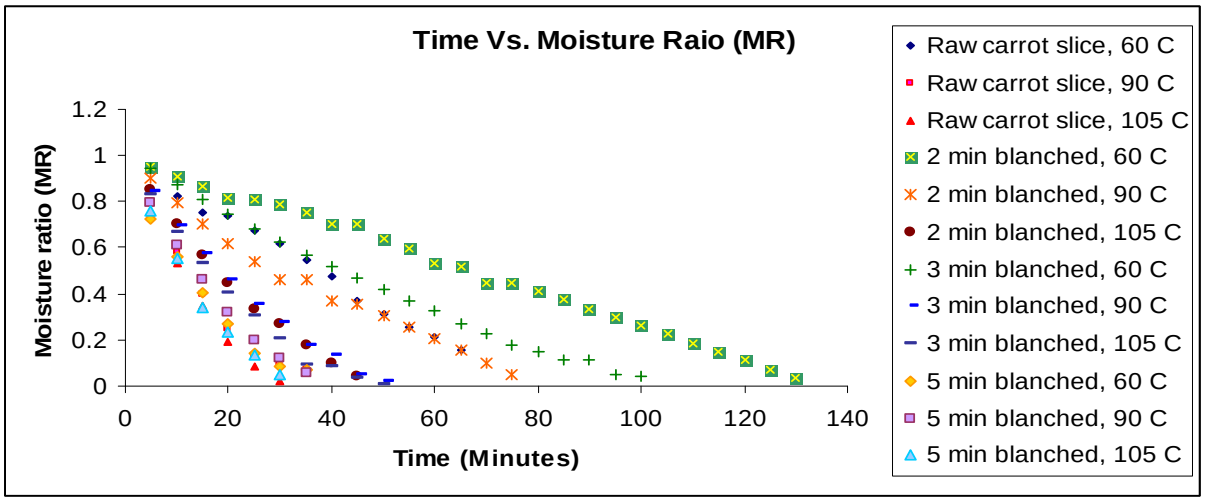

Figure 1: Changes in MR w.r.t time for different condition of carrot slices

The initial weight of the carrot slices was varied 0.738±0.223 for raw carrot slices, 2.19±0.241 for 2 minutes blanched, 1.278±0.244 for 3 minutes blanched, 0.558±0.116 for 5 min blanched slices, which also implies that there was a variation in size of the carrot slices. In case of drying at 60^0C, 90^0C, 105^0C the slices blanched for 2 and 3 minutes have taken much longer time to dry than 5 minutes blanched slices as well as raw carrot slices as the initial weight was much higher than raw carrot slices. It is also noticeable that the 5 minutes blanched slices taken less time to dry than raw slices at 60^0C, and almost same time for drying at 90^0C, and 105^0C (fig 1) as the initial weight was more closer to each other. So, if the size of the slices remains same then it is clearly understand that the blanching has a significant effect on increasing the drying efficiency. The similar observation for positive effect of blanching on drying efficiency or drying rate was reported earlier for sugar beet (33), carrot cubes (34), apples and peaches (35), and red peppers (36). But it is noticeable that more increment in blanching time than 2 or 3 minutes has no significant positive effect on drying efficiency. It is also noticeable that size of the carrot slices has an effect on drying time; carrot size or volume is proportional to drying time.

3.2 MODELING OF DRYING PROCESS

The results of model fitting criteria showed that all models had good fitness

ISSN:2348-4098

to the experimental data under all drying conditions. For all models the R^2 are higher than 0.90, χ^2 and RMSE, lower than 0.02 and 0.13, respectively except for Thomson and regression model-2. To determine the overall fitness of each model for all drying temperatures, the average values of R2, χ^2, and RMSE are calculated and reported in Table 10. The results showed that the Wang and Singh model had the best fitness to experimental data for drying of both raw/fresh and blanched carrot. Similar observation for good fitness of Wang and Singh model was reported earlier for foam mat drying of mango pulp (35). , page model also had a very good fitness for the blanched carrot slices as its χ^2, and RMSE was lower than Wang and sing model but it's R^2 also slightly lower than Wang and Singh model (Table 10). The similar observation for good fitness of page model was reported by for carrot pomace (37, 38).

Table 2: Henderson and Pebis model

Condition of Carrot	Temperature (^{0}C)	Constants		R^2	χ^2	RMSE
		a	k			
Raw	60^{0}C	1.2578	0.0283	0.95	0.0051	0.0666
Raw	90^{0}C	1.3052	0.0852	0.99	0.0008	0.0255
Raw	105^{0}C	2.141	0.1388	0.92	0.0219	0.1251
2 mins blanched	60°C	1.516	0.0201	0.86	0.0206	0.1383
2 mins blanched	90°C	1.292	0.0341	0.91	0.0056	0.0701
2 mins blanched	105°C	1.547	0.0682	0.93	0.0069	0.0747
3 mins blanched	60°C	1.483	0.0296	0.93	0.0122	0.1049
3 mins blanched	90°C	1.791	0.0748	0.91	0.0214	0.1322
3 mins blanched	105°C	2.385	0.0985	0.86	0.0512	0.2047
5 mins blanched	60°C	1.266	0.0844	0.98	0.0025	0.0438
5 mins blanched	90°C	1.506	0.0865	0.96	0.0068	0.0716
5 mins blanched	105°C	1.533	0.1043	0.96	0.0050	0.0602

ISSN:2348-4098

Table 3: Wang and Singh model

Condition of Carrot	Temperature (^{0}C)	Constants		R^2	χ^2	RMSE
		a	b			
Raw	60^{0}C	0.00001	-0.0139	0.99	0.0005	0.0212
Raw	90^{0}C	0.0007	-0.0503	0.99	0.0010	0.0281
Raw	105^{0}C	0.0007	-0.0544	0.99	0.0001	0.0103
2 mins blanched	60°C	0.0000006	-0.0075	0.99	0.0002	0.0144
2 mins blanched	90°C	0.0001	0.0196	0.99	0.0008	0.0266
2 mins blanched	105°C	0.0002	-0.0324	0.99	0.0031	0.0495
3 mins blanched	60°C	0.00004	-0.0138	0.99	0.0001	0.0103
3 mins blanched	90°C	0.0002	-0.032	0.99	0.0026	0.0464
3 mins blanched	105°C	0.0003	0.0364	0.99	0.0139	0.1066
5 mins blanched	60°C	0.0007	-0.0512	0.99	0.0003	0.0158
5 mins blanched	90°C	0.0005	-0.0431	0.99	0.0032	0.0490
5 mins blanched	105°C	0.0007	-0.0528	0.99	0.0002	0.0129

 ISSN:2348-4098

Table 4: Newton model

Condition of Carrot	Temperature (^{0}C)	Constants k	R^2	χ^2	RMSE
Raw	60^{0}C	0.0232	0.91	0.0054	0.0708
Raw	90^{0}C	0.0746	0.97	0.0045	0.0631
Raw	105^{0}C	0.103	0.86	0.0127	0.1045
2 mins blanched	60°C	0.015	0.8	0.0118	0.1065
2 mins blanched	90°C	0.029	0.88	0.0033	0.0553
2 mins blanched	105°C	0.054	0.88	0.0073	0.0808
3 mins blanched	60°C	0.0239	0.88	0.0084	0.0892
3 mins blanched	90°C	0.0582	0.86	0.0105	0.0977
3 mins blanched	105°C	0.0737	0.8	0.0161	0.1212
5 mins blanched	60°C	0.075	0.97	0.0026	0.0482
5 mins blanched	90°C	0.07	0.92	0.0060	0.0727
5 mins blanched	105°C	0.846	0.92	0.0057	0.0701

ISSN:2348-4098

Table 5: Page model

Condition of Carrot	Temperature (^{0}C)	Constants		R^2	χ^2	RMSE
		k	n			
Raw	60^{0}C	0.0066	1.3122	0.98	0.0014	0.0346
Raw	90^{0}C	0.0259	1.3233	0.99	0.0002	0.0135
Raw	105^{0}C	0.0266	1.4089	0.98	0.0010	0.0276
2 mins blanched	60°C	0.004	1.2541	0.94	0.0027	0.0505
2 mins blanched	90°C	0.0158	1.1362	0.98	0.0011	0.0315
2 mins blanched	105°C	0.0176	1.3033	0.99	0.0007	0.0242
3 mins blanched	60°C	0.0061	1.2965	0.99	0.00081	0.0271
3 mins blanched	90°C	0.017	1.3156	0.98	0.0011	0.0305
3 mins blanched	105°C	0.0152	1.3901	0.97	0.0006	0.0228
5 mins blanched	60°C	0.0457	1.1427	0.99	0. 0008	0.0243
5 mins blanched	90°C	0.0266	1.2805	0.99	0.0005	0.0209
5 mins blanched	105°C	0.0311	1.3074	0.99	0.0003	0.0163

ISSN:2348-4098

Table 6: Modified Page model

Condition of Carrot	Temperature (^{0}C)	Constants		R^2	χ^2	RMSE
		k	n			
Raw	60^{0}C	0.0218	1.3122	0.98	0.0014	0.0346
Raw	90^{0}C	0.0633	1.3233	0.99	0.0002	0.0133
Raw	105^{0}C	0.0762	1.4089	0.98	0.0010	0.0272
2 mins blanched	60°C	0.0143	1.2541	0.94	0.0065	0.0778
2 mins blanched	90°C	0.026	1.1362	0.98	0.0011	0.0316
2 mins blanched	105°C	0.045	1.3033	0.99	0.0007	0.0240
3 mins blanched	60°C	0.0198	1.2965	0.99	0.0010	0.0302
3 mins blanched	90°C	0.0452	1.3156	0.98	0.0011	0.0305
3 mins blanched	105°C	0.0512	1.3901	0.97	0.0006	0.0228
5 mins blanched	60°C	0.0672	1.1427	0.99	0.0008	0.0245
5 mins blanched	90°C	0.0589	1.2805	0.99	0.0006	0.0212
5 mins blanched	105°C	0.0703	1.3074	0.99	0.0003	0.0161

ISSN:2348-4098

Table 7: Thompson model

Condition of Carrot	Temperature (^{0}C)	Constants		R^2	χ^2	RMSE
		a	b			
Raw	60^{0}C	-16.475	-64.431	0.99	2.147	1.3566
Raw	90^{0}C	-1.5964	-16.788	0.98	2.880	1.4699
Raw	105^{0}C	-2.0888	- 15.75	0.99	0.6097	0.6599
2 mins blanched	60°C	-20.76	-104.28	0.98	4.5647	2.0558
2 mins blanched	90°C	-8.3378	-50.165	0.99	3.7646	1.8149
2 mins blanched	105°C	-4.4734	-28.187	0.99	0.4859	0.6234
3 mins blanched	60°C	-10.905	-64.721	0.99	4.9969	2.1262
3 mins blanched	90°C	-3.9517	-27.697	0.99	1.6747	1.1705
3 mins blanched	105°C	-2.4093	- 22.09	0.98	3.8433	1.7732
5 mins blanched	60°C	-1.778	-17.185	0.99	1.6708	1.1194
5 mins blanched	90°C	-3.1586	-21.107	0.99	0.2348	0.4196
5 mins blanched	105°C	-2.4278	-17.283	0.99	0.2670	0.4367

ISSN:2348-4098

Table 8: Regression model-1

Condition of Carrot	Temperature (^{0}C)	Constants		R^2	χ^2	RMSE
		a	b			
Raw	60^{0}C	0.0003	0.0082	0.99	0.0010	0.0294
Raw	90^{0}C	0.0006	0.0582	0.98	0.0017	0.0357
Raw	105^{0}C	0.0038	0.0119	0.99	0.0037	0.0515
2 mins blanched	60°C	0.0002	-0.0012	0.95	0.0064	0.0774
2 mins blanched	90°C	0.0003	0.011	0.96	0.0032	0.0532
2 mins blanched	105°C	0.0011	0.0145	0.98	0.0018	0.0388
3 mins blanched	60°C	0.0002	0.0057	0.99	0.0025	0.0479
3 mins blanched	90°C	0.0013	0.0083	0.98	0.0035	0.0541
3 mins blanched	105°C	0.0019	-0.0016	0.95	0.0078	0.0803
5 mins blanched	60°C	0.0007	0.0548	0.99	0.0004	0.0191
5 mins blanched	90°C	0.0015	0.0269	0.99	0.0007	0.0237
5 mins blanched	105°C	0.002	0.0352	0.99	0.0006	0.0215

ISSN:2348-4098

Table 9: Regression model-2

Condition of Carrot	Temperature (^{0}C)	Constants			R^2	χ^2	RMSE
		a	b	c			
Raw	60^{0}C	6.02	-82.59	76.80	0.99	3.3775	1.6290
Raw	90^{0}C	43.38	-73.69	36.87	0.95	4.7589	1.7246
Raw	105^{0}C	27.35	-53.6	30.1	0.99	0.6396	0.6045
2 mins blanched	60°C	-5.01	-131.5	134.6	0.99	3.7857	1.8344
2 mins blanched	90°C	47.08	-130.37	83.45	0.99	4.1614	1.9082
2 mins blanched	105°C	30.24	-75.54	47.72	0.99	0.2688	0.4377
3 mins blanched	60°C	47.83	-148.03	103.1	0.99	2.3922	1.4319
3 mins blanched	90°C	35.30	-82.42	50.03	0.99	1.0705	0.8823
3 mins blanched	105°C	45.57	-87.34	47.24	0.98	4.1591	1.739
5 mins blanched	60°C	39.78	-71.98	36.92	0.98	3.4268	1.4634
5 mins blanched	90°C	28.34	-63.02	37.53	0.99	0.4797	0.5475
5 mins blanched	105°C	33.03	-60.89	32.60	0.99	0.4612	0.5133

 ISSN:2348-4098

Table 10: Overall fitness of different models for IR drying of carrot

Models Name	Raw Carrot			Blanched Carrot		
	R^2	χ^2	RMSE	R^2	χ^2	RMSE
Henderson and Pabis	0.95333	0.009267	0.072400	0.92222	0.014689	0.100056
Wang and Singh	0.99000	0.000533	0.019867	0.99000	0.002711	0.036833
Newton	0.91333	0.007533	0.079467	0.87888	0.007967	0.082411
Page	0.98333	0.000867	0.025233	0.98000	0.000957	0.027567
Modified Page	0.98333	0.000867	0.025033	0.98000	0.001411	0.030967
Thompson	0.98666	1.878900	1.162133	0.98777	2.38918	1.282189
Regression model-1	0.98666	0.002133	0.038867	0.97555	0.002989	0.046222
Regression model-2	0.97666	2.925333	1.319367	0.98777	2.045244	1.195300

3.3 DETERMINATION OF SHRINKAGE VOLUME

The Shrinkage volume of the carrot under different drying condition was given in fig 2. The shrinkage is dependent on proper combination of drying temperature and blanching time (fig 2). The increment in blanching time leads to less the shrinkage percentage in carrot slices (fig 2), this might be due to increase in replacement of the air bound in carrot cell matrix by water and salt combination during blanching as the more air is replaced the carrot slice required higher temperature to dry. The drying at 60^0C, 90^0C, and 105^0C has effectively dried that sample that was passed through 2 minutes blanching but further increment in blanching time may leads to more replacement of air of cell matrix which required higher temperature to properly dry.

ISSN:2348-4098

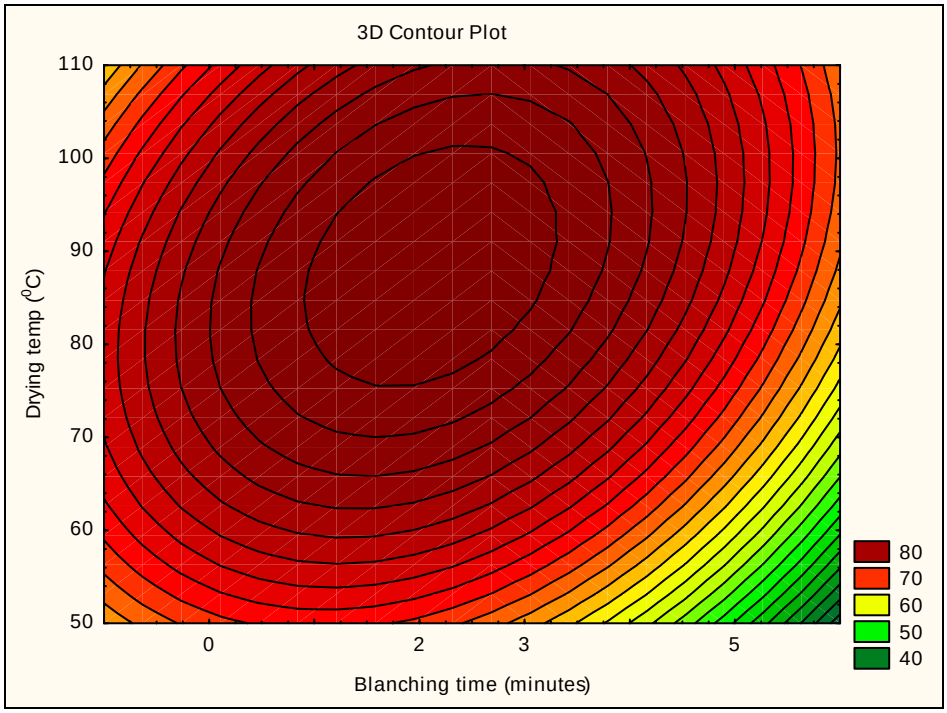

Figure 2: Combined effect of blanching time & drying temperature on shrinkage percentage

3.4 DETERMINATION OF PERCENTAGE MASS LOSS

The mass loss is mainly dependent on temperature of drying, as the drying temperature increases the mass loss also increases with respect to time. The more is the mass loss the more the drying is effective, the maximum mass loss occur at 105^0C for every condition of drying (fig 3). In every cases of drying under 105^0C, percentage mass loss is more than 86%. The results also indicate that for 2 minutes blanching and drying at 90^0C is the good combination for effective drying where 86.33% percentage mass loss takes place.

ISSN:2348-4098

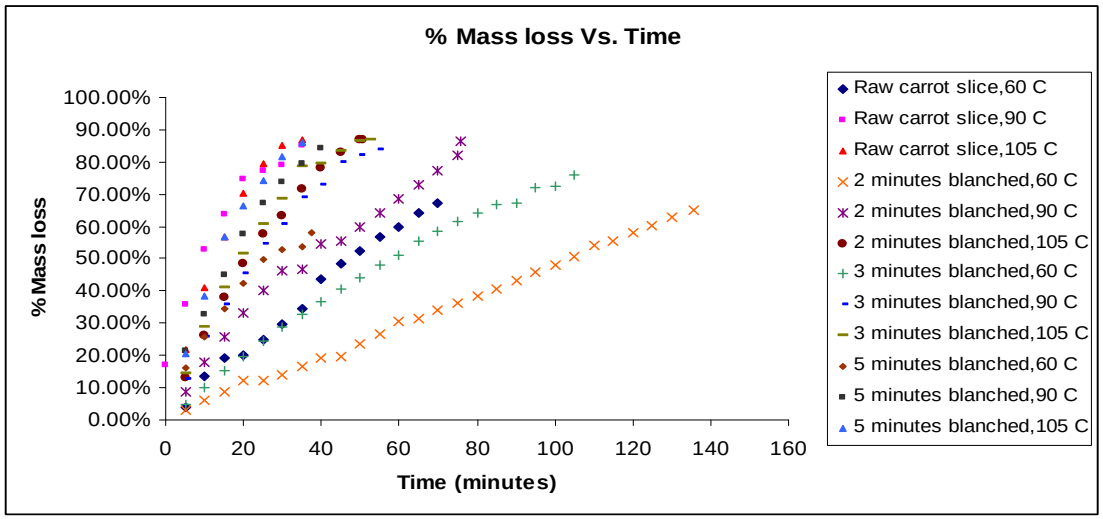

Figure 3: Percentage mass loss w.r.t for different condition of drying

3.5 HUNTER LAB COLORIMETER ANALYSIS

The change of colour of raw carrots and blanched carrots takes place during the drying process. L, a*, b*, ΔE, C*and H^{o} values of raw and blanched carrots are given in table 11. The assessment of the colour quality can be made according to the closeness of the values of the colour parameters of the dried product to those of the control. The colour characteristics of 105^{o}C dried raw carrot were relatively much closer with respect to control. Therefore, it can be concluded that the most preferable raw carrot drying temperature was 105^{o}C.In case of blanched carrot, 3 min blanched and 105^{o}C dried carrot showed best with respect to other samples, so it was best acceptable condition for blanched carrot drying. Color of blanched carrots was brighter than raw carrot due to liberation of trapped air from cell matrix of carrot sample. a*, b* were much low at 105^{o} C for 5 min blanched carrot .It may happened because of higher blanching time.

 ISSN:2348-4098

Table 11: colorimeter analysis of carrot slices for different drying condition

Condition of carrot	Drying temperature (°C)	L	a*	b*	ΔE	C*	H°
Raw (control)	-	41.38	8.49	7.77	-	±11.51	42.46
Raw	60	42.07	2.83	3.07	±7.38	±4.17	42.46
Raw	90	40.78	16.14	12.47	±8.99	±20.39	37.69
Raw	105	40.44	8.07	7.86	±1.03	±11.26	44.24
2 min blanched (control)	-	40.60	16.89	13.28	-	±21.48	38.17
2 min blanched	60	40.74	11.68	8.31	±7.26	±14.33	35.43
2 min blanched	90	40.37	3.30	2.78	±17.17	±4.31	40.11
2 min blanched	105	40.99	2.05	2.02	±18.63	±2.87	44.57
3 min blanched (control)	-	37.06	2.71	3.18	-	±3.96	49.56
3 min blanched	60	39.19	5.14	4.53	±3.50	±6.85	41.39
3 min blanched	90	40.27	9.45	7.81	±8.6	±12.26	39.57
3 min blanched	105	38.35	1.22	1.63	±2.51	±2.04	53.19
5 min blanched (control)	-	40.77	2.89	3.36	-	±4.43	49.30
5 min blanched	60	42.58	1.03	1.63	±3.12	±1.93	57.71
5 min blanched	90	44.03	0.05	0.80	±5.02	±0.8	86.42
5 min blanched	105	43.99	0.06	0.74	±5.02	±0.74	85.37

ISSN:2348-4098

4. CONCLUSION

In the study, it is very clearly seen that blanching increases the drying efficiency but the thickness and size of the slices should be kept thin. The proper combination of blanching time and drying temperature may increase the drying efficiency further, which requires more research in this field. Among several models Wang and Sing model fit well for all condition of drying of raw and blanched carrot, as well as page model also fit well for the blanched sample drying. So, these two models can be applied in further research study to predict the moisture ratio. To maintain of original/fresh colour which destructed during drying or blanching require more research to obtained the better combination of blanching time and drying temperature.

REFERENCES

[1] Lewicki P P. "Effect of pre drying, drying andrehydration on plant tissue properties. A review". International Journal of Food Properties, 1, 1–22. (1998).

[2] Bal S, Wratten F T, Chesnen J L, Faulkner M D. "Ananalytical and experimental study of radiant heating of rice grain". Transactions of the ASAE, 13(5), 644–655. (1970).

[3] Ginzburg A S. "Application of Infrared Radiation in Food Processing". Chemical and Process Engineering Series. Leonard Hill, London. (1969).

[4] Baysal, T., Icier, F., Ersus, S., & Yldz, H. "Effects of microwave and infrared drying on the quality of carrot and garlic". European Food Research and Technology, 218(1), 68-73. (2004).

[5] Wang, J., & Sheng, K. "Far-infrared and microwave drying of peach". Food Science and Technology, 39(3), 247-255. (2006).

[6] Togrul, H. "Suitable drying model for infrared drying of carrot". Journal of Food Engineering, 77(3), 610-619. (2006).

[7] Wang, J. "A single-layer model for far-infrared radiation drying of onion slices". Drying Technology, 20(10), 1941-1953. (2002).

[8] Afzal, T. M., & Abe, T. "Combined convection and far infrared radiation drying of rough rice". ASAE Annual International Meeting, 10-14 August, Minneapolis, MN, USA. (1997).

[9] Volonchuck, S. K., & Shornikova, L. P. "Full-value nutrition and infrared

ISSN:2348-4098

drying of raw vegetables". Pishchevaya Promyshlennost, 5, 16-17. (1998).

[10] Jain, D., & Pathare, P. B. "Selection and evaluation of thin layer drying models for infrared radiative and convective drying of onion slices". Biosystems Engineering, 89(3), 289-296. (2004).

[11] Praveenkumar, D. G., Umesh Hebber, H., & Ramesh, M. N. "Suitability of thin layer models for infrared-hot air-drying of onion slices". Food Science and Technology, 39(6), 700-705. (2006).

[12] Sharma, G. P., Verma, R. C., & Pathare, P. "Mathematical modeling of infrared radiation thin layer drying of onion slices". Journal of Food Engineering, 71(3), 282-286. (2005).

[13] Abe, T., & Afzal, T. M. "Thin-layer infrared radiation drying of rough rice". Journal of Agricultural Engineering Research, 67(4), 289-297. (1997).

[14] Hashimoto, A. M. U., & Kameoka, T. "Effect of infrared irradiation on drying characteristics of wet porous materials". Drying Technology, 17(7-8), 1613-1626. (1999).

[15] İbrahim DOYMAZ. "Determination of Infrared Drying Characteristics and Modelling of Drying Behaviour of Carrot Pomace" Journal of Agricultural Sciences, 19 (44-53). (2013).

[16] D. Mihoubia, S. Timoumi, F. Zagrouba. "Modelling of convective drying of carrot slices with IR heat source". Chemical Engineering and Processing, 48 (808–815). (2009).

[17] Parry, J. L. "Mathematical modelling and computer simulation of heat and mass transfer in agricultural grain drying". Journal of Agricultural Engineering Research, 32 (339-352). (1985).

[18] Diamante, L. M., & Munro, P. A. "Mathematical modelling of the thin layer solar drying of sweet potato slices". Solar Energy, 51 (271-276). (1993).

[19] Karim, M. A., & Hawlader, M. N. A. "Drying characteristics of banana: theoretical modelling and experimental validation". Journal of Food Engineering, 70(1), 35-45. (2005).

[20] Meeso, N., Nathakaranakule, A., Madhiyanon, T., & Soponronnarit, S. "Modelling of far-infrared irradiation in paddy drying process". Journal of Food Engineering, 78(4), 1248-1258. (2007).

[21] Wang, Z., Sun, J., Chen, F., Liao, X., & Hu, X. "Mathematical modelling on thin layer microwave drying of apple pomace with and without hot air pre-drying". Journal of Food Engineering, 80(2), 536-544. (2007).

ISSN:2348-4098

[22] Henderson, S. M., & Pabis, S. "Grain drying theory. I: temperature effects on drying coefficients". Journal of Agricultural Engineering Research, 6(3), 169-174. (1961).

[23] Wang, C. Y., & Singh, R. P. "Use of variable equilibrium moisture content in modeling rice drying". Transactions of ASAE, 11, 668-672. (1978).

[24] Ayensu, A. "Dehydration of food crops using a solar dryer with convective heat flow". Solar Energy, 59(4e6), 121-126. (1997).

[25] Praveenkumar, D. G., Umesh Hebber, H., & Ramesh, M. N. "Suitability of thin layer models for infrared-hot air-drying of onion slices". Food Science and Technology, 39(6), 700-705. (2006).

[26] Doymaz, I. "Air-drying characteristics of tomatoes". Journal of Food Engineering, 78(4), 1291-1297. (2007).

[27] Togrul, H. "Simple modeling of infrared drying of fresh apple slices". Journal of Food Engineering, 71(3), 311-323. (2005).

[28] Vega, A., Fito, P., Andres, A., & Lemus, R. "Mathematical modeling of hot-air drying kinetics of red bell pepper (var. Lamuyo)". Journal of Food Engineering, 79(4), 1460-1466. (2007).

[29] Thompson, T. L., Peart, R. M., & Foster, G. H. "Mathematical simulation of corn drying, A new model". Transactions of the ASAE, 11(4), 582-586. (1968).

[30] Junling Shi, Zhongli Pan, Tara H. McHugh, Delilah Wood, Edward Hirschberg, Don Olson. "Drying and quality characteristics of fresh and sugar-infused blueberries dried with infrared radiation heating". LWT - Food Science and Technology 41, 1962-1972. (2008).

[31] Altunakar, B., Sahin, S., & Sumnu, G. "Functionality of batters containing different starch types for deep-fat frying of chicken nuggets". European Food Research and Technology, 218, 318–322. (2004).

[32] Eliçin, A.K. and K. Saçılık. "An experimental study for solar tunnel drying of apple". Ankara Üniversitesi Tarım Bilimleri Dergisi, 11(2):207-211. (2005).

[33] Vaccarezza, L.M. & Chirife, J. "On the mechanism of moisture transport during air drying of sugar beet root". Journal of Food Science, 40, 1286–1289. (1975).

[34] Mazza, G. "Drying of carrots: effect of pre-drying treatments on moisture transport and product quality". Journal

ISSN:2348-4098

of Food Technology, 18, 113–123. (1983).

[35] Barbanti, D., Mastrocola, D., Pinnavaia, G., Severini, C. & Dalla Rosa, M. "Air drying of fruit: effects of different pre-treatments on drying rate and product quality". In: Drying _91 (edited by A.S. Mujumdar& I. Filkova). Pp. 471–482. Amsterdam: Elsevier Applied Science Publishers. (1991).

[36] Robin A. Wilson, Dattatreya M. Kadam, Sonia Chadha , Monika Sharma. "Foam Mat Drying Characteristics of Mango Pulp". International Journal of Food Science and Nutrition Engineering, 2(4): 63-69. (2012).

[37] Upadhyay A, Sharma HK, Sarkar BC. "Characterization of dehydration kinetics of carrot pomace". Agricultural Engineering International: The CIGR Ejournal FP 07 35. Vol. X. (2008).

[38] Navneet Kumar, B. C. Sarkar & H. K. Sharma. "Mathematical modelling of thin layer hot air drying of carrot pomace". Journal of Food Science and Technology 49(1), 33–41. (January–February 2012).

ISSN:2348-4098

THE ALL-OPTICAL REVERSIBLE NEW UNIVERSAL GATE USING MACH- ZEHNDER INTERFEROMETER

[1]ASHIS KUMAR MANDAL, [2]GOUTAM KUMAR MAITY

[1]Lecturer, Physics, Chakur Haris Seminary High School, West Bengal, India,

[2]Associate Professor, Electronics & Communication Engineering, MCKV Institute of Engineering, West Bengal, India

ABSTRACT

At present time, reversible logic, one of the vital issue, has originated as a promising computing paradigm having application in low-power CMOS, quantum computing, nanotechnology and optical computing, DNA computing, etc. With much efficiency optical logic gates have the potential to perform at macroscopic (light pulses carry information), or quantum (single photons carry information) levels. Now, we propose and configure a great scheme of TAND gate in all-optical domain. We have explained their principle of operations and used a theoretical model to fulfill this task, finally confirming through numerical simulations In the field of ultra-fast all-optical signal processing Mach–Zehnder interferometer (MZI), semiconductor optical amplifier (SOA)-based, has an important function. The different logical (realization of Boolean function) operations can be executed by designed circuits in the domain of reversible logic-based information processing. The logic blocks in our traditional computer are irreversible because after generating the output bits the blocks lose the input bits permanently. The classical gates like AND, OR, NAND, etc. are such type of gates because they have multiple-input but single output. The reversible gates have inputs and outputs which are one-to-one correspondence. The inputs of such gates can be determined from its outputs. So, this type of gates has same number of inputs and outputs. In conventional irreversible hardware computation does in energy dissipation due to information loss [1]. But, the reversible logic circuits give us the computation with arbitrary small energy dissipation [2]. For the field of information processing a promising technology has been developed by reversible logic circuits. Many optical logic gates have been suggested to perform irreversible logic function [3-14]. A gate is universal if any logical reversible circuit can be designed using these gates. This paper

 ISSN:2348-4098

presents a circuit for realization of universal TAND gate in all-optical domain. This paper is built as follows. In Section 1 the principle and operation Mach–Zehnder interferometer (MZI)-based optical switch is explained. All-optical circuit of MZI-based universal TAND gate is discussed in Section 2. Designing of various gates in all-optical domain are reported in Section 3 by universal TAND gate. Corresponding simulation (by Matlab-7.0) results confirm gate's properties are also attached in this paper.

INDEX TERMS: Reversible logic gates, Mach–Zehnder interferometer (MZI), and TAND gate.

1. MZI-BASED ALL-OPTICAL SWITCH

When the incoming signal is to be switched into the interferometer, it is split between the arms of the interferometer. The incoming signal emerges from crossbar port in the absence of a control signal. The presence of control pulse changes the refractive index of

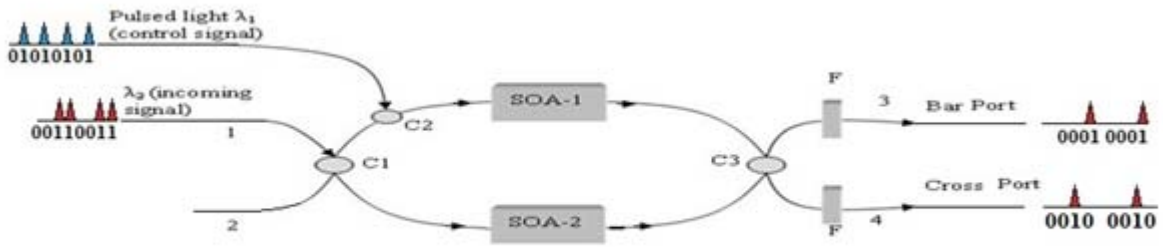

Figure: 1(a)

the medium given by $\triangle n = n_2 I$, here, $\triangle$ n is the change in the refractive index of the medium, n2 the nonlinear refractive coefficient and I the intensity of the light incident on the medium. The incoming signal is switched over to bar port due to a change in the index adds a phase shift between the two arms of the interferometer.

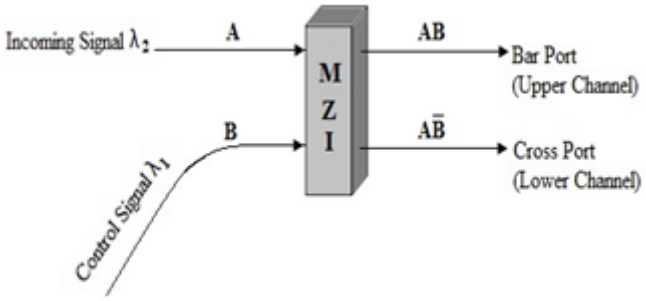

Figure 1(b)

This switching process is based on cross phase modulation (XPM). The XPM used SOA-Mach–Zehnder interferometer is the great important interferometric structure due to

ISSN:2348-4098

its low-energy requirement, simplicity, compactness and stability [15-25]. Symmetric MZI-SOA all-optical switch is shown in Fig. 1(a) and (b).

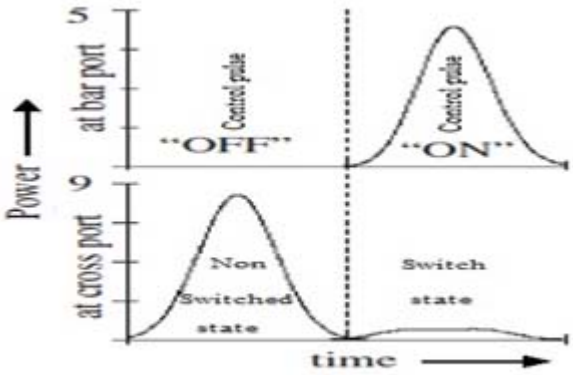

Figure 1(c)

Two semiconductor optical amplifiers (SOA-1 and SOA-2) are inserted in each arm of a MZ interferometer [15-18]. It has two input ports (port-1 and port-2) and two output ports (port-3 or Bar-port and port-4 or Cross-port). The incoming signal pulse of wavelength $\lambda 2$ enters through port-1, is divided equally by the coupler C1 (50:50) and propagates simultaneously in the two arms and port-2 is kept open. At that time, through coupler C2 a pulsed signal of wavelength $\lambda 1$ enters to the upper arm in such a way that most power goes through upper arm. This pulsed signal saturates the SOA-1 and changes its refractive index, while the SOA-2 remains the unsaturated gain state. As a consequence, a differential phase shift can be gained between the data signal of two arms. So, light is present in the port-3 (bar port), as shown in Fig. 1(a) and no light is present in the port-4 (cross port). This is known as 'switched state'. Both SOA (SOA-1 and SOA-2) get the same unsaturated gain when control signal is absent. Then no light is present in the port-3 (bar port) but light is present in the port-4 (cross port).This is called 'no-switched state'.

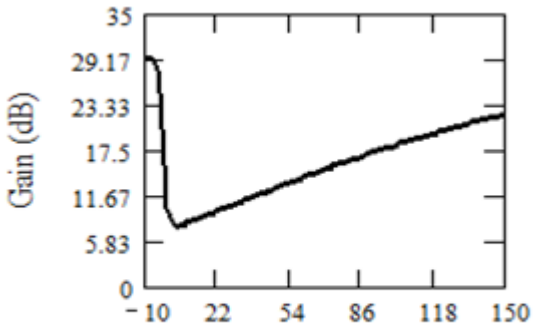

Figure 1(d)

ISSN:2348-4098

Optical filters (F) are inserted in front of the output ports for blocking the $\lambda 1$ signal (control signal). The MZ scheme is desirable for cross-gain saturation as it does not reverse the bit pattern and results in a higher on–off contrast because nothing exits from bar port during 0 bits. Schematic block diagram of MZI is shown in Fig. 1(b). Truth table of Fig. 1(a) is given in Table 1.

Table-1: Truth table of Fig-1(a)

Input		Output	
Incoming signal	Out coming signal	Port-3 (cross port)	Port-4 (bar port)
0	0	0	0
0	1	0	0
1	0	0	1
1	1	1	0

1.1 THEORETICAL MODEL

Mach-Zehnder interferometer (MZI) switch (fig. 1a & 1b) is a very powerful optical device to realize ultra fast all-optical switching. This switch has a semiconductor amplifier (SOA) in each arm of a MZ interferometer [15-16, 18]. The pulsed signal at the wavelength λ_1 enters to the upper arm through coupler C2 such that most power passes through upper arm. At the same time, the incoming signal pulse at the wavelength λ_2 enters port-1, is split equally by this coupler C1 and propagates simultaneously in the two arms.

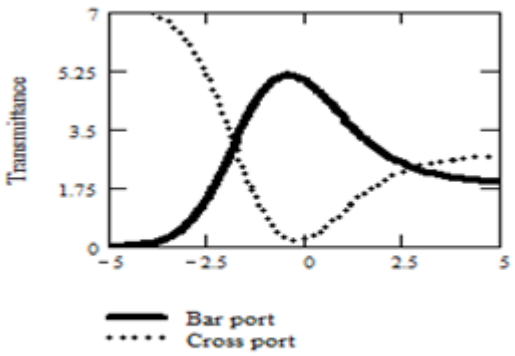

Figure 1.1(a)

At port-3 and port-4 the intensity transmission characteristics can be expressed as [26]

$$T_3(t) = \frac{1}{4}G_1\left\{k_1k_2 + (1-k_1)(1-k_2)R_G - 2\sqrt{k_1k_2(1-k_1)(1-k_2)R_G}\cos(\Delta\Phi)\right\} \quad (1)$$

$$T_4(t) = \frac{1}{4}G_1\left\{k_1(1-k_2) + (1-k_1)k_2R_G - 2\sqrt{k_1k_2(1-k_1)(1-k_2)R_G}\cos(\Delta\Phi)\right\} \quad (2)$$

Where $R_G = G_2/G_1$, G_1 and G_2 are the time dependent gain, $\Delta\Phi(t) = -\frac{\alpha}{2}\ln\left(\frac{G_2}{G_1}\right)$, α is the line width enhancement factor (taken 7.5 here), k_1 and k_2 are the ratios of the couplers C1 and C2 respectively. For simplicity we take $k_1 = k_2 = 1/2$. The output signal power at port-3 and port-4 are,

$$P_j(t) = P_{ip}(t)\cdot T_j(t), \qquad j = 3, 4. \quad (3)$$

Where $P_{ip}(t)$ is the power of the incoming signal pulse. When both beams are present simultaneously, the control pulse saturates SOA-1 on change in carrier density inside SOA. The gain of the SOA during this period is [27-29],

$$G(t) = \frac{1}{1 - \left(1 - \frac{1}{G_0}\right)\exp\left(-\frac{U_{in}(t)}{U_{sat}}\right)} \quad (4)$$

Where U_{sat} is the saturation energy of the SOA and $U_{in}(t) = \int_{-\infty}^{t} P_{in}(t')dt'$. Here we consider a Gaussian Pulse $P_{in}(t) = \frac{E_{in}}{\sigma\sqrt{\pi}}\exp\left(-\frac{t^2}{\sigma^2}\right)$ as control signal, where E_{in} is the input pulse energy, σ is the full width at half maximum (taken 2.8 here). Now the gain recovery is happened in SOA-1 with time constant τ_e. The momentarily gain during this time is [30]

$$G(t) = G_0\left[\frac{G(t_s)}{G_0}\right]^{\exp\left[-(t-t_s)/\tau_e\right]}, \qquad t > t_s \quad (5)$$

Where, $G(t_s)$ is the gain after saturation of SOA-1. We show the gain change for SOA-1 in the Figure3. (c) (All the simulation and calculation is done with Mathcad-7). Physically the pulse is so short that the gain has no time to recover [10].

Here we take G_0 = unsaturated amplifier gain =29.6 dB, τ_e = 95 ps, E_{in}/U_{sat} = 0.1. From the graph in the Figure1(c) we find t_s= 5.5 ps and $G(t_s)$ = 7.969 dB. The beam in the

 ISSN:2348-4098

lower arm experiences the unsaturated amplifier gain G_0 (as there is no strong optical pulse to saturate the SOA-2) i.e. $G_1 \neq G_2$, recombine at the coupler C3. So that $\Delta\Phi \approx \pi$.

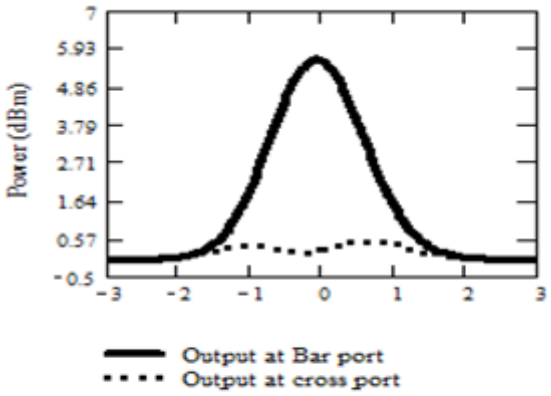

Figure 1.1(b)

Hence, all one bits are directed toward the bar port (upper port-3 in the figure). In the presence of control pulse, the output pulse at port-3 and port-4 is shown in the Figure1.1(b) and the transmitted intensity for both port are also shown in Figure1.1(a). However, in the absence of the λ_1 beam, the both the incoming signal beam in two arms experiences the same unsaturated amplifier gain G_0 in both SOA (i.e. $G_1 = G_2$), recombine at the coupler C3. So $\Delta\Phi = 0$. From equation (3), we can say $P_3(t) = 0$ and the pulse only exits at the cross port (lower port-4 in the figure). In the absences of control pulse, the output pulse at port-3 and port-4 is shown in the Figure1.1(c).

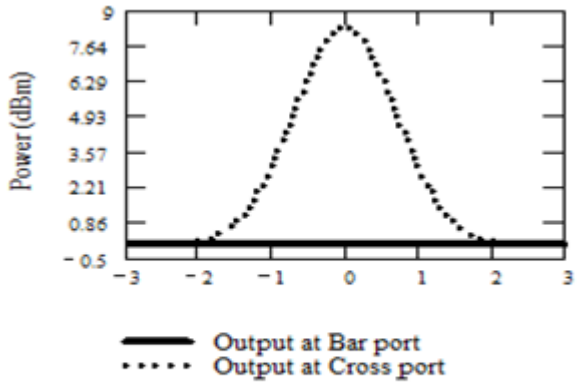

Figure 1.1(c)

Optical filters are placed in front of the output ports for blocking the λ_1 signal. The MZ scheme is preferable over cross-gain saturation as it does not reverse the bit pattern

 ISSN:2348-4098

and results in a higher on-off contrast simply because nothing exits from bar port during 0 bits. Now, it is clear that in the absence of control signal (λ_1), the incoming signal (λ_2) exits through cross-port (lower channel) of MZI as shown in Fig. 3. (a).In this case no light is present in the bar-port (upper channel). But in the presence of control signal, the incoming signal exits through bar port of MZI as shown in Fig. 1.1(b). In this case no light is present in the cross port. In the absence of incoming signal, bar-port and cross- port receives no light as the filter blocks the control signal. Schematic block diagram of MZI is shown in Fig.-1 (b).

2. MZI-BASED NEW GATE: TAND GATE

TAND gate is also a (2*2) conservative reversible gate. It has two inputs (A, B) and two outputs (P, Q) satisfy the relation as follows:

$$\left.\begin{aligned} P &= A \\ Q &= A\bar{B} \end{aligned}\right\} \qquad (6)$$

Table-2: Truth table of TAND gate

Inputs		Outputs	
A	B	P	Q
0	0	0	0
0	1	0	0
1	0	1	1
1	1	1	0

2.1 PRINCIPLE AND DESIGN

Schematic diagram is given in Fig. 2(b). The MZI-based circuit for all-optical reversible TAND gate is given in Fig. 2(a). Here input 'A' is connected with MZI as incoming signal. The control signal of the corresponding gate comes from the input 'B'. The output 'P' is taken by combining the light through a beam combiner (BC) from the bar port (B) and from the cross port (C) of MZI by splitting it by BS .The output 'Q' is taken from the cross port (C) of MZI. The operational principle of this gate is discussed below in details.

(1) When A=B=0, i.e. input A and B do not receive any light, the final output P and Q receives no light from the MZI. So P=Q=0, which satisfy the first row of the truth table 2

 ISSN:2348-4098

(2) When A = 0 and B = 1, then only the control signal is present at MZI. No incoming signal is present at MZI. According to the working principle of MZI described in the Section 1, all the ports do not receive any light. So the final output is P=0 and Q=0, which satisfy the second row of the truth table 2.

(3) When A=1 and B=0, then only the incoming signal is present at MZI and no control signal is present at MZI. According to the working principle of MZI described in the Section 1, only the cross port of MZI(C) receives light. Other port does not receive light. So P=1 and Q=1, which satisfy the third row of the truth table 2.

(4) When A=1 and B=1, then bar port of MZI(B) receives light (as both incoming and control signal of MZI receive light) and cross port does not receive light. So P=1 and Q=0, which satisfy the fourth row of the truth table 2.

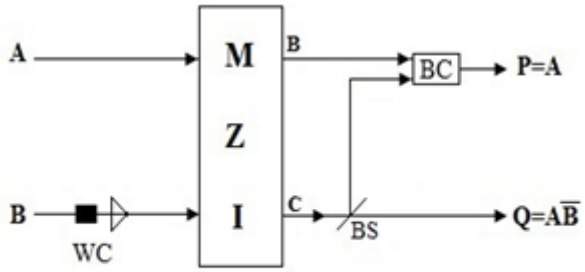

Figure 2(a)

BC : Beam Combiner, ⁄ BS: Beam Splitter, ▷ EDFA: Erbium Doped Fiber Amplifier, ■ WC: Wavelength Converter

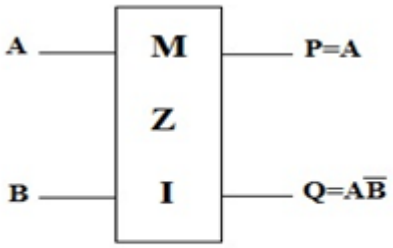

Figure 2(b)

ISSN:2348-4098

3. TAND GATE CAN BE USED TO PERFORM AS UNIVERSAL LOGIC GATE

Proposed arrangements to perform various gate operations are as follow-

3.1 NOT OPERATION

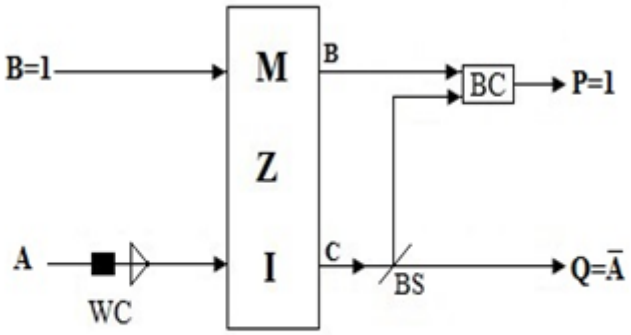

Figure 3.1(a)

BC : Beam Combiner, ⁄ BS: Beam Splitter, ▷ EDFA: Erbium Doped Fiber Amplifier, ■ WC: Wavelength Converter

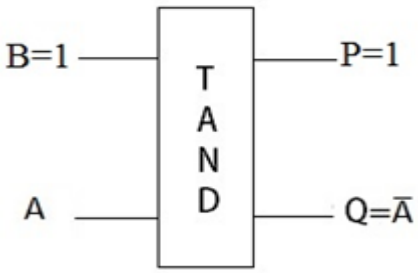

Figure 3.1(b)

Schematic diagram is given in Fig. 3.1(b). The MZI-based circuit for NOT gate by all-optical reversible TAND gate is given in Fig. 3.1(a). Here input 'B'(=1) is connected with MZI as incoming signal. The control signal of the corresponding gate comes from the input 'A'. The output 'P' is taken by combining the light through a beam combiner (BC) from the bar port (B) and from the cross port (C) of MZI by splitting it by BS .The output 'Q' is taken from the cross port (C) of MZI. The operational principle of this gate is discussed below in details.

Table-3.1: Truth table of Figure3.1(a)

A	Q
0	1
1	0

 ISSN:2348-4098

(1) When B=1 and A=0, then only the incoming signal is present at MZI and no control signal is present at MZI. According to the working principle of MZI described in the Section 1, only the cross port of MZI(C) receives light. Other port does not receive light. So P=1 and Q=1, which satisfy the first row of the truth table 3.1.

(2) When A=1 and B=1, then bar port of MZI (B) receives light (as both incoming and control signal of MZI receive light) and cross port does not receive light. So P=1 and Q=0, which satisfy the second row of the truth table 3.1.

3.2 AND OPERATION

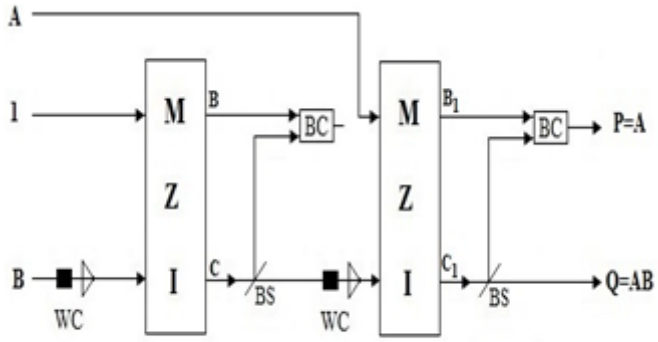

Figure 3.2(a)

BC : Beam Combiner, BS: Beam Splitter, EDFA: Erbium Doped Fiber Amplifier, WC: Wavelength Converter

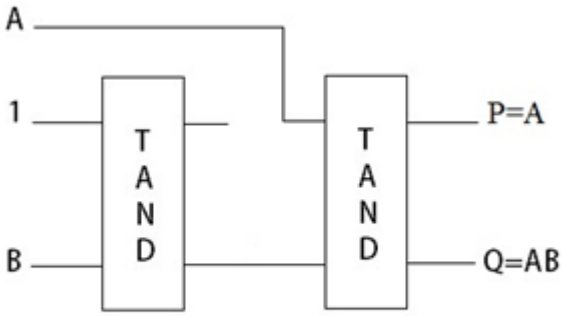

Figure 3.2(b)

Schematic diagram is given in Fig. 3.2(b). The MZI-based circuit for AND gate by all-optical reversible TAND gate is given in Fig. 3.2(a). Here input 'A' is connected with MZI-based TAND gate as incoming signal. The control signal of another gate (TAND gate based NOT gate) comes from the input 'B' and the output (C)of this gate is connected as

ISSN:2348-4098

a control signal of other gate. The final output 'Q' is taken from the cross port (C1) of MZI. The operational principle of this gate is discussed below in details.

Table-3.2: Truth table of Figure3.2(a)

A	B	P	Q
0	0	0	0
0	1	0	0
1	0	1	0
1	1	1	1

(1) When A=B=0, i.e. input A and B do not receive any light, the final output P and Q receives no light from the MZI. So P=Q=0, which satisfy the first row of the truth table 3.2.

(2) When A = 0 and B = 1, then only the control signal is present at MZI. No incoming signal is present at MZI. According to the working principle of MZI described in the Section 1. So the final output is P=0 and Q=0, which satisfy the second row of the truth table 3.2.

(3) When A=1 and B=0, then only the incoming signal is present at MZI and no control signal is present at MZI. According to the working principle of MZI described in the Section 2, P=1 and Q=0, which satisfy the third row of the truth table 3.2.

(4) When A=1 and B=1, then both incoming and control signal of MZI receive light and according to the working principle of MZI described in the Section 1 and TAND gate, P=1 and Q=1, which satisfy the fourth row of the truth table 3.2.

3.3 OR OPERATION

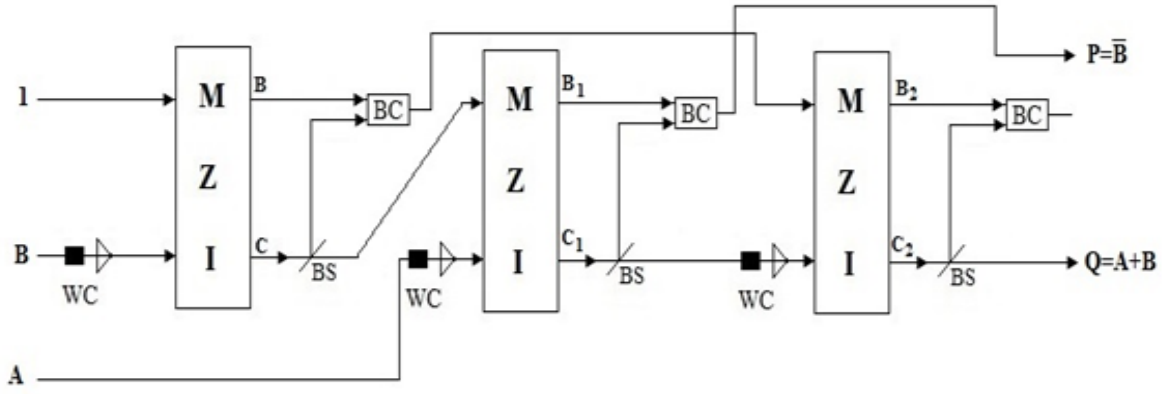

Figure 3.3(a)

ISSN:2348-4098

BC : Beam Combiner, BS: Beam Splitter, EDFA: Erbium Doped Fiber Amplifier, WC: Wavelength Converter

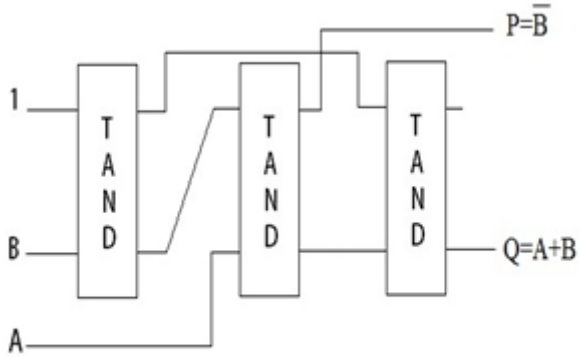

Figure 3.3(b)

Schematic diagram is given in Fig. 3.3(b). The MZI-based circuit for OR gate by all-optical reversible TAND gate is given in Fig. 3.3(a). Here input 'A' is connected with MZI-based TAND gate as control signal. The control signal of the TAND based NOT gate comes from the input 'B' and its cross port (C) is connected as an input signal of above TAND gate. And cross port (C1) of this gate is connected as a control signal of another TAND based NOT gate. The output 'P' is taken form bar port (B1) and output 'Q' is taken form cross port (C2). The operational principle of this gate is discussed below in details.

Table-3.3: Truth table of Figure3.3(a)

A	B	P	Q
0	0	1	0
0	1	0	1
1	0	1	1
1	1	0	1

(1) When A=B=0, i.e. input A and B do not receive any light, the final output P and Q accordingly is P=1 and Q=0, which satisfy the first row of the truth table 3.3.

(2) When A = 0 and B = 1, then only the control signal is present at MZI-based TAND gate. No incoming signal is present at TAND based NOT gate. According to the working principle of MZI and TAND gate described in the Section 1 Section 2, all the final output is P=0 and Q=1, which satisfy the second row of the truth table 3.3.

(3) When A=1 and B=0, then only the incoming signal is present at MZI-based TAND gate and no control signal is present at TAND based NOT gate. According to the working

 ISSN:2348-4098

principle of MZI and TAND gate described in the Section 1 Section 2, the cross port (C2) receives light. Other port also receives light. So P=1 and Q=1, which satisfy the third row of the truth table 3.3.

(4) When A=1 and B=1, then as both control signal of corresponding gates receive light and cross port (C2) receive light. So P=0 and Q=1, which satisfy the fourth row of the truth table 3.3.

3.4 NAND OPERATION

Schematic diagram is given in Fig. 3.4(b). The MZI-based circuit for NAND gate by all-optical reversible TAND gate is given in Fig. 3.4(a). Here input 'A' is connected with MZI-based TAND gate as incoming signal. The control signal of the TAND based NOT gate comes from the input 'B'. The output of this gate, cross port (C), is connected to the control port of above gate. The out of this MZI-based TAND gate, cross port (C1), is connected to another TAND based NOT gate and its output, cross port (C2), is taken as final output 'Q'. 'P' is taken from bar port (B1) of MZI-based TAND gate. The operational principle of this gate is discussed below in details.

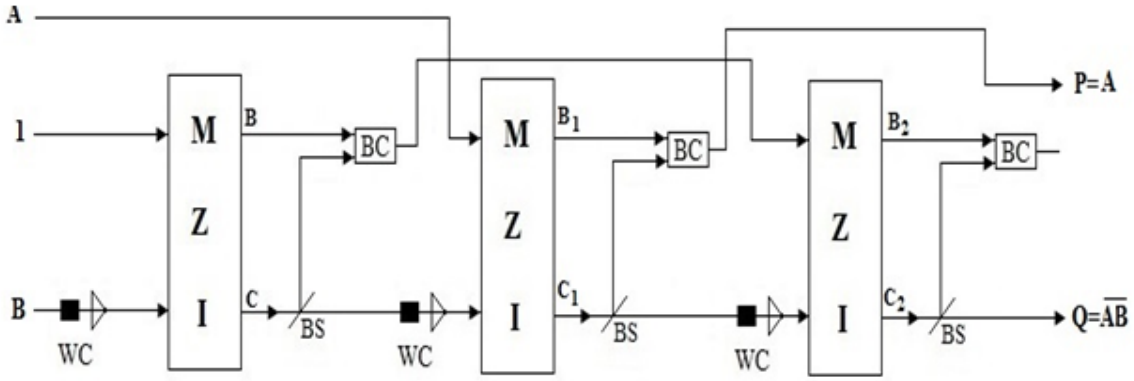

Figure 3.4(a)

BC : Beam Combiner, BS: Beam Splitter, EDFA: Erbium Doped Fiber Amplifier, WC: Wavelength Converter

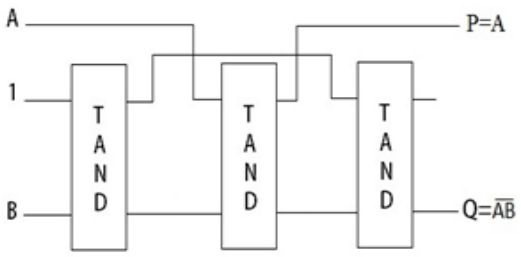

Figure 3.4(b)

ISSN:2348-4098

Table-3.4: Truth table of Figure 3.4(a)

A	B	P	Q
0	0	0	1
0	1	0	1
1	0	1	1
1	1	1	0

(1) When A=B=0, i.e. input A and B do not receive any light, the final output P receives no light and Q receives light from the MZI. So P=0 and Q=1, which satisfy the first row of the truth table 3.4.

(2) When A = 0 and B = 1, then only the control signal is present at TAND based NOT gate. No incoming signal is present at MZI-based TAND gate. According to the working principle of MZI and MZI-based TAND gate described in the Section 1 and Section 2, the final outputs are P=0 and Q=1, which satisfy the second row of the truth table 3.4.

(3) When A=1 and B=0, then only the incoming signal is present at MZI-base TAND gate and no control signal is present at TAND based NOT gate. According to the working principle of MZI and MZI-based TAND gate described in the Section 1 and Section 2, the final outputs are P=1 and Q=1, which satisfy the third row of the truth table 3.4.

(4) When A=1 and B=1, According to the working principle of MZI and MZI-based TAND gate described in the Section 1 and Section 2, the final outputs are P=1 and Q=0, which satisfy the fourth row of the truth table 3.4.

3.5 NOR OPERATION

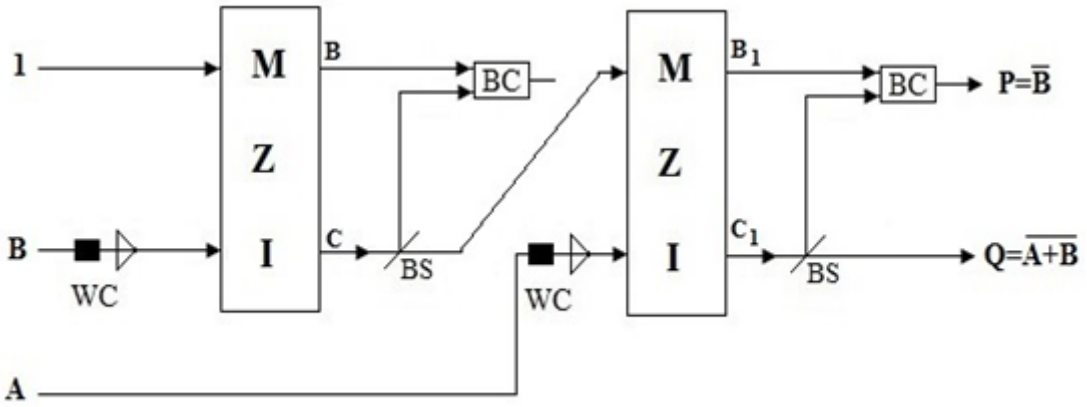

Figure 3.5 (a)

ISSN:2348-4098

BC : Beam Combiner, BS: Beam Splitter, EDFA: Erbium Doped Fiber Amplifier, WC: Wavelength Converter

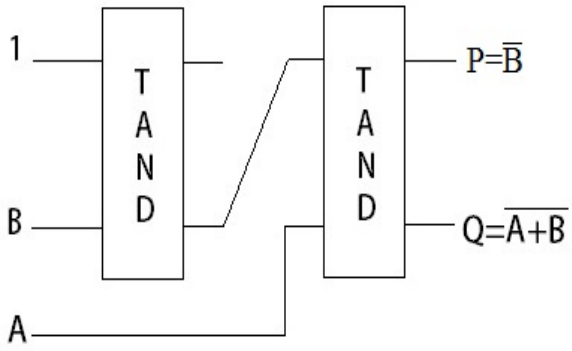

Figure 3.5(b)

Schematic diagram is given in Fig. 3.5(b). The MZI-based circuit for NOR gate by all-optical reversible TAND gate is given in Fig. 3.5(a). Here input 'A' is connected with MZI-based TANT gate as control signal. The control signal of TAND based NOT gate comes from the input 'B'. The output of this gate, cross port (C), is connected to the incoming signal of above gate, MZI-based TAND gate. The output 'Q' and 'P' are taken from the cross port (C1) and bar port (B1) of this MZI-based TAND gate. The operational principle of this gate is discussed below in details.

Table-3.5: Truth table of Figure3.5(a)

A	B	P	Q
0	0	1	1
0	1	0	0
1	0	1	0
1	1	0	0

(1) When A=B=0, i.e. input A and B do not receive any light, the final output P and Q receives light from the MZI-based TAND gate. So P=Q=1, which satisfy the first row of the truth table 3.5.

(2) When A = 0 and B = 1, then only the control signal is present at TAND based NOT gate. No control signal is present at MZI-based TAND gate. According to the working principle of MZI and MZI-based TAND gate described in the Section 1 and Section 2, the final outputs are P=0 and Q=0, which satisfy the second row of the truth table 3.5.

ISSN:2348-4098

(3) When A=1 and B=0, then only the control signal is present at MZI-based TAND gate and no control signal is present at TAND based NOT gate. According to the working principle of MZI and MZI-based TAND gate described in the Section 1 and Section 2, the final outputs are P=1 and Q=0, which satisfy the third row of the truth table 3.5.

(4) When A=1 and B=1, then both control signals of MZI-based TAND gate and TAND based NOT gate receive light. So P=0 and Q=0, which satisfy the fourth row of the truth table 3.5.

3.6 XNOR OPERATION

Schematic diagram is given in Fig. 3.6(b). The MZI-based circuit for X-NOR gate by all-optical reversible TAND gate is given in Fig. 3.6(a). Here input 'A' and 'B' are connected with two MZI-based TAND gates as incoming and also control signal at the same time. The outputs of the cross port (C, C2) are connected to the control port of TAND based NOT gate and MZI-based TAND gate respectively. The output from cross port (C1) is connected to the input port of MZI-based TAND gate which gives final output 'Q' through cross port C3. And output 'P' is taken from bar port (B). The operational principle of this gate is discussed below in details.

BC : Beam Combiner, BS: Beam Splitter, EDFA: Erbium Doped Fiber Amplifier, WC: Wavelength Converter

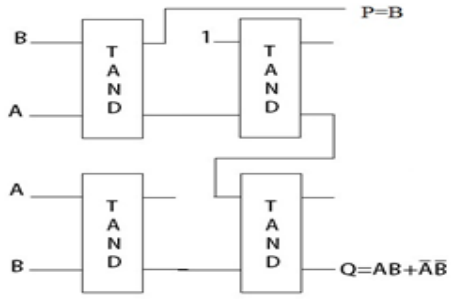

Figure 3.6(b)

Table-3.6: Truth table of Figure3.6(b)

A	B	P	Q
0	0	0	1
0	1	1	0
1	0	0	0
1	1	1	1

ISSN:2348-4098

(1) When A=B=0, i.e. input A and B do not receive any light, the final output P receives no light and Q receives light from the corresponding gate. So P=0 and Q=1, which satisfy the first row of the truth table 3.6.

(2) When A = 0 and B = 1, according to the working principle of MZI and MZI-based TAND gate described in the Section 1 and Section 2, the final outputs are P=1 and Q=0, which satisfy the second row of the truth table 3.6.

(3) When A=1 and B=0, according to the working principle of MZI and MZI-based TAND gate described in the Section 1 and Section 2, the final outputs are P=0 and Q=0, which satisfy the third row of the truth table 3.6.

(4) When A=1 and B=1, the final outputs are P=1 and Q=1, which satisfy the fourth row of the truth table 3.6.

3.7 XOR OPERATION

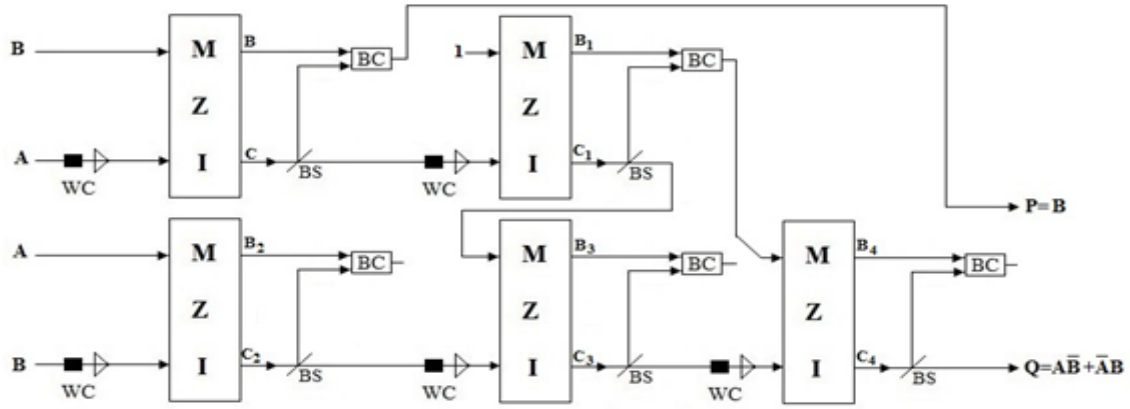

Figure 3.7(a)

BC : Beam Combiner, BS: Beam Splitter, EDFA: Erbium Doped Fiber Amplifier, WC: Wavelength Converter

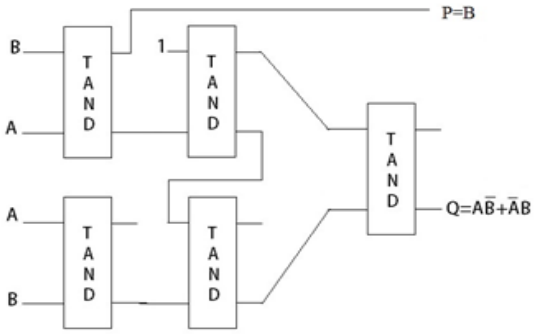

Figure 3.7(b)

ISSN:2348-4098

Schematic diagram is given in Fig. 3.7(b). The MZI-based circuit for X-OR gate by all-optical reversible TAND gate is given in Fig. 3.7(a). First, a circuit is done like X-NOR gate operation. Then outputs from cross port (C3) and bar port (B1) are connected to a MZI-based TAND gate as control signal and incoming signal respectively. The final outputs 'Q' and 'P' are taken from cross port (C4) and bar port (B). The operational principle of this gate is discussed below in details.

Table-3.7: Truth table of Figure3.7(a)

A	B	P	Q
0	0	0	0
0	1	1	1
1	0	0	1
1	1	1	0

(1) When A=B=0, i.e. input A and B do not receive any light, the final output P and Q receives no light from the used MZI-based TAND gate. So P=Q=0, which satisfy the first row of the truth table 3.7.

(2) When A = 0 and B = 1, according to the working principle of MZI and MZI-based TAND gate described in the Section 1 and Section 2, the final outputs are P=1 and Q=1, which satisfy the second row of the truth table 3.7.

(3) When A=1 and B=0, according to the same working principle of the used gate, the final outputs are P=0 and Q=1, which satisfy the third row of the truth table 3.7.

(4) When A=1 and B=1, the both incoming and control signal of MZI-based TAND gate receive light and cross port does not receive light. And then similar working principle we get the final outputs are P=1 and Q=0, which satisfy the fourth row of the truth table 3.7.

4. SIMULATION (BY MATLAB-7.0) RESULT OF ABOVE DESIGNED GATES

The vertical axis in Figure4(a) to 4(j) indicates power in dB, while horizontal axis represents time scale in ps. The timing instant for the occurrence of bit pattern is at 1,3,5,7 ps. Upper first two (Figure4(a) and Figure4(b)) set waveforms indicate the input bit sequences, **0011** and **0101** for the input variables A and B respectively.

ISSN:2348-4098

Let us test the reversible operation from the simulation results with chosen arbitrary time at 5 ps for the Figure4(a), 4(b) and 4(c) of TAND gate. The output signal P=1, Q=1. Using these specific outputs we get from equation-6, A=1, B=0. Similarly, from different output bit patterns gives the different input bit combinations which satisfies the reversibility condition.

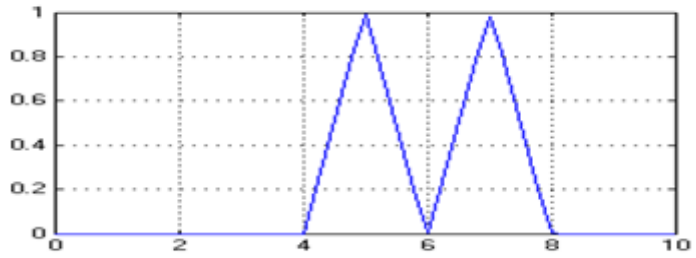

Figure 4(a): Input A

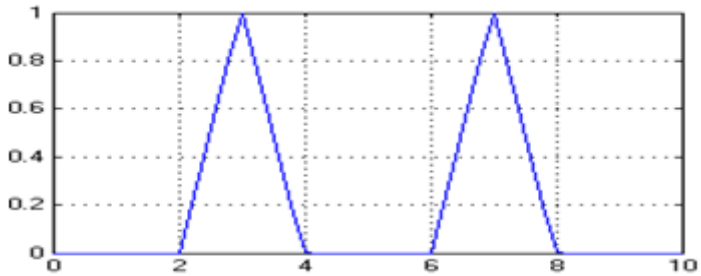

Figure 4(b): Input B

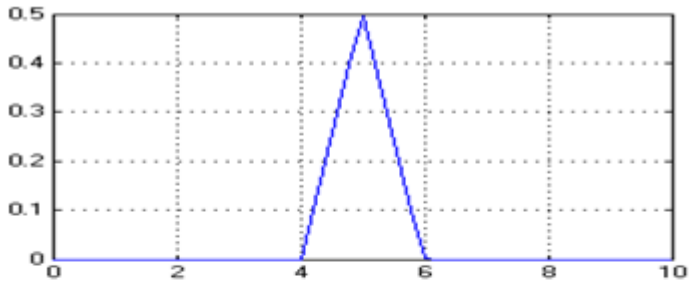

Figure 4(c): 'Q' Output (cross port C) of TAND gate

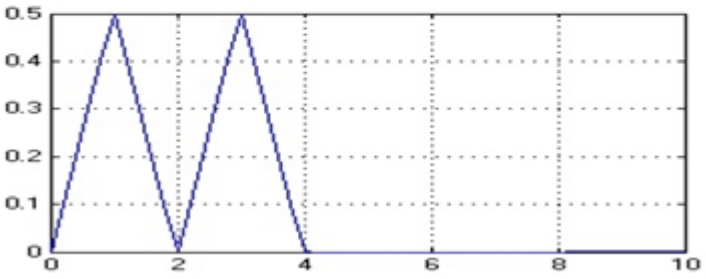

Figure 4(d): Output of NOT operation

ISSN:2348-4098

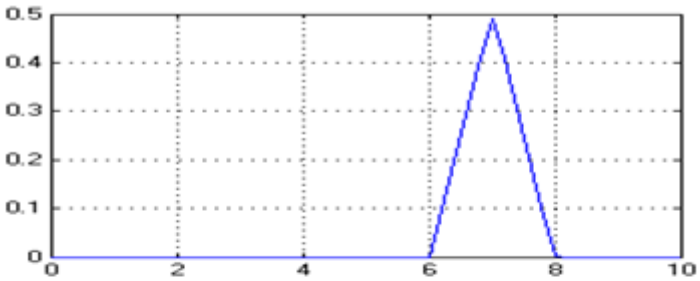

Figure 4(e): Output of AND operation

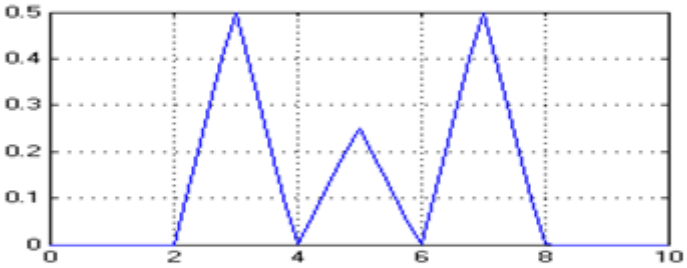

Figure 4(f): Output of OR operation

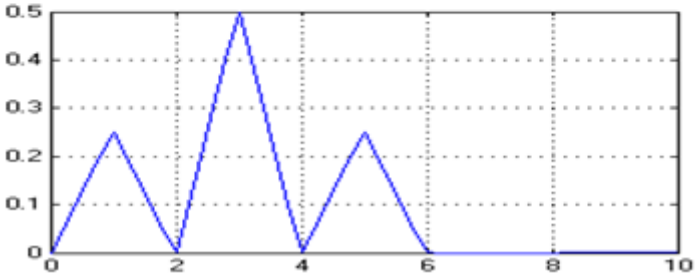

Figure 4(g): Output of NAND operation

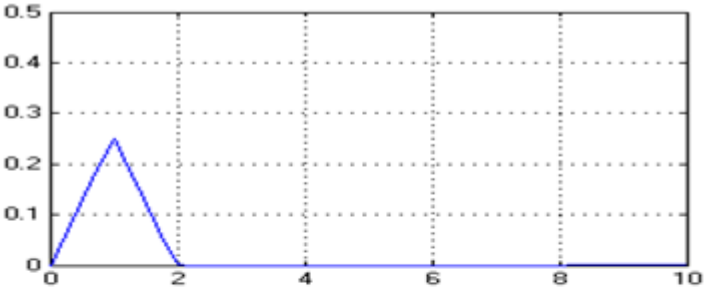

Figure 4(h): Output of NOR operation

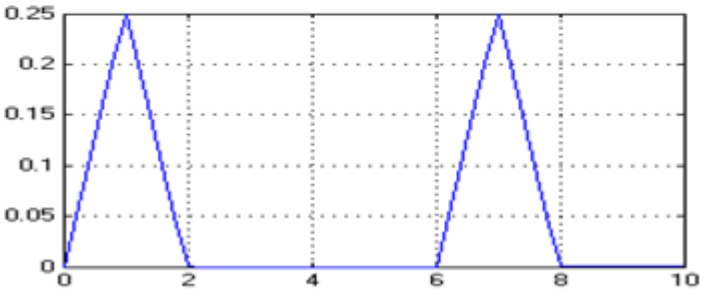

Figure 4(i): Output of X-NOR operation

ISSN:2348-4098

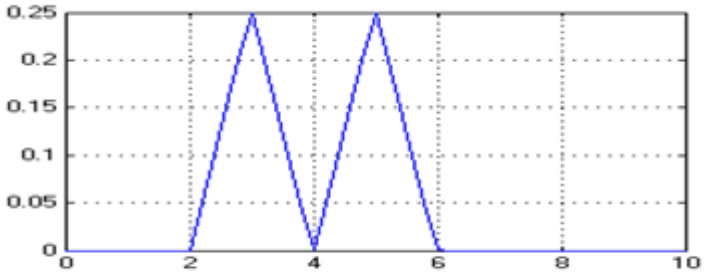

Figure 4(j): Output of X-OR operation

5. CONCLUSION

Here, in this paper, the all-optical scheme of reversible TAND gate is proposed and discussed. Simulation result verifies the functionality of those designed gates with verified reversibility. This is important that the above explanations are based on simple model. We have used Mach–Zehnder interferometer as it is often used in practice due to it can be easily integrated by using SiO2/Si or InGaAsP/InP waveguides, resulting in a compact device [31]. The theoretical models developed and the results obtained numerically are useful to future all-optical reversible logic computing system. Different logic operations in reversible system can easily be achieved with these gates. It is worth noting that the synthesis of reversible logic is different from irreversible logic synthesis. The major constraints in reversible logic are to minimize the number of reversible gates used and garbage outputs produced. The output, which is not used for further computations, is known as garbage output. Future work would concentrate realization of various Boolean expression and arithmetic operations using TAND gate.

REFERENCE

[1]. Landauer R. Irreversibility and heat generation in the computational process. IBM Journal of Research and Development 1961;5:183–91.

[2]. Bennett CH. Logical reversibility of computation. IBM Journal of Research and Development 1973;17:525–32.

[3]. Kim J-Y, Kang J-M, Kim T-Y, Han S-K. All-optical multiple logic gates with XOR, NOR, OR, and NAND functions using parallel SOA-MZI structures: theory and experiment. Journal of Light Wave Technology, IEEE 2006;24(9):3392–9.

[4]. John Caulfield H, Westphal Jonathan. The logic of optics and the optics of logic. Information Sciences 2004;162:21–33.

[5]. Yi Jin, Huacan He, Yangtian Lu. Ternary optical computer architecture. Physica Scripta 2005;T118:98–101.

[6]. Zaghloul YA, Zaghloul ARM. Complete all-optical processing, polarizationbased binary logic gates and optical processors. Optics Express 2006;14(21): 9879–9895.

[7]. Ginzburg P, Hayat A, Vishnyakov V, Orenstein M. Photonic logic by linear unidirectional interference. Optics Express 2009;17(6):4251–6.

[8]. Yatagai T. Optical space variant logic gate array based on spatial encoding technique. Optics Letter 1986;11:260–2.

[9]. Roy JN. Mach–Zehnder Interferometer based tree architecture for all-optical logic and arithmetic operations. Optik 2009;120(7):318–24.

[10]. Chattopadhyay T, Roy JN. Polarization encoded all-optical quaternary multiplexer and demultiplexer—a proposal. Optik. doi:10.1016/j.ijleo.2008.03.030, in press.

[11]. Chattopadhyay T, Roy JN. Polarization encoded all-optical quaternary R-S flipflop using binary latch. Optics Communication 2009;282(7):1287–92.

[12]. Lohmann AW. Polarization and optical logic. Applied Optics 1986;25(10): 1594–1599.

[13]. Cuesta-Soto F, Mart´ınez A, Blasco J, Mart´ı J. Numerical analysis of the performance of Mach–Zehnder interferometric logic gates enhanced with coupled nonlinear ring-resonators. Optics Express 2007;15(5):2323–35.

[14]. Gayen DK, Roy JN. All-optical arithmetic unit with the help of terahertz optical asymmetric demultiplexer (TOAD) based tree architecture. Applied Optics 2008;47(7):933–43.

[15]. Agrwal GP. Applications of nonlinear fibre optics. India: Academic Press; 2001 [(An imprint of Elsevier, San Diego, USA) Chapter 3–4].

[16]. Schreieck R, Kwakernaak M, Jackel H, Gamper E, Gini E, VogtW, et al. Ultafast switching dynamics of Mach–Zehnder interferometer switches. IEEE Photonics Technology Letters 2001;13(6):603–5.

[17]. Li Junqing, Li L, Jin L, Li C. All-optical switch and limiter based on nonlinear polarization in Mach–Zehnder interferometer coupled with a polarization maintaining fiber-ring resonator. Optics Communication 2006;260:318–23.

[18]. Agrwal GP. Fibre-optic communication systems, 3rd ed.. New York: Wiley, Inc. Publication; 2002 [Chapter 8 (WDM Components)].

[19]. Ueno Y, Nakamura S, Tajima K. Penalty-free error-free all-optical data pulse regeneration at 84 Gb/s by using a symmetric-Mach–Zehnder-type semiconductor regenerator. IEEE Photonics Technology Letters 2001;13(5): 469–471.

[20]. Zhang M, Zhao Y, Wang L, Wang J, Ye P. Design and analysis of all-optical XOR gate using SOA-based Mach-Zehnder Interferometer. Optics Communications 2003;223:301–8.

[21]. Chen H, Zhu G, Wang Q, Jaques J, Leuthold J, Piccirilli AB, et al. All-optical logic XOR using differential scheme and Mach-Zehnder interferometer. Electronics Letters 2002;38(21):1271–3.

[22]. Ye X, Ye P, Zhang M. All-optical NAND gate using integrated SOA-based Mach–Zehnder interferometer. Optical Fiber Technology 2006;12(4):312–16.

[23]. Dong H, Sun H, Wang Q, Dutta NK, Jaques J. 80 Gb/s All-optical logic AND operation using Mach–Zehnder interferometer with differential scheme. Optics Communications 2006;265(1):79–83.

[24]. Li Z, Li G. Ultrahigh-speed reconfigurable logic gates based on four-wave mixing in a semiconductor optical amplifier. IEEE Photonics Technolgy Letters 2006;18:1341–3.

[25]. Martinez JM, Herrera J, Ramos F, Marti J. All-optical correlation employing single logic XOR gate with feedback. Electronics Letters 2006;42(20):1170–2.

[26]. J.N.Roy and S.Mukhopadhyay, "A minimization scheme of optical space variant logic operation in a combinational architecture,"Opt.commun.119, 499-504(1995).

[27]. M. H. Hu, C. G. Caneau, H. P. LeBlanc, V. X. Liu, H. K. Nguyen, N. Nishiyama, S. Tsuda and C. –E. Zah, "Semiconductor optical amplifier for amplification and switching applications", Proc. SPIE, 5280, 128-133 (2004).

[28]. W.Li, M. Zhang, P. ye, "Simulation of all-optical XOR gate with a semiconductor optical amplifier Mach-Zehnder interferometer sped up by a Continuos-wave light", Journal of Optical Networking 2005; 4 (8): 524-530.

[29]. I. Armstrong, I. Andonovic and A. E. Kelly, "Semiconductor optical amplifiers: performance and applications in optical packet switching", Journal of Optical Networking, 3(12), p.882 (2004).

[30]. F. Qian, G. Li, M. S. Alam and M. A. Karim, "Digit-set-restricted modified signed-digit arithmetic based on optoelectronic shared content-addressable memory", Proc. SPIE, 5201, 167-173 (2003)

[31]. Leuthold J, Besse PA, Eckner J, Gamper E, D¨ ulk M, Fischer S, et al. All-optical Mach-Zehnder interferometer wavelength converters and switches with integrated data and control-signal separation scheme. Journal of Lightwave Technology 1999;17(6):1056–66.

ISSN:2348-4098

BIOGRAPHIES:

Ashis Kumar Mandal was born in Howrah, West Bengal on 15th March, 1980. He received BSc (Hons. in Physics) degree from Calcutta University & MSc (in Pure Physics) degree from Madurai Kamaraj University. He is presently working as an Assistant Teacher in Chakur Haris Seminary High School. With nearly 8 years of teaching experience he passed CSIR-UGC NET-Dec, 2012(LS, Rank-70) in India. Also, he has published some research papers in international journal. He is interested in Digital Electronics, optical information processing in communication system & organic solar cell.

ISSN:2348-4098

Goutam Kumar Maity had started his carrier with Lectureship at Panskura Banamali College, after completing his post graduation in Eletronics from Jadavpur University, Kolkata, West Bengal, India in 2000. He left Lectureship in 2005 & switched to reputed private engineering colleges since last ten years. He did M.Tech. from West Bengal University of Technology& Ph.D from Bengal Engineering and Science University, Shibpur, Howrah, West Bengal, India in Information Technology & Optical Communications respectively. He has teaching and research experience of more than 14 years. Presently he is working as Associate Professor in ECE Department at MCKV Institute of Engineering, Liluah, Howrah, West Bengal, India. His interests include embedded systems, optical information processing in communication Systems and optical cryptography.

ISSN: 2348-4098
Volume-02
Issue-04
April-May 2014

Publication Fee :

For Online Version	
For Indian Author **INR 2500₹**	for Foreign Author **USD 100$**
For Print Version	
For Indian Author **INR 3200₹**	for Foreign Author **USD 120$**
Both Online & Print Version	
for Indian Author **INR 3500₹**	for Foreign Author **USD160$**

Address :
E-310A,
Civil Lines, Jaipur-
(INDIA) Pin- 302019
Contact No.: +91- 9929435130
Super Fax No.: +91- 8824479077

Innovative Journal Publication and Research Consultancy
E-mail : editor@ijset.in
Website: www.ijset.in/www.ijprc.com